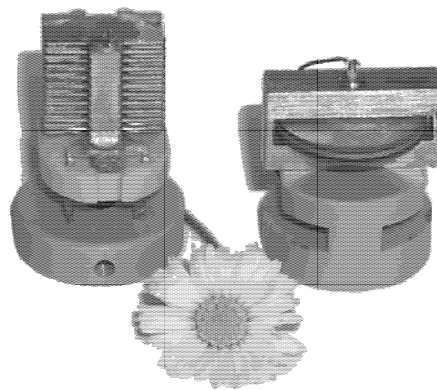# Dielectric and Shear Mechanical Relaxation in Glass Forming Liquids

—

A thorough analysis and experimental test of the DiMarzio-Bishop model

Kristine Niss & Bo Jakobsen
Master thesis in physics
Supervised by: Niels Boye Olsen

Kristine Niss and Bo Jakobsen: *Dielectric and Shear Mechanical Relaxation in Glass Forming Liquids – A thorough analysis and experimental test of the DiMarzio-Bishop model*
Master thesis supervised by Niels Boye Olsen

Abstract

The goal of this thesis is to elucidate whether a relation can be established between shear mechanical and dielectric relaxation in glass forming liquids. The starting point is a generalized Debye model, which has been proposed by Dimarzio & Bishop (1974).

The DiMarzio-Bishop model is thoroughly analyzed and reformulated in such a way that different unphysical simplifications that have been used earlier, are avoided. New testable qualitative predictions of the DiMarzio-Bishop model are formulated and the model is put in a form where quantitative tests can be made by using only one macroscopic parameter.

The DiMarzio-Bishop model is tested by extensive dielectric and shear mechanical measurements on various molecular liquids. The shear mechanical measurements are performed using a transducer that has been developed at IMFUFA by Christensen & Olsen (1995). This transducer allows measurements to be made in an exceptionally large frequency range (1mHz-50kHz). The systematic errors and uncertainties of the two measuring methods are analyzed in detail. Furthermore these errors and uncertainties are taken into account in the reformulation and tests of the DiMarzio-Bishop model.

It is found that the DiMarzio-Bishop model to a large extend has qualitative agreement with our data and data from the literature, whereas the quantitative agreement is moderate or poor depending on the liquid tested. This suggests that the model is too coarse grained to capture details of the relaxation processes, but that it does in fact capture the fundamentals of the physics involved, and consequently that there is a direct relation between shear mechanical relaxation and dielectric relaxation.

Front cover illustration: Photograph of the multilayered capacitor used for dielectric measurements, the piezoelectric shear modulus gauge, and a daisy (scale 1:1).

Preface

This text is a slightly revised version of our master thesis in physics. The work reported has been carried out under the supervision of Niels Boye Olsen in the passed year. It is an experimental project and the measurements have been performed in the student laboratory at the old IMFUFA.

During our work we have been met with much goodwill and have received invaluable help and support from many sides.

We thank the glass research group at IMFUFA for the interest they have taken in our work and for giving us the great opportunities of participating in the "III Workshop on Non Equilibrium Phenomena in Supercooled Fluids, Glasses and Amorphous Materials" in Pisa, and to speak at the "Viscous Liquids and the Glass Transition (III)", workshop at Sømine Stationen.

Niels L. Ellegaard, Claus F. Behrens, Eva Uhre, Rasmus Godiksens, and Esben Thormann are thanked for the discussions and the helpful inputs.

The cumbersome task of proof reading has been shared by Marianne Niss, Ulrik Stervbo-Kristensen, Christian Johannessen, and Maj M. Rydbjerg, whom we all thank for their effort.

We thank Thomas H. Aagaard and Fritz Duus (Chemistry department, RUC) for finding, and allowing us to use, the PZO RL3 refractometer.

We are indebted to the technical staff at IMFUFA, Oda Brandstrup, David B. Andersen, Michael Jensen, Ib Høst Pedersen, Torben S. Rasmussen, and Ebbe H. Larsen, for the practical services that made the experimental part of our project possible, and for helping out with multiple unexpected problems ranging from short circuits in the cryostat to the cooling water flood in our lab.

A special thank to Ranko Richert (Arizona State University) for providing high quality dielectric squalane data.

Jeppe C. Dyre (IMFUFA) is thanked, as much for his critical attitude, as for his strong support.

We are grateful to Tage Christensen (IMFUFA) for all the times he has spent 15 minutes (read: entire afternoons) helping us, especially in the laboratory and understanding the details of the PSG.

Last and most of all we wish to thank Niels Boye Olsen for being a qualified and committed supervisor and for sharing his knowledge from a lifetime in the lab with us.

Kristine Niss and Bo Jakobsen
October 2003

iii

Dansk Resumé

I dette speciale arbejder vi med dielektrisk og shearmekanisk relaksation i seje væsker[1].

Det er karakteristisk for seje væsker, at temperaturafhængigheden af viskositeten hyppigt er ikke-Arrhenius, og at relaksationsprocesserne er ikke-Debye[2]. Disse to forhold er ikke forstået og udgør således de to mest grundlæggende spørgsmål for forskningen i seje væsker.

Baggrund og mål for vores arbejde

Udgangspunktet for dette projekt er en udbredt formodning om, at der eksisterer en sammenhæng mellem væskers shearmekaniske egenskaber og deres dielektriske opførsel. Denne hypotese er interessant, fordi en klarlægning af en sådan sammenhæng oplagt vil bidrage til den overordnede forståelse af dynamikken i seje væsker.

Ideen om en sammenhæng mellem shearmekaniske egenskaber og dielektrisk relaksation går tilbage til Debye [1929]. Debye var inspireret af Einsteins arbejde med translationel diffusion, og beskrev det rotationelle bidrag til dielektricitetskonstanten ved at betragte den enkelte dipol som en kugle, der roterer i et viskøst medie. Debyes model forudsiger Debye-relaksation, og holder derfor generelt ikke for seje væsker.

Vores mål med dette arbejde er at bidrage til forståelsen af den mulige sammenhæng mellem dielektrisk og shearmekanisk relaksation. Vores arbejde er bygget på en generalisering af Debyes model, som er blevet foreslået af Dimarzio & Bishop [1974]. I modsætning til den oprindelige Debye-model, tager DiMarzio-Bishop-modellen væskens viskoelastiske egenskaber i betragtning.

Eksperimentel test af sammenhængen mellem shearmodul og dielektricitetskonstant

Undersøgelser af sammehænge mellem to responsfunktioner stiller meget store krav til målingerne, da man skal være sikker på, at de to typer målinger er sammenlignelige. Dermed skal forstås, at det skal sikres, at det undersøgte stof er kemisk stabilt, samt at de eksperimentelle omstændigheder er de samme. Det er desuden svært at foretage mekaniske målinger på meget viskøse stoffer, da stivheden af stofferne bliver sammenlignelige med typiske stivheder i måleudstyret. Disse forhold gør, at mængden af tilgængelige data, som tillader direkte sammenligning mellem dielektricitetskonstant og shearmodul, er meget begrænsede. Det har derfor været vores ambition at producere grundige målinger på en række stoffer med forskellige egenskaber.

---

[1] Med seje væsker forstår vi væsker med viskositeter i størrelsesordenen $10^4 - 10^{12}$ Pa s, svarerende til relaksationstider på ca. $10^{-6} - 10^3$ s.

[2] Hvis viskositetens temperaturafhængighed går som $e^{\frac{E}{k_B T}}$ kaldes den Arrhenius. Debye-relaksation betyder, at væsken relakserer mod ligevægt på en simpel eksponentiel måde.

Vi har foretaget målinger på syv forskellige stoffer, som har varierende dielektrisk relaksationsstyrke og relaksationsegenskaber. Stofferne er udvalgt ud fra et ønske om både at undesøge stoffer med og uden en eksperimentelt tilgængelig beta-relaksation[3]. Vi har begrænset os til at arbejde med væsker i ligevægt[4], samt begrænset os til lineære eksperimenter.

Alle målinger er udført på IMFUFAs studenteropstilling som tillader kapacitansmålinger med høj pressision og god temperaturkontrol. De dielektrisk målinger er foretaget med en pladekondensator, og dækker frekvensintervallet $1\text{mHz} - 1\text{MHz}$.

Vi har anvendt den såkaldte "piezoelectric shear modulus gauge", PSG, til shearmålingerne. Denne transducer, som er udviklet på IMFUFA (se Christensen & Olsen [1995]), gør det muligt at finde shearmodulet ud fra kapacitetsmålinger. Metoden dækker et frekvens- og shearmodulinterval, der er exceptionelt stort ($1\text{mHz} - 50\text{kHz}$ og $0.1\text{MPa} - 10\text{GPa}$).

I forbindelse med sammenligningen af de to forskellige typer data, er det centralt at have styr på de indgående fejl og usikkerheder. Derfor analyserer og beskriver vi disse fejl og usikkerheder grundigt.

Resultater

Vi reformulerer den makroskopiske version af DiMarzio-Bishop modellen, hvorved højfrekvensopførslen behandles fysisk korrekt og tidligere ufysiske forsimplinger undgås. Det bemærkes blandt andet, at højfrekvens-plateauværdien af dielektricitetskonstanten dels er styret af den atomare polarisabilitet og dels af et rotationelt elastisk bidrag.

Gennem en analyse af temperaturafhængigheden af netop højfrekvens-plateauværdien i de dielektriske målinger, viser vi, at en stigning af denne værdi med temperaturen betyder, at der eksisterer et *elastisk* bidrag til dielektricitetskonstanten. Et fald i den dielektriske højfrekvens-plateauværdi ved temperaturstigning er derimod ikke et bevis for, at et sådant elastisk bidrag ikke findes. Eksperimentelt ser vi en stigning i højfrekvens-dielektricitetskonstanten, og dermed et sikkert tegn på et elastisk bidrag, i ét af de undersøgte stoffer.

Ved en analyse af DiMarzio-Bishop-modellen finder vi, at den forudsiger at maksimum i tabet ligger ved en højere frekvens for shearmodulet end for dielektricitetskonstanten, samt at relaksationskurven for shearmekanikken er bredere end for dielektricitetskonstanten. Vi har for alle de undersøgte stoffer fundet, at forudsigelsen om forskellen i position af maksimum i tabet er som modellen forudsiger, hvilket også er, hvad der rapporteres i litteraturen. Når formen på tabskurverne sammenlignes ses den forudsete forskel i de fleste tilfælde. Forskellen er dog ikke nær så udtalt som forudsagt af DiMarzio-Bishop modellen.

Vi formulerer desuden en simpel én-parameter-version af DiMarzio-Bishop-modellen med henblik på kvantitativ test af denne. Formuleringen er meget anvendelig, fordi

---

[3]Beta-relaksation er en sekundær relaksation som ses ved højere frekvenser end den primære relaksation.

[4]Almindeligvis undersøges underafkølede molekylære væsker, men andre væsker med stor viskositet undersøges også. I denne sammenhæng er det således ikke afgørende om væsken er i en metastabil ligevægt eller en ægte termodynamisk ligevægt, og vi henviser derfor til væskens tilstanden som "ligevægt" i begge situationer. At vi begrænser os til ligevægtsvæsker skal derfor ses som i modsætning til at undersøge væsker i glas tilstanden.

den er robust over for absolutte fejl i målingerne, og fordi parameteren er direkte relateret til makroskopiske målbare størrelser. De fysisk rimelige værdier for parameteren er således nedadtil begrænset af kvadratet på brydningsindekset og opad begrænset af det målte højfrekvensplateau for dielektricitetskonstanten.

Vi finder at DiMarzio-Bishop modellen giver rimelige kvantitative forudsigelser for stoffer med lille dielektrisk styrke og ingen beta-relaksation. Derimod er modellens kvantitative forudsigelser for stoffer med stor styrke dårlige. Det findes desuden at DiMarzio-Bishop modellen i alle tilfælde giver en dårlig beskrivelse af beta-relaksationen.

Ved at analysere hvilken betydning valget af lokalfelt har for DiMarzio-Bishop modellens forudsigelser finder vi, at den dårlige overensstemmelse mellem modellen og data, for stoffer med stor styrker, sandsynligvis ikke skyldes valget af lokalfelt.

Vi diskuterer om grunden til, at modellen passer for stoffer med lille styrke og ikke for stoffer med store styrke er, at der er forskel i hvordan shearmodul og dielektricitetskonstant kobler i de to tilfælde. Vi foreslår, at lokal orden måske påvirker shearmodulet og dielektricitetskonstanten på forskellige måder. Lokal orden kan have større betydning for beta-relaksationen, da denne menes at have en lokal karakter. Tilsvarende er det let at forestille sig, at stor dielektrisk styrke, hvilket er direkte relateret til stort dipolmoment af de enkelte molekyler, kan lede til en mere udtalt lokal orden. Derved vil den lokale orden naturligt få større betydning for stoffer med stor dielektrisk styrke. Som alternativ til ovenstående forklaring viser vi, at det er en mulighed at DiMarzio-Bishop modellen kun passer godt for stofferne med lille styrke, fordi vi her har løsere bånd på den styrende parameter.
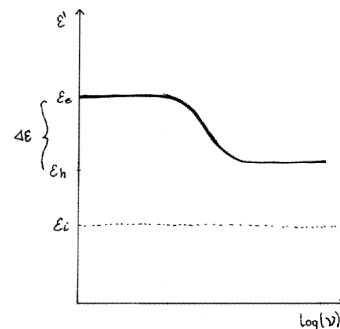
Opsummering

Overenstemmelsen mellem DiMarzio-Bishop modellens kvantitative forudsigelser og virkeligheden svinger mellem rimelig og dårlig. Derfor mener vi ikke, at modellen er anvendelig i forbindelse med kvantitative forudsigelser.

Derimod finder vi god overensstemmelse mellem de kvalitative forudsigelser fra DiMarzio-Bishop modellen og resultaterne af vores målinger. Vi mener derfor at DiMarzio-Bishop modellen indfanger den grundlæggende fysik i dielektrisk relaksation, hvilket dermed understøtter at shearmekanisk relaksation og dielektrisk relaksation er tæt forbundet.

List of commonly used symbols

$\langle \cdot \rangle$ Ensemble average

$\cdot'$ Real part of complex number

$\cdot''$ Imaginary part of complex number

T Temperature

T_g The glass temperature

lp As subscript indicates that the function should be evaluated at the loss peak frequency

ω Angular frequency

ν Frequency

ω_{lp} Loss peak (angular) frequency

ν_{lp} Loss peak frequency

$G, G(\omega)$ Complex frequency dependent shear modulus

G_∞ High frequency plateau value of shear modulus

$\eta, \eta(\omega)$ Complex frequency dependent viscosity

η_0 Frequency independent viscosity, equilibrium viscosity

τ Some relaxation time

τ_M Maxwell time

$\varepsilon, \varepsilon(\omega)$ Complex frequency dependent dielectric constant

$\chi, \chi(\omega)$ Complex frequency dependent dielectric susceptibility

α_i Molecular induced polarization coefficient

ε_i Molecular induced dielectric constant

ε_e Equilibrium (low frequency limit of) dielectric constant

ε_h High frequency plateau of dielectric constant

a Elastic contribution to the dielectric constant; $a = (\varepsilon_h - \varepsilon_i)/(\varepsilon_e - \varepsilon_i)$

ε_0 Vacuum permittivity

$\alpha_r, \alpha_r(\omega)$ Complex frequency dependent rotational polarization coefficient

$\zeta, \zeta(\omega)$ Complex frequency dependent friction coefficient

ζ_0 Frequency independent frictions coefficient

E_m Macroscopic field

E_d Local average directing field

E_i Local average inducing field

E_L Lorentz field

μ Dipole moment

$\mu(t)$ A memory function

r Radius of rotating sphere in Debye and DiMarzio-Bishop model

N Dipoles per volume

θ Angel between field direction and dipole

K_1, K_2, K_3 Parameters in our formulation of the DiMarzio-Bishop model (see section 4.7.2)

The figure illustrates our definitions of the different dielectric quantities. $\Delta\varepsilon$ is the dielectric relaxation strength, we often refer to it as "the dielectric strength" or merely "the strength". ε_i is the part of the dielectric constant which is due to induced polarization of the molecules (see section 3.2.1).

Contents

1 Introduction

Glass forming liquids have a diverse phenomenology, which has been investigated over a large range of temperatures and frequencies. Dielectric spectroscopy data are the most abundant, because dielectric measurements are easy to perform with high accuracy over a large frequency span. It is therefore of great interest to understand what microscopic processes are actually probed via the macroscopic dielectric constant.

The results of dielectric measurements are often compared to the shear mechanical behavior of the liquid either via the Debye-Stoke-Einstein (DSE) time, or by direct comparisons of the shear relaxation and the dielectric relaxation. This is done because it is a common conjecture that dielectric relaxation is somehow connected to the shear meachanical properties of the liquid. The believe in such a connection can at least be dated back to Debye [1929]. In the Debye model the rotation of a dipole in a liquid is governed by the viscosity of the surroundings, in analogy with the result of Einstein on translational diffusion. However, the Debye model does not generally hold for glass forming liquids because it predicts too simple and too narrow a relaxation.

Motivation and goal

A better qualitative understanding of the possible connection between the two relaxations would contribute to achieving an overall consistent picture of the relaxation processes in glass forming liquids. Especially because it would qualify the interpretation of dielectric data.

Models of glass forming liquids often relate to the mechanical properties of the liquid. The question of the glass forming itself is normally connected to an increase in shear viscosity, but the frequency dependent shear modulus is also considered a fundamental property. An example of this is the shoving model, which has been developed at IM-FUFA. This model connects the high frequency plateau value of the shear modulus to the viscosity [Dyre et al., 1996]. However, it is often difficult to obtain reliable shear data especially at high frequencies, which complicates direct tests of the shoving model. Therefore reliable estimates of shear behavior based on dielectric measurements could play an important role in testing the shoving model and other models involving shear behavior.

Our aim is to contribute to the understanding of the possible connection between the shear mechanical relaxation and the dielectric relaxation, both qualitatively and quantitatively. The studies, we perform, are largely based on the simple model of Dimarzio & Bishop [1974], which is a generalized version of the original Debye model. Our objectives can be summarized by the following two questions.

- Does the DiMarzio-Bishop model capture the underlying physics of dielectric relaxation in glass forming liquids?

1

- Does the DiMarzio-Bishop model provide a method for estimating shear relaxation spectra from dielectric relaxation spectra?

We believe that a model-based approach is desirable since it provides testable predictions. Without a model it is impossible to evaluate which correlations that could be expected between the two relaxation processes. However, the drawback of studying a model is that it limits the conclusions that can be drawn. Hence, if the model gives poor results it is of course still possible that a connection between shear relaxation and dielectric relaxation can be found by another approach.

Method

In order to test the DiMarzio-Bishop model we have to analyze it in great detail, and we restate it in appropriate formulations that enable simple quantitative and qualitative predictions. One of our main objectives, is to include a systematic treatment of the significance of the local fields used in the macroscopic formulation. Besides these analyses it is of course necessary to test the predictions of the model against data, in order to answer the questions we have posed.

The viscosity spans many order of magnitude in the relevant temperature regime, leading to very high demands on the measurement equipment used for mechanical spectroscopy. Thus, to span the full dynamical range several techniques have to be used. [Etienne et al., 2003]

At high viscosity near the glass temperature, problems using a conventional rheometer emerge, as deformation of the rheometer has to be taken into account [Christensen & Olsen, 1995]. Due to these problems the amount of shear mechanical data are limited, and the amount of shear mechanical and dielectric measurements taken on samples from the same batch and in the same lab, ensuring comparable conditions for the measurements are even further limited. It is therefore a main ambition to produce reliable dielectric and shear mechanical data from liquids with a varied phenomenology.

Comparing measurements from two different methods put great demands on the precision, as absolute errors and temperature independent errors, which are sometimes ignored, can influence the conclusions. Therefore, we have performed a study of the errors and uncertainties on our data and have taken care not to draw conclusions which could be altered by these.

The report

The study of glass forming liquids has been a central research area at IMFUFA for over a decade, and it has at the same time been the object of many student projects. It is our hope that the next group of students entering the field will profit from reading this report as we have profitted from the earlier projects. We have thus attempted to introduce the subjects from a starting point that more or less corresponds to the level of understanding we had a year ago.

Chapter one has given a general introcuction to the thesis. Chapter two and three will introduce the general questions and phenomenology of glass forming liquids, in particular shear and dielectric relaxation in glass forming liquids. The focal point of this introduction is the issues, which are relevant for our studies.

In chapter 4 the original derivations of the Debye model and the DiMarzio-Bishop model are presented before a reformulation of the macroscopic version of the DiMarzio-Bishop model is introduced. Finally, the chapter ends with an account of the approach we use to test the DiMarzio-Bishop model experimentally.

The experimental setup and practical procedures are described in chapter 5, including our analysis of the errors and uncertainties.

Chapters 6-11 present our data and further analysis of the DiMarzio-Bishop model, which leads to a range of predictions that subsequently are tested. Based on these findings an overall discussion of the DiMarzio-Bishop model is made in chapter 12.

In relation to our data we have looked at a few phenomenological issues, which are central to the general discussions about glass forming liquids, and to a lesser extend to the DiMarzio-Bishop model. These issues are presented in chapter 13.

Finally, the conclusion is presented in chapter 14.

A list of commonly used symbols is found before the table of contents, however symbols will also be defined the first time they are used. In the report we use the standard SI system of units. This may lead to some confusion as it is customary to use cgs units in the literature on dielectric behavior. It is, however, easy to translate formulas from SI units to cgs units, merely interchange ε_0 with $1/(4\pi)$.

2 Glass forming liquids; relaxation and response

This chapter gives an introduction to those of the general results and questions from glass physics, which are related to the specific questions we deal with. The focus is on relaxation processes and response functions.

2.1 What is a glass?

The equilibrium value of volume (and enthalpy) of a liquid will in general decreases with decreasing temperature. Whenever the temperature is decreased by some amount the volume has to adjust to its new equilibrium value. This does not happen instantaneously[1], rather the liquid equilibrates in some way over time. The characteristic time for this process is closely related to the viscosity of the liquid, and as the viscosity grows upon cooling so does the time required to reach equilibrium[2]. Due to this there will be a temperature, T_g, at which the volume can no longer reach its equilibrium value within the time scale of a given cooling experiment. At lower temperatures the liquid will no longer be an equilibrium liquid but a *glass*. The volume of the glass is also dependent on temperature, but this temperature dependence is weaker than that of the liquid. The glass only contracts due to the isostructural contraction, which happens instantaneously upon cooling[3] whereas the liquid has both isostructural contraction and contraction due to better packing of the molecules.

The change in compression rate at T_g gives rise to an abrupt change in slope on a $V - T$ plot. A stereotype of this plot is shown in figure 2.1. The plot also shows a re-heating curve and it is seen that the system exhibits hysteresis, as it is typical for a system which has been taken out of equilibrium. If the system is kept below T_g the liquid will approach equilibrium, though it happens slowly, and the volume will therefore be time dependent.

A liquid will have a T_g corresponding to each cooling rate (lower cooling rates give lower T_g). However, the term T_g is traditionally used about the temperature at which the liquid falls out of equilibrium when cooled at standard experimental rates [Ediger et al., 1996]. Alternatively T_g is sometimes defined as the temperature where the viscosity is 10^{12}Pa s, or the temperature where the characteristic time (τ) of whatever response in question is $100s$ or $1000s$.

---

[1] In some sense it can be said that equilibrium is never achieved but only approached asymptoticly. Equilibrium will however be reached within experimental resolution - making this a rather academic argument.

[2] The liquid will of course reach its melting point at some point, but if the cooling is fast enough crystallization can be avoided (the liquid becomes supercooled), and the liquid behavior is continued. When a liquid is supercooled it is in a metastable state. Through this thesis we refer to this metastable state as "the equilibrium liquid", when we wish to distinguish it from the glassy state.

[3] In practice it is not really possible to make an instantaneous jump in temperature, but the isostructural change in volume will happen at the same time scale as the temperature change.
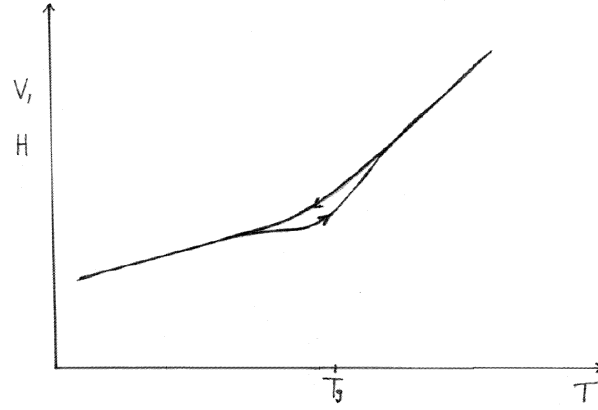
Figure 2.1 Stereotypic $V, H - T$ plot of cooling and re-heating of a liquid through the falling out of equilibrium. [Angell et al., 2000]

2.2 Non-Arrhenius

There is nothing surprising in the behavior described above. The viscosity is expected to increase with decreasing temperature, and the falling out of equilibrium is a natural consequence of this. The puzzling part is the dramatic rate at which the viscosity and the characteristic times increase with decreasing temperature.

The simplest model of the temperature dependence would be an activated behavior, where the viscosity/characteristic times are controlled by some temperature independent activation energy (E_a). This would lead to an Arrhenius temperature dependence:

$$\eta = \eta_p e^{E_a/k_B T} \quad \text{or} \quad \tau = \tau_0 e^{E_a/k_B T}, \tag{2.2.1}$$

where η_p and τ_0 are the high temperature limits of the viscosity and the characteristic time, respectively.

However, most liquids have a much stronger temperature dependence than the above – they are *non-Arrhenius*. Figure 2.2 shows a classical illustration of how the temperature dependence of time/viscosity deviates from Arrhenius.

In the past decades there has been a vast amount of work in attempt to characterize the non-Arrhenius behavior and resolve its origin, and it has undoubtedly been one of the main areas of research within the research field of glass forming liquids.

The temperature dependence is commonly reported in terms of the Angell fragility index , which when found from a relaxation time is given by

$$m = \left. \frac{\mathrm{d} \log_{10}(\tau)}{\mathrm{d} T_g/T} \right|_{T_g} \tag{2.2.2}$$

 [Richert & Angell, 1998].

An alternative index which has been suggested by N. B. Olsen is

$$\gamma(T) = -\frac{\mathrm{d} \log E(T)}{\mathrm{d} \log T} \tag{2.2.3}$$

 [Olsen, 2003][Dyre & Olsen, 2003], where $E(T)$ the apparent activation energy, defined by

$$\tau(T) = \tau_0 e^{\frac{E(T)}{k_B T}} \quad \Leftrightarrow \quad E(T) = k_B T(\ln \tau(T) - \ln(\tau_0)). \tag{2.2.4}$$
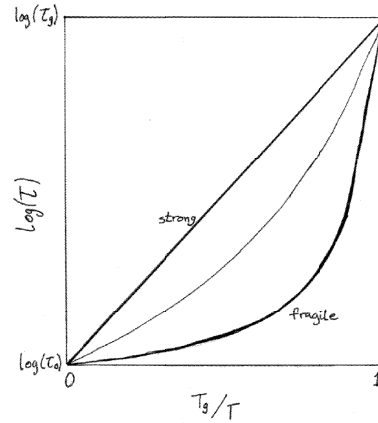
Figure 2.2 Sketch of classical fragility plot (also sometimes called an Angell plot after C. A. Angell). τ_0 is the high temperature characteristic time and τ_g is the characteristic time at the glass temperature. Liquids with temperature behavior close to Arrhenius are called "Strong liquids" and liquids which deviates much from Arrhenius are called "Fragile liquids" [Richert & Angell, 1998].

The Olsen index gives the relative change in apparent activation energy as function of relative change in temperature. This is a very convenient way of measuring fragility, because the non-Ahrrenius behavior is often modeled in terms of the apparent activation energy. The Olsen index is 0 in the case of an Ahrrenius liquid whereas the Angell index is $(\log_{10}(\tau_g/\tau_0))$. The general relation between the two is

$$m = \log_{10}(\tau_g/\tau_0)\left(1 + \gamma(T_g)\right). \tag{2.2.5}$$

There has been a number of models trying to account for the temperature dependence of the viscosity [Angell et al., 2000]. One of these is the shoving model by Dyre et al. [1996], which connects the high frequency shear modulus G_∞ to the viscosity

$$\eta = \eta_p e^{\frac{V_c G_\infty(T)}{k_B T}}, \tag{2.2.6}$$

where V_c is a characteristic volume.

Our work does not directly deal with the non-Arrhenius behavior, but our discussions will return briefly to the subject in section 13.3. The possibility of testing the shoving model by dielectric measurements, which was mentioned in the introduction, will be discussed in section 10.3.

2.3   The general dynamics of a liquid

The most general question we can ask regarding the dynamics of the equilibrium liquid is of course the following: Where are all the molecules and how are they oriented as a function of time? That is, we ask the time dependence of $6N$ coordinates (N being the number of particles). But these $6N$ values are of course not accessible (except in computer simulations) and moreover it is difficult, if not impossible, to interpret such an overwhelming amount of information. It is, however, very common in glass physics to think and argue in terms of the potential energy landscape. The energy landscape is a hyper-surface which describes the potential energy of the system as a function of the $6N$ coordinates. This view of the liquid dynamics was introduced by Goldstein [1969]

and it has been used extensively in the last decade as a tool in computer simulations and theoretical work.

In the temperature interval we study, that is temperatures a little above T_g, it is generally agreed that the long time dynamics are dominated by hopping between energy minima, whereas short time dynamics can be viewed as vibrational modes determined by the shape of the minima (see for example Schrøder et al. [2000]).

The different properties of the liquid, which can be measured will all be given by the (unknown) time dependent values of these $6N$ coordinates. However, some of the properties do not depend on all $6N$ coordinates. The macroscopic polarization of dipolar substance is for example independent of the position of the molecules and only dependent on the orientation of the dipolar axis. Likewise, it does not probe the individual orientation of the molecules, nor the distribution of orientations, but only the average orientation.

Different measurements contain information on different aspects of the coordinates of the molecules, and different types of measurements can probe quantities which are totally different in nature as for example the volume and polarization. It is therefore possible that different types of measurements on the liquid can give uncorrelated information on the system. We picture this by saying that different measurements probe different projections of the liquids movement in its $6N$-dimensional phase space. In addition to measurements of totally different quantities it is also possible to access properties which are closely related. The background for our work is a conjecture about the existence of a connection between the rotation of dipoles in the liquid and the shear mechanical properties of the liquid.

2.4 Linear response in viscous liquids

When the glass is formed as described in section 2.1 the liquid is taken far out of equilibrium which results in nonlinear effects. The experiments we have performed are linear experiment on the equilibrium liquid. Before describing some of the known phenomenology of linear relaxation we give a brief introduction linear response theory.

In linear experiments the liquid is subjected to an input so small that the resulting changes can be assumed to depend linearly on the input. The output response at time t depends on the input at all times t' before t (causality), and on how much time has passed since the input $(t - t')$. The time itself is assumed to have no significance.

Such a linear response is described by

$$B(t) = \int_{-\infty}^{t} \mu(t - t')h(t')dt' = \int_{0}^{\infty} \mu(t')h(t - t')dt'. \tag{2.4.1}$$

with $B(t)$ being the time dependent output and $h(t)$ the applied input. $\mu(t)$ is called the memory function, as it describes how the system remembers its past. The output can of course not depend on the future. This can mathematically be expressed by setting $\mu(t) = 0$ for $t < 0$.

A convenient input is the Heaviside step input:

$$H(t) = \begin{cases} 0 & t \leq 0 \\ 1 & t > 0 \end{cases}$$

The time (domain) response function, $R(t)$ is defined as the output of a Heaviside input:

$$B(t) = \int_{-\infty}^{t} \mu(t-t')\, H(t')\, dt' = \int_{0}^{t} \mu(t')dt' = R(t), \qquad (2.4.2)$$

from which it is seen that the memory function (μ) is the time derivative of the time response function. It is also seen that $R(t) = 0$ for $t < 0$.

Again the input could be a change in temperature and the monitored response could be the relative change in volume of the liquid, in which case the investigated quantity is the linear expansion coefficient. Many other linear responses can be measured and even more can be defined.

2.4.1   Fluctuation versus response

The linear response of a system is directly related to the fluctuation of the system in equilibrium through the fluctuation dissipation theorem (FD-theorem). This is important in the interpretation of the experiments since it shows that a linear experiment in fact probes the dynamics of the equilibrium liquid. Further it allows for direct comparisons to be made between linear response measurements and measurements on the fluctuations via two time correlation functions in the equilibrium system.

Given the general description of a linear response (equation 2.4.1) the general formulation of the FD-theorem states

$$\mu(t) = -\frac{1}{k_B T}\frac{\mathrm{d}}{\mathrm{d}t}\left\langle B(t)A(0)\right\rangle.$$

$A(t)$ has to be a physical quantity which is conjugated to the applied input $h(t)$, which means that $A(t)h(t)$ is a component of the potential energy of the system.   The FD-theorem leads to an easily interpretable result when $B(t)$ itself is conjugated to h, for example if B is the polarization and h an electric field. In this case the time response function $R(t)$ corresponding to a Heavyside input is directly proportional to the mean square variation of the quantity $B(t)$ in equilibrium:

$$
\begin{aligned}
R(t) &= \int_{0}^{t} \mu(t')dt' \\
&= \left(-\frac{1}{k_b T}\left\langle B(t)B(0)\right\rangle + \frac{1}{k_b T}\left\langle B(0)B(0)\right\rangle\right) \\
&= \frac{1}{2}\frac{1}{k_b T}\left\langle B(0)B(0)\right\rangle + \frac{1}{2}\frac{1}{k_b T}\left\langle B(t)B(t)\right\rangle - \frac{1}{k_b T}\left\langle B(t)B(0)\right\rangle \\
&= \frac{1}{2}\frac{1}{k_b T}\left(\left\langle B(0)B(0)\right\rangle + \left\langle B(t)B(t)\right\rangle - 2\left\langle B(t)B(0)\right\rangle\right) \\
&= \frac{1}{2}\frac{1}{k_b T}\left(\left\langle (B(t) - B(0))^2\right\rangle\right) \qquad (2.4.3)
\end{aligned}
$$

The calculation above follows Doi & Edwards [1986], but is slightly expanded.

A consequence of the result is that our measurements on the dielectric constant gives a measure of the mean square fluctuation of the polarization in the equilibrium liquid, and the shear modulus is a measure of the mean square fluctuation of the shear stress.

2.4.2   Time versus frequency domain

Linear response measurements can be performed by experiments in either the time domain or the frequency domain. All the experiments we have performed are made in the frequency domain. The information obtained in the two situations is equivalent and transformations can be performed to go from one to the other.

The time domain response function $R(t)$ was defined above (see equation 2.4.2) as the output of a Heaviside step input.

In the frequency domain an oscillating input is applied, $h(t) = \text{Re}\left(h_0 e^{i\omega t}\right)$ and the frequency dependent response function $R(\omega)$ is defined by:

$$B(t) = \int_{-\infty}^{t} \mu(t - t')\ \text{Re}\left(h_0 e^{i\omega t'}\right) dt' \tag{2.4.4}$$

$$= \text{Re}\left(h_0 \int_0^\infty \mu(t') e^{i\omega(t-t')} dt'\right) \tag{2.4.5}$$

$$= \text{Re}\left(h_0 e^{i\omega t} \int_0^\infty \mu(t') e^{-i\omega t'} dt'\right) \tag{2.4.6}$$

$$= \text{Re}\left(h(t) R(\omega)\right). \tag{2.4.7}$$

Hence the frequency dependent response function is the Laplace transformed memory function, with $i\omega$ as Laplace Frequency.

Combining the above result with the observation that the memory function is the time derivative of the time response function, leads to the relation between the two response functions

$$R(\omega) = \int_0^\infty \left.\frac{dR(t)}{dt}\right|_{t=t'} e^{-i\omega t'} dt' = i\omega \int_0^\infty R(t') e^{-i\omega t'} dt'. \tag{2.4.8}$$

When working in the frequency domain the input and output is normally taken to be complex valued functions $h = h_0 e^{i\omega t}$ and $B = B_0 e^{i\omega t}$ where h_0 and B_0 are complex numbers describing phase and amplitude. If the actual physical output is needed the real part of B should be used. This "complex formalism" has the advantaged that the frequency domain response function $R(\omega)$ is given directly by

$$R(\omega) = \frac{B_0}{h_0}. \tag{2.4.9}$$

We will in the rest of this thesis use the complex formalism when dealing with frequency domain experiments and response functions.

2.5   Phenomenology of relaxations in glass forming liquids

The following is an overview of how the phenomenology of relaxations in glass forming liquids is usually characterized and of the questions commonly connected to it. The phenomenology of the relaxation process will depend on which specific relaxation is in question, though it is possible to make some general assertions. Dielectric measurements, which are probably the easiest to make, and definitely the type of data which is the most abundant, have played a central role in the determination of these characteristics [Lunkenheimer & Loidl, 2002]. This is, as we mentioned in the introduction, why it is central to understand dielectric relaxation.

2.5.1   Non-Debye

The simplest linear relaxation experiment, at least for a gedanken experiment, is to consider a Heavyside step input, and then to monitor how the output reaches a new equilibrium behavior. The simplest possible output in this experiment is an output that instantaneously reaches its equilibrium behavior. This would be found in the case where the output behavior is independent of the history of the input. Such a behavior is generally not found in viscous liquids, because here the response does depend on the history of the input. When the step input is applied to a liquid it is taken linearly out of equilibrium and will subsequently relax into its new equilibrium state. If a harmonic input is applied the response will correspondingly depend on frequency. The equilibrium behavior will be seen at low frequencies whereas the instantaneous contributions to the relaxation is seen at high frequencies.

The simplest relaxation process are exponential, commonly referred to as Debye relaxation.

The following equations show two examples of such a exponential relaxations (expressed as the time and frequency response functions)

$$
R(t) = \begin{cases} R_0 \left(1 - e^{-t/\tau}\right) & t \geq 0 \\ 0 & t < 0 \end{cases} \qquad R(t) = \begin{cases} R_0 \left(e^{-t/\tau}\right) & t \geq 0 \\ 0 & t < 0 \end{cases}
$$

$$
R(\omega) = R_0 \frac{1}{1 + i\omega\tau} \qquad\qquad R(\omega) = R_0 \frac{i\omega\tau}{1 + i\omega\tau}
\tag{2.5.1}
$$

The left set of equations could for example describe the polarization of a substance when an electric field is applied, while the right set of equations for example could describe the force response to a deformation in a viscoelastic[4] substance (this type of response is illustrated in figure 2.3). The frequency dependent response functions exhibit a peak in the imaginary part called the loss peak, because it corresponds to the maximum loss. Both sides of the loss peak in a Debye relaxation show power law behavior, and the slope (in a log-log plot) is 1 on the low frequency side of the peak and -1 on the high frequency side.

A relaxation of this type is very rarely found in viscous liquids, hence the relaxation is non-Debye. The reason for this is not understood and it is regarded as one of the main questions in the research area of viscous liquid [Angell et al., 2000].

The relaxation spectrum is found to be broader than a Debye relaxation. This is often described as a superposition of Debye processes or sometimes by one of the numerous phenomenological fitting functions which are used in the area.

The most general question, concerning non-Debye relaxation in macroscopic quantities, is whether it is due to an intrinsic non-Debye relaxation or whether it is due to heterogeneous dynamics. The two extreme scenarios are either a homogeneous relaxation or a heterogeneous relaxation. In a homogeneous relaxation all the relaxation entities have relaxations identical to the average relaxation. In a heterogeneous scenario every entity behaves differently, and in this case it is possible that the individual relaxation is Debye. In this case the non-Debye average relaxation stems from the fact that it is an average. [Richert, 2002]

---

[4]A short introduction to viscoelasticity is given in the beginning of the next chapter.
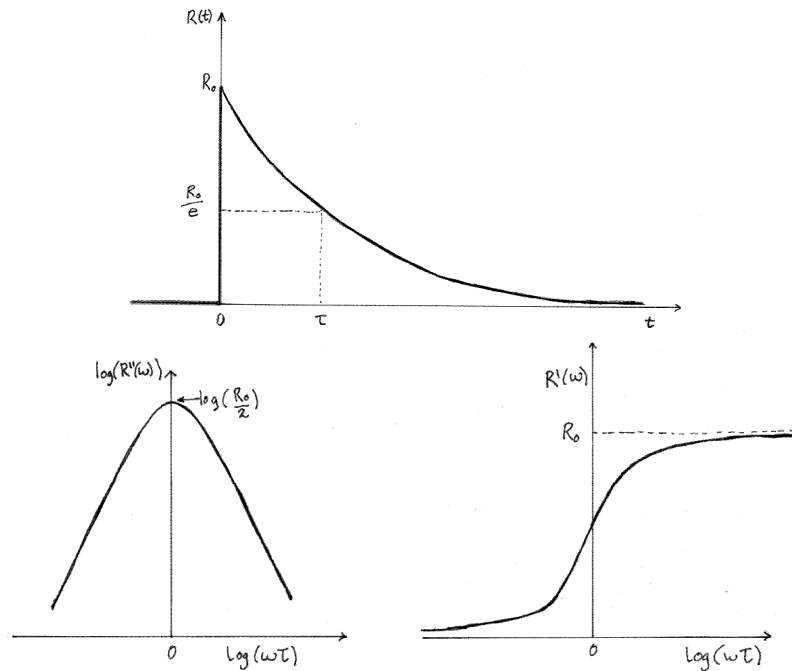
Figure 2.3 An example of relaxation functions that are Debye (corresponding to the right hand equations in equation 2.5.1).

In the last decade there has been extensive studies, using different experimental techniques and simulations, of the heterogeneity of viscous liquids. The most common conclusion is that the liquid is structurally homogeneous but that the dynamics is heterogenous. This means that different parts of the liquid move in different ways at a given time. [Richert, 2002]

2.5.2   Time Temperature Superposition

The relaxation process is non-Debye, and the characteristic time is temperature dependent. The next question is whether the nature of the relaxation process itself is temperature dependent and if so, how this temperature dependence is. The first part of the question can be posed as a question of whether there is time temperature superposition (TTS) or not.

TTS holds if the relaxations at different temperatures can be made to coalesce if the frequency/time is scaled by a characteristic time scale and the relaxation is normalized by its strength. If TTS holds then the response function, in the frequency domain, can be written in the following way

$$R(\omega, T) = R_0(T)R_n(\omega\tau(T)), \tag{2.5.2}$$

where R_n is a temperature independent function, which describes the shape of the relaxation, $\tau(T)$ is a temperature dependent time scale, and $R_0(T)$ is a temperature dependent relaxation strength [Olsen et al., 2001]. It follows from this definition that all characteristic times of the relaxation will be proportional, through temperature independent constants, if TTS holds. This is a convenient result because it relates the easily accessible time scales (eg. the reciprocal loss peak frequency) to other time scales, which might be relevant for models or theory.

If time temperature superposition holds it can be interpreted by saying that the liquid does not "know" the difference between different temperatures; it always behaves in the same way. It is only the speed at which things happen that change.

It is generally agreed that time temperature superposition is not universal, but that it is sometimes obeyed. Whether it is obeyed or not should probably be tied to other properties of the liquid and the nature of the relaxation in question. [Angell et al., 2000],[Olsen et al., 2001]

It was earlier believed that TTS was universal [Olsen et al., 2001], and this notion has been used to construct relaxation curves over a wide time/frequency-range [Ferry, 1961]. This is of course not justified since TTS is not universal, however, TTS is still sometimes assumed due to the lack of better ways to obtain data over a large time/frequency-range (see for example [Ribierre et al., 2003]).

We will later use the term "TTS plot" about plots where the imaginary part of the relaxation function is normalized by the value at the loss peak and is plotted against a frequency that is reduced by the loss peak frequency.

2.5.3   Beta relaxation

The Johari-Goldstein beta relaxation is a secondary relaxation, which is sometimes seen at higher frequencies than the primary relaxation (also known as the alpha relaxation). Its relaxation strength is usually $5 - 20\%$ of the total relaxation, and the beta relaxation time has a much weaker temperature dependence than that of the alpha relaxation [Olsen et al., 2000]. The beta relaxations can be seen in the equilibrium liquid as well as in the glass (see for example Olsen [1998]).

It was originally debated whether the beta relaxation is due to intramolecular relaxation, or it is due to the same kind of relaxation process as the alpha relaxation [Goldstein, 1969], [Johari & Goldstein, 1970]. Today the debate is focused on wether all or just some of the relaxing entities participate in the relaxation. Johari and Goldstein originally proposed a picture of islands of mobility in which some parts of the liquids are more mobile than the rest giving rise to this extra faster relaxation, (see for example Johari [1973] Johari [2002]). Another explanation, which has strong support, is that every relaxation entity makes a small relaxation at a fast time scale corresponding to the beta relaxation (see for example Vogel & Rössler [2001]).

It is debated whether the beta relaxation is fundamental for glass forming liquids – fundamental in the sense that there is always a beta relaxation. The beta relaxation can not always be seen, but it is possible that the temperature where the alpha and beta relaxations merge is below T_g, making it impossible to observe a distinct beta peak in measurements taken above T_g. An example supporting this view is found in Lunkenheimer & Loidl [2002]. Here a shoulder, which could be a hidden beta, is found to appear in the spectrum for a number of liquids when they are cooled and relaxed making the alpha relaxation time very large.

The general introduction that has been given in this chapter is followed by definitions and more details regarding shear and dielectric relaxation in the next chapter.

3 Shear and dielectric relaxation

The first two sections in this chapter give definitions and basic phenomenology of shear and dielectric relaxation, while the final section provides some of the background for comparing the two.

3.1 Shear relaxation

This section gives a very short introduction to viscoelasticity; shear modulus, viscosity and their generalization. The section follows the notation and presentation in Harrison [1976] and Lautrup [1999].

3.1.1 Basic concepts

Elastic substances

The shear modulus, G, is a measure of how difficult it is to make a deformation of a substance.

In the case of a pure shear deformation (that is a shear deformation with constant volume) in an isotropic elastic material, the shear modulus connects the linearized strain tensor u_{ij} with the stress tensor σ_{ij} in the following way (there might be a constant contribution to the stress tensor from pressure, but this is ignored).

$$\sigma_{ij} = 2Gu_{ij} \tag{3.1.1}$$

By turning to a one dimensional case and assuming that the stress and strain are harmonic functions of time, it is seen that:

$$\sigma = 2Gu \tag{3.1.2}$$
$$\tag{3.1.3}$$

where $\sigma = \sigma_0 e^{i\omega t}$ and $u = u_0 e^{i\omega t}$ are the relevant components of the tensors.

Viscous substances

For viscous substances the shear viscosity η plays a similar role to the shear modulus. It connecting the linearized rate of strain tensor $\frac{\mathrm{d}u_{ij}}{\mathrm{d}t}$ with the stress tensor. The connection is given as (in the case of a pure shear strain, and ignoring hydrostatic pressure)

$$\sigma_{ij} = 2\eta \frac{\partial u_{ij}}{\partial t}. \tag{3.1.4}$$

Here the one dimensional harmonic situation with $\sigma = \sigma_0 e^{i\omega t}$ and $u = u_0 e^{i\omega t}$ yields

$$\sigma = 2i\omega\eta u \tag{3.1.5}$$

where it is seen that stress and strain are out of phase.

Viscoelastic substances

All the liquids we are going to investigate, show viscoelastic behavior. By this is meant that they behave as something between a pure elastic substance and a pure viscous substance.

The generalized complex shear modulus G^* is defined as

$$G^* = \frac{1}{2}\frac{\sigma}{u}. \tag{3.1.6}$$

It is seen that for a pure elastic substance $G^* = G$, while $G^* = i\omega\eta$ for a pure viscous liquid.

It is likewise possible to define a generalized viscosity

$$\eta^* = \frac{1}{2}\frac{\sigma}{\frac{\mathrm{d}u}{\mathrm{d}t}} \tag{3.1.7}$$

and it can be seen that $\eta^* = \frac{1}{i\omega}G^*$.

The above definitions are general, and can also be used on system with inertial effect. However, we will always assume that we are in a frequency domain where such effects can be neglected.

3.1.2   Phenomenology

In the viscoelastic case, G^* generally becomes a frequency dependent complex number $G^* = G'(\omega) + iG''(\omega)$.

In the high frequency limit, the substance acts as a pure elastic substance, while it acts like a pure viscous liquid in the low frequency limit:

$$\lim_{\omega\to 0} G^* = 0 + i\omega\eta_0 \tag{3.1.8a}$$

$$\lim_{\omega\to\infty} G^* = G_\infty + 0i \tag{3.1.8b}$$

where η_0 is the equilibrium viscosity, and G_∞ is the instantaneous shear modulus (where ∞ should be understood as a limit where initial effects still can be neglected).

In the rest of this thesis, we will write the complex frequency dependent shear modulus as G, and the complex frequency dependent shear viscosity as η.

The Maxwell model

The simplest model which has a behavior resembling that of a real viscoelastic liquid is the Maxwell model. The model can be described by the electric network model[1] shown on figure 3.1.

The shear modulus of the Maxwell model is

$$G = G_\infty\frac{i\omega\tau_M}{i\omega\tau_M + 1} = G_\infty\frac{(\omega\tau_M)^2}{1 + (\omega\tau_M)^2} + iG_\infty\frac{\omega\tau_M}{1 + (\omega\tau_M)^2} \tag{3.1.9}$$

where $\tau_M = \frac{\eta_0}{G_\infty}$, τ_M is also known as the Maxwell time. It is seen that this model has the limiting behavior described in equation 3.1.8. It is also seen that the Maxwell model
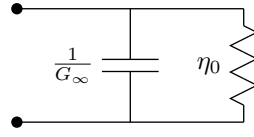
Figure 3.1 Electric diagram representing the Maxwell model. A capacitor with capacitance $1/G_\infty$ in parallel with a resistor with resistance η_0.

is one of the examples of a Debye relaxation presented in equation 2.5.1 (see figure 2.3 for the typical spectrum of the Maxwell model). The Maxwell model is inadequate to describe real shear mechanical data, since Debye relaxation is rarely seen in viscoelastic liquids.

We will sometimes use an extended Maxwell model (see appendix B) to describe data.

3.1.3   The shear compliance

The complex frequency dependent shear compliance is defined as

$$J = \frac{1}{G} = \frac{G'}{G'^2 + G''^2} - i\frac{G''}{G'^2 + G''^2} \tag{3.1.10}$$

The imaginary part of the shear compliance has the low frequency behavior $-1/\omega\eta_0$. A quantity which is related to the compliance is the retardation part of the compliance defined as $J - 1/G_\infty - 1/i\omega\eta_0$. This quantity is sometimes claimed to exhibits a peak in the imaginary part (for example in Schröter & Donth [2002]). However, the fitting function commonly used for shear moduli data (see appendix B), does not imply the existence of such a peak.

3.2   Dielectric relaxation

3.2.1   Basic concept

The dielectric constant[2] ε, or equivalently the dielectric susceptibility χ, is a measure of how polarized a substance gets when subjected to an electric field in the linear regime. The macroscopic polarization is parallel to the electric field in the case of an isotropic liquid, and the dielectric constant is therefore a scalar. The definitions are

$$\boldsymbol{P} = \varepsilon_0\chi\boldsymbol{E_m}, \quad \boldsymbol{D} = \boldsymbol{P} + \varepsilon_0\boldsymbol{E_m} = \varepsilon_0(\chi + 1)\boldsymbol{E_m} = \varepsilon_0\varepsilon\boldsymbol{E_m}, \tag{3.2.1}$$

where $\boldsymbol{P}$ is the polarization per unit volume, $\boldsymbol{E_m}$ is the applied electric field, $\boldsymbol{D}$ is the displacement field, and ε_0 is the vacuum permittivity.

An alternative representation of the liquids dielectric proporteis which is sometimes used is the dielectric modulus

$$\boldsymbol{E_m} = \frac{M}{\varepsilon_0}\boldsymbol{D} \text{ thus, } M = \frac{1}{\varepsilon}. \tag{3.2.2}$$

---

[1]In an electric network model of a rheological system, charge is the two times the strain and voltages the stress. The modulus of the model corresponds the shear modulus, with these definition.

[2]The term constant is a bit misleading, as it is not constant but a function of both temperature and frequency.

In the frequency dependent case we describe the phase difference between the field and the polarization by the standard complex formalism, which has been introduced earlier. We will show some standard examples of frequency dependence in section 3.2.3, but we will first look a bit more into what it is we measure.

The polarization stems from two physical processes: Polarization of the molecules due to a change in the electron distribution and reorientation of the permanent dipoles[3]. We refer to the first process as *induced molecular polarization* or just *induced polarization*, and we call the latter process *the rotational polarization*.

Induced molecular polarization

The induced molecular polarization is a quantity which is related to the single molecule, and it gives information about how tightly bound the electrons are to nuclei. It can be described by a proportionality between the polarization of the molecule and the local field that acts on it. The proportionality will in general be given by a tensor, a the polarization will be favored in some directions, due to the geometry of the molecule. The average induced polarization in an isotropic liquid, which has an uniform distribution of angular directions, will however be parallel to the field. We assume that this is always the case and this allows us to introduce that following notation

$$\boldsymbol{p}_i = \alpha_i \boldsymbol{E}_i \tag{3.2.3}$$

where $\boldsymbol{p}_i$ is the average induced polarization per molecule, α_i is the induced polarization coefficient and $\boldsymbol{E}_i$ is the average local inducing field. The average local field acting on the dipoles in the liquid is in this context assumed to be proportional to, but not in general equal to, the average macroscopic field (see section 3.2.2).

The induced polarization governs the refraction index. The contribution to the dielectric constant from induced polarization can therefore be found if the refraction index is known. We designate this contribution by ε_i, and the relation to the refraction index[4] n is simply $\varepsilon_i = n^2$. What we call ε_i is almost everywhere termed ε_∞, we prefer not to use this notation due to the confusion it can lead to, (see the discussion elsewhere in this report, for example section 4.3).

Rotational polarization

The rotational polarization is controlled by how easy the molecules rotate when an electric field is applied. In a gas the molecules are free to move and the rotational polarization will be given by a Boltzmann distribution. In a liquid the rotation will be limited due to the interaction with the surroundings, and it is possible that it is the macroscopic mechanical properties of the liquid, which control the rotation of the dipoles. It is the possible connection between the shear modulus and the rotational polarization which we seek to study in our work.

A major problem with studying the rotational polarization is that it is difficult to access directly by experiments. The modeled quantity is the average polarization due to the

---

[3]If the substance in question is not totally non-polar.

[4]The induced polarization can also include a contribution from atomic stretching, that is polarization due to changed position of the atoms within the molecule. Such a contribution will not be seen in a refraction experiment, because the inertia of the atoms will inhibit the streching at high frequencies. This means that n^2 really is a lower bound for ε_i. Normally the contribution from atomic stretching is small, that is $\varepsilon_i \approx 1.05n^2$ [Böttcher, 1973].

orientation of the molecules. It is often modeled by a proportionality to an average local directing field, E_d, in which case the rotational polarization coefficient α_r can be defined

$$\langle \boldsymbol{\mu} \rangle = \alpha_r \boldsymbol{E}_d, \tag{3.2.4}$$

where $\boldsymbol{\mu}$ is the permanent dipole moment of a molecule.

The measurable macroscopic susceptibility differs from the rotational polarization coefficient in two aspects, firstly the susceptibility contains the contribution from the induced molecular polarization, secondly the susceptibility relates the polarization to the macroscopic average field rather than to an average local directing field. It is not trivial to determine the relationship between the macroscopic average field and the local directing field. This problem is complicated by the fact that the local directing field is not equal to the local inducing field.

The rotational polarizability is in many cases modeled without taking a stand on which local field should be used. The assumptions about the local field are introduced in the end of the modeling process and can in principle be chosen differently. This approach is applied by Debye [1929], Dimarzio & Bishop [1974] and Christensen & Olsen [1994]. A different approach is to integrate the assumptions about the local field in the fundamental "building" of the model. In section 4.5 we discuss an example from Fatuzzo & Mason [1967] where this method is used. Common to the models mentioned here – the models we study – is that the interaction between the dipole and its surroundings is handled by treating the surroundings as a continuum liquid. The continuum approach is used regarding the dielectric as well as the mechanical properties of the surroundings. An averaged description might not be adequate for capturing the dynamics of the interaction of the field and the dipoles. However, if this is the case then the whole concept of a model, which relates a macroscopic mechanical property to the rotation of dipoles needs to be reinterpreted. Therefore we restrict our discussion of the local fields to average fields.

3.2.2   Relation between macroscopic and microscopic: the local field

It is necessary to chose a local field when comparing measurements on the macroscopic dielectric constant to models of the microscopic rotational polarization coefficient. In this thesis we aim to treat the significance of this choice systematically. The following section supplies the background for understanding the problem, as well as for our treatment of it.

This section is generally restricted to the static situation, except for brief final discussion on how the local fields generalize with regard to a harmonic input field.

The basic equation relating the polarization coefficients to the susceptibility arises by determining the total specific polarization from the macroscopic and microscopic entities, respectively:

$$\boldsymbol{P} = \chi \varepsilon_0 \boldsymbol{E}_m = N \left(\alpha_i \boldsymbol{E}_i + \langle \boldsymbol{\mu} \rangle \right) = N \left(\alpha_i \boldsymbol{E}_i + \alpha_r \boldsymbol{E}_d \right) \tag{3.2.5}$$

where N is the number of dipoles per volume, and other symbols are as defined earlier.

Setting $\boldsymbol{E}_m = \boldsymbol{E}_i = \boldsymbol{E}_d$ is the simplest possible approach. The macroscopic average field is also called the Maxwell field, and the result of using the Maxwell field as local fields is simply obtained by dividing equation 3.2.5 by the field:

$$\chi \varepsilon_0 = N \left(\alpha_i + \alpha_r \right). \tag{3.2.6}$$

The field within each particular molecule, due to the distribution of charge in the molecule itself, is included in the Maxwell field. This leads to the implicit assumption that the molecule acts on itself with a torque, but that is of course is impossible.

Clausius-Mossotti approximation

In most of the studies we refer to later the Clausius-Mossotti approximation is used. To obtain the Clausius-Mossotti approximation it is assumed that the directing local field equals the inducing local field. This single local field is called the Lorentz field and can be found as the field in a spherical *imaginary* vacancy in the liquid. By imaginary is meant that the polarization of the rest of the liquid is calculated as if the dipole was there. This description includes the polarization of the surroundings due to the dipole, and the fact that this polarization give rise to a field acting back on the dipole. Only the field from the dipole itself is excluded in the description.

The Lorentz field is given by

$$E_L = \left(1 + \frac{\chi}{3}\right) E_m = \frac{\varepsilon + 2}{3} E_m. \tag{3.2.7}$$

Setting $E_i = E_d = E_L$ in equation 3.2.5, leads to the Clausius-Mossotti relation[5]:

$$\frac{\chi}{\chi + 3} = \frac{\varepsilon - 1}{\varepsilon + 2} = \frac{N}{3\varepsilon_0}(\alpha_r + \alpha_i) \tag{3.2.8}$$

An alternative route to finding the Lorentz field is to use an Onsager-like argument. Moreover, this method makes it very eaisy to understand the difference between the Lorentz field and the Onsager fields, and we will therefore present it before discussing the Onsager fields. The presentation follows Böttcher [1973].

A dipole in a dielectricum (which in our case is made up of the same type of dipoles) will polarize its surroundings, and this polarization of the surroundings will give rise to an electric field at the position of the original dipole, this field is known as the reaction field of the dipole. The reaction field will itself have contributed to the polarization of the dipole. This recursiveness can easily be handled in equilibrium. The reaction field at the position of a dipole is proportional to the dipole itself, and the average reaction field is proportional to the average polarization. A derivation of the reaction field is shown in appendix A.

The Lorentz field is the field which can be found in a physical spherical cavity in a dielctricum plus the mean reaction field from the dipole which is induced/rotated by the field.

$$E_L = G + R \tag{3.2.9}$$

Where E_L is the Lorentz field, G is the cavity field and R is the average reaction field.

---

[5]Isolating the susceptibility in the Clausius-Mossotti equation yields

$$\chi = \frac{3}{\frac{3\varepsilon_0}{N\alpha} - 1} \quad \text{where} \quad \alpha = \alpha_i + \alpha_r.$$

From this it is seen that χ diverges for $3\varepsilon_0/N\alpha = 1$ and attains negative values for $3\varepsilon_0/N\alpha < 1$, this "problem" is referred to as the Clausius-Mossotti catastrophe. According to Böttcher [1973] there is no problem when $\alpha_r = 0$ because experiments show that the critical value of α_i is not reached. When $\alpha_r > 0$ the problem can be resolved by turning to the Onsager field instead of the Lorentz field [Onsager, 1936].

G can be found by a standard textbook solution of the Laplace equation to be:

$$G = \frac{3\varepsilon}{2\varepsilon + 1} E_m. \tag{3.2.10}$$

The reaction field is the reaction field of the mean molecular polarization in the liquid, the mean polarization has as described a contribution both from rotation of permanent dipoles and from induced polarization. Using the results of appendix A and $E_i = E_d = E_L$ yields

$$R = f(\alpha_i + \alpha_r)E_L = f\alpha E_L = f\alpha(G + R) \tag{3.2.11}$$

f is the reaction field factor, which is the proportionality between a dipole and the reaction field it generates. R can easily be isolated from this equation.

Substituting the hereby obtained expressions for R and G into equation 3.2.9 and rearanging a bit leads to

$$E_L = \frac{1}{1 - f(\alpha_i + \alpha_r)} \frac{3\varepsilon}{2\varepsilon + 1} E_m. \tag{3.2.12}$$

In order to get to the Clausius-Mossotti approximation from this, the expression for the reaction field factor f, should of course be inserted. The radius of the sphere enters in the reaction field factor (see equation A.6) and the final step is to eliminate this radius by use of the Onsager approximation[6]. For the present purpose we find it instructive to keep the Lorentz field in the above formulation.

Onsager fields

Onsagers important contribution was to realize that the reaction field of the permanent dipole does not contribute to the directional polarization. This section is based on Böttcher [1973] and Onsager [1936]. The average rotational polarization of the dipoles is parallel to the macroscopic field and so is the average reaction field due to these. But this reaction field has not contributed to aligning the dipoles, since the reaction field of each specific dipole is parallel to the dipole and therefore it acts with no torque on the dipole. The reaction field from the permanent dipoles does, however, contribute to the induced molecular polarization, hereby leading to a difference between the two local fields.

The first step is to determine the directing field. The directing field has two contributions. The cavity field G and the reaction field due to the molecular polarization, which is induced by the directing field

$$E_d = G + f\alpha_i E_d. \tag{3.2.14}$$

By inserting equation 3.2.10 and isolating E_d the following result is obtained

$$E_d = \frac{1}{1 - f\alpha_i} \frac{3\varepsilon}{2\varepsilon + 1} E_m. \tag{3.2.15}$$

Notice how this resembles the Lorentz field (equation 3.2.12).

---

[6]The Onsager approximation relates the molecular radius to the macroscopic volume of the liquid:

$$\frac{4\pi r^3}{3} = \frac{1}{N}. \tag{3.2.13}$$

To find the local inducing field the average reaction field of the permanent dipole has to be added to the directing field.

$$E_i = R + E_d \tag{3.2.16}$$

This reaction field has to be the reaction field of a permanent dipole with a molecular polarization coefficient. This is because the reaction field of the permanent dipole induces an additional dipole moment in the direction of the permanent dipole, which again has a contribution to the reaction field. This last term was not, and should not be, included in the directing field as it is parallel to the permanent dipole but should of course be included in the inducing field.

The expression for the reaction field of a permanent dipole which can be further polarized is given in equation A.7: In order to get the average reaction field the average permanent dipole moment ($\alpha_r E_d$) is inserted

$$R = \frac{f}{1 - f\alpha_i} \alpha_r E_d. \tag{3.2.17}$$

Inserting this in equation 3.2.16 along with the expression for for the directing field (equation 3.2.15) leads to the Onsager inducing field

$$E_i = \left(1 + \frac{f}{1 - f\alpha_i}\alpha_r\right) \frac{1}{1 - f\alpha_i} \frac{3\varepsilon}{2\varepsilon + 1} E_m. \tag{3.2.18}$$

If $\alpha_r = 0$ this Onsagers inducing field, reduces to the Lorentz local field given in equation 3.2.12. Hence there is no difference between the Onsager field and the Lorentz field for substances with no permanent dipole moment.

In order for the Onsager fields to lead to the Onsager equation the fields are inserted in equation 3.2.5, the reaction field factor is inserted and the Onsager approximation is applied. Finally the Clausius-Mossotti relation is used to introduce ε_i instead of α_i. This use of Clausius-Mossotti is consistent because as we just saw the Lorentz field and the Onsager field agree when there is only induced polarization.

The Onsager equation reads [Onsager, 1936]:

$$\mu^2 = \frac{9k_B T \varepsilon_0}{N} \frac{(\varepsilon - \varepsilon_i)(2\varepsilon + \varepsilon_i)}{\varepsilon(\varepsilon_i + 2)^2} \tag{3.2.19}$$

Lorentz field compared to Onsager field

In a lot of the work done in this area, the Clausius-Mossotti relation is used (we will later return to the question about what local field should be used in connection to the model that we test), that is the Lorentz field is assumed as both the directing and the inducing field.

$$E_d = E_i = E_L = \frac{1}{1 - f(\alpha_i + \alpha_r)} \frac{3\varepsilon}{2\varepsilon + 1} E_m.$$

Comparing this to the Onsager directing field (equation 3.2.15) it is seen that if $\alpha_r \ll \alpha_i$ then there is only a little difference between the Lorentz field and the Onsager directing field.

By using the Lorentz field the reaction field of the permanent dipole is assumed to be part of the direction field. If the permanent dipole moment is small then the mistake maken is also small.

Likewise it is seen that if

$$\frac{f}{1 - f\alpha_i}\alpha_r \ll 1 \text{ and } \alpha_r \ll \alpha_i \tag{3.2.20}$$

then the local inducing field found from the Onsager approach is approximately equal to the Lorentz field. This issue is a little more subtle. The inducing Onsager field is in principle the cavity field plus a reaction field just as the Lorentz field is it. The difference lies in the part of the reaction field which is due to the permanent dipole. In the Onsager direction field it is taken into account that the average permanent dipole is determined by the directing field alone, hence leading to a different reaction field from the permanent dipoles than in the case of the Lorentz field.

The local fields and frequency dependency

As long as we are in a quasistatic regime where the different fields in the dielectricum and whatever cavities, we might imagine, can still be found from solving the Laplace equation, then the Lorentz field is generalized straight forward to the frequency dependent situation. There will be a phase difference between the macroscopic field and the Lorentz field, but this does not lead to any complications.

The generalization to the frequency dependent case is not trivial for the Onsager fields. This is because a crucial point in deriving the Onsager relation is that the reaction field of the permanent dipole does not contribute to the directing field because one particular dipole and its reaction field will be parallel. However, if a harmonic field is applied there will be a phase difference between a dipole and the reaction field it generates, and they will no longer be parallel. Therefore, the reaction field will act on the dipole with a torque.

In the next chapter, where we introduce the Debye model and its generalization we will also discuss the Onsager-like frequency dependent field of Fatuzzo & Mason [1967] (see section 4.5).

3.2.3   Typical frequency dependence

In this section we describe the basic phenomenology of the frequency dependent macroscopic dielectric constant.

At low frequencies the dielectric constant will approach its equilibrium value, ε_e, asymptotically. At higher frequencies the molecules will no longer be able to adjust their orientation to the field and the real part of the dielectric constant approaches a new lower plateau value ε_h. The dielectric constant will never go to one, because there will always be a contribution from the induced molecular polarization, that is $\varepsilon_i = n^2 > 1$ (as noted before, we call the dielectric constant from the induced molecular polarization ε_i, it is commonly called ε_∞). It is however very possible that the plateau value which is reached by dielectric spectroscopy ε_h (at about 1MHz) is greater than ε_i. The difference between ε_h and ε_i is actually a central point in our this work and it will be discussed extensively in chapter 4 and chapter 7.

Between the equilibrium value and the high frequency plateau the dielectric constant exhibits a loss peak because the motion of the dipolar molecules is out of phase with the applied field. This is an example of a relaxation process as we have described it earlier. A typical dielectric relaxation spectrum with one relaxation process is depicted in figure 3.2. Sometimes there is also a Johari-Goldstein beta relaxation (see section 2.5.3) or the spectrum exhibits a high frequency wing. Figure 3.3 gives an illustration of a characteristic dielectric spectrum with a beta relaxation.
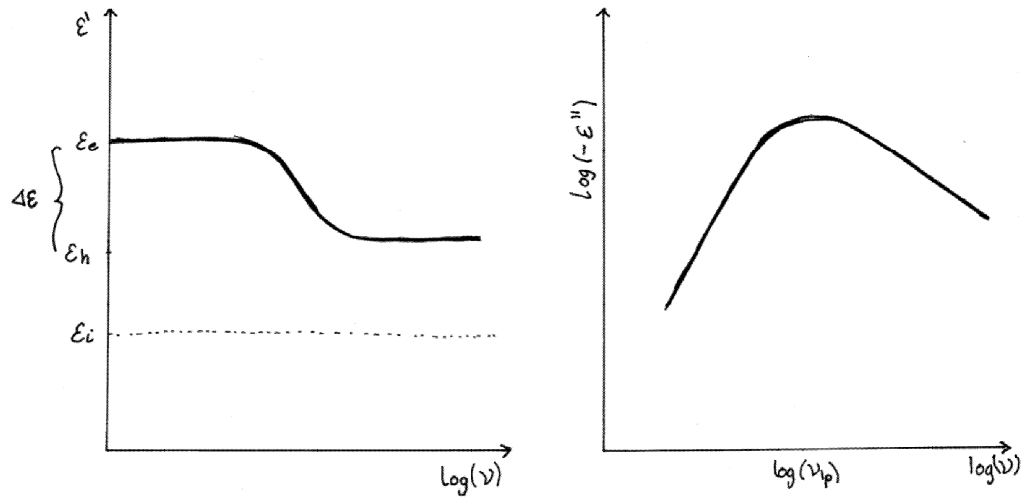

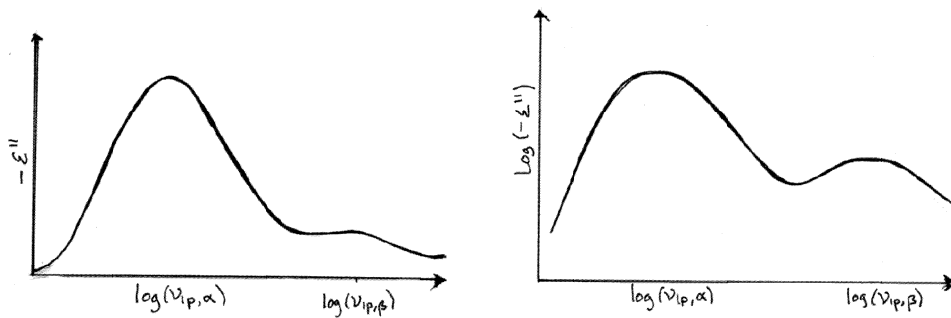**Figure 3.2** Typical real and imaginary part of a dielectric relaxation.

Figure 3.3 Sketch of dielectric loss, including an alpha and a beta relaxation.

3.3   The connection between shear and dielectric relaxation

The hypothesis of a connection between shear behavior and dielectric relaxation goes back to Debye [1929], and this possible connection is still investigated. In this section we give a very brief overview of how the two properties are commonly compared, in order to place our studies of the DiMarzio-Bishop model in a context.

3.3.1   The Debye model

In the Debye model [Debye, 1929] it is assumed that the dipoles are spherical and non-interaction, and that the surroundings of each dipole can be described by the frequency independent viscosity η_0 of a continuum viscous liquid. The rotation of the dipole is controlled by the Stokes friction term for a sphere rotating in a viscous liquid. The classical derivation of the Debye model is postponed until section 4.1, where we return to the Debye model, because it is the basis for the model we are testing.

The Debye model predicts Debye relaxation. This is, as we have already discussed, rarely found. The Debye model is therefore rarely used to describe the dielectric relaxation function. The Debye relaxation time, is however, often used.

3.3.2   The Debye relaxation time

The Debye model predicts a relaxation time and this is frequently studied and used. The Debye relaxation time is closely related to the Stokes-Einstein relation where a connection is made between the Stokes friction term for a sphere dragged trough a viscous liquid and the translational diffusion coefficient

$$D = \frac{k_B T}{6\pi\eta_0 r} \tag{3.3.1}$$

[Einstein, 1905], where r is the radius of the sphere, which is related to some mean radius of the molecule.

The equivalent results of the Debye model is that the microscopic rotational relaxation time (τ) is given as

$$\tau = \frac{8\pi r^3 \eta_0}{2k_B T} \tag{3.3.2}$$

[Debye, 1929]. This relation is know as the Debye-Stokes-Einstein (DSE) relation.

Decoupling

The DSE prediction holds in many ordinary liquids, though the molecular radii, which are used, are smaller than what should be expected from the geometry of the molecule. [Rössler, 1990].

It is known that the translational diffusion decouples from the viscosity at high viscosities for many liquids. The typical finding is that the diffusion is too fast compared to the prediction of the Stokes-Einstein equation [Angell et al., 2000].

A similar decoupling between the rotational relaxation time and the time defined by the Debye-Stokes-Einstein equation could exist. This possibility has been tested a number of times, see for example [Menon et al., 1994], [Deegan et al., 1999], [Chang & Sillescu, 1997], [Suchanski et al., 2000] and [Schröter & Donth, 2000]. The deviation from of the DSE prediction are generally rather small.

The decoupling is usually measured by a decoupling index. It can be defined in various different ways, a version which is sometimes used [Chang & Sillescu, 1997] is

$$R = \frac{\eta_0}{\tau T} \tag{3.3.3}$$

where τ is some measure of the dielectric/rotational time; $\tau = 1/\nu_{dielec,peak}$ is most frequently used.

The general picture is that R (or an equivalent index) varies a factor of 3 to 10 when the relaxation time is changed about 10 decades. [Menon et al., 1994], [Deegan et al., 1999], [Chang & Sillescu, 1997], [Schröter & Donth, 2000]

It is of course also possible to do more direct test of the DSE predictions using microscopic methods. This is for example done in Rössler [1990], where NMR data is used for the rotational relaxation time. In the studied liquid it is found that two regimes exist; a high temperature region where DSE might hold, and a low temperature region where the diffusion mechanisms appear to be different. A comparison between rotational dynamics and the shear modulus where probe molecules are used is found in Yang & Richert [2002]. It is found that the time dependencies of the two relaxations is similar if the size of the probe molecules is of the same order of magnitude as the size of the molecules of the host liquid. If the probe molecules are significantly bigger the rotational relaxation becomes slower and more exponential.

3.3.3   Direct comparison of the relaxations

The shape of the dielectric and shear mechanical relaxations functions and their peak positions have also been compared directly in several papers Menon et al. [1994], Deegan et al. [1999], Christensen & Olsen [1994], Suchanski et al. [2000] Ribierre et al. [2003], Richert et al. [2003], and Schröter & Donth [2000]. We will return to the subject in chapter 8 where we discuss qualitative predictions from the DiMarzio-Bishop model which we have studied in this work.

It is sometimes discussed whether a modulus or susceptibility formulation is more appropriate when the shear and dielectric relaxation are compared. The dielectric constant and the shear modulus is most commonly used, but also the dielectric modulus and the retardation part of the mechanical compliance are used.

3.3.4   A simple connection of the relaxation times

It is a general assumption that the relaxation time in the dielectric and mechanical measurements are related (A commonly used substitute for the mean time is the time defined by the maximum in the loss). The assertion is justified by connecting the two relaxation times via the Maxwell and the Debye model (see for example Deegan et al. [1999]).

If the dielectric relaxation time (τ_{dielec}) is determined by the DSE equation and the mechanical relaxation time is taken as the Maxwell time (τ_M), then solving for the viscosity yields

$$\eta_0 \quad \propto \quad \frac{T}{r^3}\tau_{dielec} \ \text{ and} \tag{3.3.4}$$

$$\eta_0 \quad = \quad G_\infty \tau_M \tag{3.3.5}$$

Combining this yields

$$\frac{\tau_{dielec}}{\tau_M} \propto \frac{G_\infty}{T}r^3 \tag{3.3.6}$$

The shear mechanical time is normally taken to be the time of the maximum loss. This is proportional to τ_M if TTS is obeyed (see section 2.5.2 for a discussion of TTS). G_∞/T, and thereby $\frac{\tau_{dielec}}{\tau_M}$, is much less temperature dependent than the time scales.

3.3.5   Models

The above described connections between shear and dielectric spectrums are rather phenomenological, because they are based on simple models which are known to not hold. More elaborated models connecting the two relaxations also exist. These models usually seek to understand the dielectric spectrum, specifically the rotational polarization via the mechanical properties of the liquid.

A few models are based on the original microscopic Debye model, but attempts to handle the local field in a more consistent way than just using the Clausius-Mossotti approximation. A static Onsager field is used in Cole [1938], and a generalized Onsager field is used in Fatuzzo & Mason [1967].

The generalized Debye model of Dimarzio & Bishop [1974], which we have studied and which is thoroughly presented and analyzed in the next chapter (and the rest of this thesis) attempts to give a more precise description of the interaction of the molecule with the environment by including the viscoelasticity of the liquid. To our knowledge two other models exist, where this is attempted.

The first model which took viscoelasticity into account was the model of Gemant [1935]. The main difference between the model of Gemant and the DiMarzio-Bishop model is that the latter is restricted to a specific viscoelastic behavior. Moreover Gemant does not provide a theoretical derivation of the model, but states it on the basis of physical arguments. Contrary to the result in Havriliak & Havriliak [1995] we are able to reproduce the spectra presented in Gemant [1935] by using the parameters given in the article.

The second model is that of Havriliak [1990] where a (frequency dependent) mechanical contribution is included in the energy connected with aligning a molecule in an applied field. A small review and discussion of the models which explicitly include the viscoelasticity is presented in Havriliak & Havriliak [1995]. It is found in this review that similar results are obtained from the model of Dimarzio & Bishop [1974] and Havriliak [1990].

4 The Debye model and the DiMarzio-Bishop model

In this chapter we will present the DiMarzio-Bishop model which is a generalization of the classical Debye model. The chapter starts with a derivation of the microscopic classical Debye model followed by the generalization suggested in Dimarzio & Bishop [1974]. We propose a new macroscopic formulation hereby avoiding two different unphysical assumptions which have been used in earlier macroscopic formulations by Dimarzio & Bishop [1974] and Christensen & Olsen [1994] respectively.

A review of results and methods presented in papers in which the DiMarzio-Bishop model is explicitly tested is included, and it is briefly discussed why further testing is needed. Furthermore we discuss how the local field problem can be partly disentangled from the microscopic DiMarzio-Bishop model.

Finally we account for the background of the experimental tests of the DiMarzio-Bishop model which is reported in the following chapters.

4.1 The Debye model

The background material for the following presentation has mainly been Debye [1929] and Dimarzio & Bishop [1974].

4.1.1 Fundamental assumptions

Debye's model is derived by treating the molecules as noninteracting ideal dipoles. This means that the dipoles in the liquid are assumed to be randomly orientated in an equilibrium situation with no external field.

The dipoles themselves are modeled as spheres with radius r and an ideal dipole, with dipole moment μ, at the center. The dipole's interaction with its surroundings is modeled as if it was a macroscopic entity in a continuous liquid.

The liquid is assumed to have a frequency independent viscosity (η_0), and the molecule is viewed as a sphere rotating in this medium with a friction coefficient according to Stokes law and a no slip boundary condition. The use of Stokes law means that the inertia of the continuous liquid is neglected, and the inertia of the molecule itself is likewise neglected. The neglection of inertia means that the model is not valid in the high frequency area, where the inertia of the molecules inhibits their rotation.

The local directing electric field (E_d) (see section 3.2.1 for a definition) is assumed to be a given homogeneous field. The model is in this aspect, as in all other aspects, an average description. This means that the model gives α_r as an average property, and not as something which can be assigned to a single molecule.

4.1.2 The governing equation

A coordinate system is chosen such that the field is in the ($\hat{z}$) direction.

The dipoles are described by a probability density function, f. f is a function of the angle θ between the $\hat{z}$ direction and the direction of the dipol, and of time. f describes the probability of finding a dipole with angle θ to $\hat{z}$, at a given time.

The dynamics of f is described by a continuity equation, and an equation describing the current of probability J. The continuity equation is:

$$\frac{\partial f}{\partial t} + \nabla \cdot J = 0. \tag{4.1.1}$$

The current is controlled by an equation which includes a diffusive term and a convection term. The first term is governed by the probability density gradient and the latter is originates from the average angular velocity (V) due to the external torque:

$$J = -D_0 \nabla f + V f. \tag{4.1.2}$$

D_0 is the diffusion constant.

The relevant coordinate system is spherical and everything becomes independent of the azimuthal angle φ due to the rotational symmetry in the system. Hence the relevant component of the angular velocity is $\dot{\theta}$. The angular velocity describes the velocity of the spheres (with moment of inertia I) rotating in the viscous media, the equation of motion is:

$$I\ddot{\theta} = -\zeta_0 \dot{\theta} + M \tag{4.1.3}$$

where M is the torque due to the external field, and ζ_0 is a friction coefficient describing the viscous forces. In the Debye model, which aims to describe the very viscous limit, the inertial term is, as mentioned already, neglected and the equation simplifies to

$$\dot{\theta} = \frac{M}{\zeta_0}. \tag{4.1.4}$$

By rewriting equation 4.1.1 in spherical coordinates, inserting equation 4.1.2, equation 4.1.4 and using the fact that everything is φ independent, the following equation is obtained

$$\frac{\partial f}{\partial t} = \frac{1}{\sin \theta} \frac{\partial}{\partial \theta} \left[\sin \theta \left(D_0 \frac{\partial f}{\partial \theta} - \frac{M}{\zeta_0} f \right) \right]. \tag{4.1.5}$$

This is the differential equation of the Debye model, and it describes rotational diffusion.

The friction term is, as mentioned earlier, taken to be the Stokes-friction term

$$\zeta_0 = 8\pi \eta_0 r^3, \tag{4.1.6}$$

and the torque can be written as

$$M = -\mu E_d \sin \theta. \tag{4.1.7}$$

4.1.3 The diffusion coefficient

Given a constant local field the equilibrium behavior of f is described by a Boltzmann distribution

$$f \propto e^{\frac{-U}{k_B T}} \tag{4.1.8}$$

U being the potential energy of a dipole in the local field. U is given by

$$U = -\mu E_d \cos \theta \tag{4.1.9}$$

that is

$$f = k e^{\frac{\mu E_d \cos \theta}{k_B T}} \tag{4.1.10}$$

where k is a constant.

Using equation 4.1.6, 4.1.7, 4.1.10 and the fact that in equilibrium $\frac{\partial f}{\partial t} = 0$ for all θ, equation 4.1.5 gives

$$
\begin{aligned}
0 &= \frac{1}{\sin \theta} \frac{\partial}{\partial \theta} \left[\sin \theta \left(D_0 k e^{\frac{\mu E_d \cos \theta}{k_B T}} \frac{-\mu E_d \sin \theta}{k_B T} + \frac{\mu E_d \sin \theta}{\zeta_0} k e^{\frac{\mu E_d \cos \theta}{k_B T}} \right) \right] & \text{(4.1.11a)} \\
&= \frac{1}{\sin \theta} \frac{\partial}{\partial \theta} \left[(\sin \theta)^2 \mu E_d k e^{\frac{\mu E_d \cos \theta}{k_B T}} \left(-\frac{D_0}{k_B T} + \frac{1}{\zeta_0} \right) \right] & \text{(4.1.11b)} \\
&\Downarrow \\
D_0 &= \frac{k_B T}{\zeta_0} & \text{(4.1.11c)}
\end{aligned}
$$

Equation 4.1.11c follows from equation 4.1.11b because the latter has to be true for all θ. Hence it is seen that the diffusion constant and the friction term are not independent but are really just two measures of the same characteristics.

4.1.4 1. order solution

Debye solves equation 4.1.5 to first order by assuming that the local field is a harmonic function of time

$$E_d = E_{d,0} e^{i\omega t} \tag{4.1.12}$$

this means that the torque is given as $M = -\mu E_{d,0} e^{i\omega t} \sin \theta$.

A first order solution of the following form

$$f = A \left(1 + B \frac{\mu E_{d,0}}{k_B T} \cos(\theta) e^{i\omega t} \right) \tag{4.1.13}$$

is used. A and B are constants. The solution is first order in $\mu E_{d,0}$, and has the angular dependence $\cos(\theta)$ which is the angular dependence that is known to hold in the low frequency limit (equation 4.1.10).

By inserting the first order solution (equation 4.1.13) into the differential equation (equation 4.1.5) and disregarding second order terms in $\mu E_{d,0}$, B can be determined

$$B = \frac{1}{1 + \frac{i\omega \zeta_0}{2k_B T}}. \tag{4.1.14}$$

A can be found by the condition that when $E_{d,0} = 0$, f is an uniform distribution, that is

$$A = \frac{1}{4\pi} \tag{4.1.15}$$

The only angular dependence of f (equation 4.1.13) is the $\cos\theta$ term and this ensures that f is normalized at all times, because integration of the $\cos\theta$ term over the spherical surface gives zero.

Combining all this yields:

$$f = \frac{1}{4\pi}\left(1 + \frac{1}{1 + \frac{i\omega\zeta_0}{2k_BT}}\frac{\mu E_{d,0}}{k_BT}\cos(\theta)e^{i\omega t}\right), \tag{4.1.16}$$

from which the average polarization is found:

$$\langle\mu_z\rangle = \langle\mu\cos\theta\rangle \tag{4.1.17}$$

$$= \int_0^{2\pi}\int_0^{\pi}\mu f\cos\theta\sin\theta d\theta\,d\varphi \tag{4.1.18}$$

$$= \frac{\mu^2 E_{0,d}e^{i\omega t}}{3k_BT(1 + \frac{i\omega\zeta_0}{2k_BT})} \tag{4.1.19}$$

using equation 4.1.6 and writing the result in terms of the rotational polarizability coefficient (defined in equation 3.2.4) finally leads to

$$\alpha_r = \frac{\mu^2}{3k_BT\left(1 + \left(\frac{4\pi r^3}{k_BT}\right)i\omega\eta_0\right)}. \tag{4.1.20}$$

There are two uncorrelated parameters in the model, μ and r.

4.2   The DiMarzio-Bishop model

In following we present the microscopic DiMarzio-Bishop model and it will be clear that the derivation is very similar to derivation if the original Debye model.

In the original model the viscosity is assumed to be independent of frequency. The consequence of the generalization by Dimarzio & Bishop [1974] is, as earlier mentioned, that the viscosity is allowed to be time dependent (or equivalent frequency dependent). All other assumptions from the original Debye model are maintained (see section 4.1.1).

The idea of the generalization is that the two controlling terms in the description of the current of probability (equation 4.1.2) are allowed to depend on the past. The diffusion term now depends on the history of the distribution, and the convection term depends on the history of the external field.

The model is restricted to linear viscoelastic liquids (see section 2.4), and the governing equation is the most general linear analog to equation 4.1.5

$$\frac{\partial f}{\partial t} = \frac{1}{\sin\theta}\frac{\partial}{\partial\theta}\left[\sin\theta\left(\int_{-\infty}^t D(t-t')\left.\frac{\partial f}{\partial\theta}\right|_{t=t'}dt' - f\int_{-\infty}^t V(t-t')M(t')dt'\right)\right] \tag{4.2.1}$$

where V is the mobility memory function and D is the diffusion memory function.

In this case the equilibrium arguments (section 4.1.3) result in the following equation connecting the diffusion memory function to the mobility memory function

$$\int_{-\infty}^{t} D(t-t')dt' = k_B T \int_{-\infty}^{t} V(t-t')dt' \qquad (4.2.2)$$

which implies that

$$D(t') = k_B T V(t') \qquad (4.2.3)$$

By inserting the expression for the torque (equation 4.1.7) and assuming that the input is of the form given in equation 4.1.12 plus a solution of the form given in equation 4.1.13, the generalized rotational differential equation (equation 4.2.1) can be rewritten in the following way

$$\frac{\partial f}{\partial t} = \frac{1}{\sin\theta}\frac{\partial}{\partial\theta}\left[\sin\theta\left(\frac{\partial}{\partial\theta}\int_{-\infty}^{t} k_B T V(t-t')A\left(1+B\frac{\mu E_{d,0}}{k_B T}\cos(\theta)e^{i\omega t'}\right)dt' - \right.\right.$$
$$\left.\left. f\int_{-\infty}^{t} V(t-t')(-\mu E_{d,0}e^{i\omega t'}\sin\theta)dt'\right)\right]. \quad (4.2.4)$$

Using the definition of the complex response functions in the frequency domain (and the fact that the complex mobility coefficient $V(\omega)$ is given as $V(\omega) = 1/\zeta(\omega)$, $\zeta(\omega)$ being the complex friction coefficient), this reduces to

$$\frac{\partial f}{\partial t} = \frac{1}{\sin\theta}\frac{\partial}{\partial\theta}\left[\sin\theta\left(-k_B T B\frac{\mu E_{d,0}}{k_B T}\sin(\theta)1/\zeta(\omega)e^{i\omega t} - \right.\right.$$
$$\left.\left. f(-\mu E_{d,0}\sin\theta)1/\zeta(\omega)e^{i\omega t}\right)\right] \quad (4.2.5)$$

which can be rewritten in terms of f and M

$$\frac{\partial f}{\partial t} = \frac{1}{\sin\theta}\frac{\partial}{\partial\theta}\left[\sin\theta\left(\frac{k_B T}{\zeta(\omega)}\frac{\partial f}{\partial\theta} - \frac{M}{\zeta(\omega)}f\right)\right]. \qquad (4.2.6)$$

The above equation is based on the assumption of a harmonic input and a solution of the form given in equation 4.1.13, hence it is not as general as 4.2.1. It is however a very convenient formulation, since it resemble the original Debye differential equation. The calculations which gives the constants in the solution and finally the rotational polarization coefficient are therefore completely equivalent to the calculations performed when deriving the original Debye model.

The result of the DiMarzio-Bishop generalization is that the viscosity in Debye's model is replaced by the frequency dependent viscosity:

$$\alpha_r(\omega) = \frac{\mu^2}{3k_B T\left(1+\left(\frac{4\pi r^3}{k_B T}\right)i\omega\eta(\omega)\right)} = \frac{\mu^2}{3k_B T\left(1+\left(\frac{4\pi r^3}{k_B T}\right)G(\omega)\right)} \qquad (4.2.7)$$

where the second equality is obtained by using the relation $G(\omega) = i\omega\eta(\omega)$.

The model has μ and r as two uncorrelated parameters, just as the original Debye model did.

4.3   Earlier macroscopic formulations, using the Clausius-Mossotti approximation

It is, as explained in chapter 3.2.2, a general problem when testing theories and models on the rotational polarization that it can not be measured directly, since the model of the rotational polarization has to be related to the macroscopic susceptibility or dielectric constant.

With one exception, which we will return to, all the earlier studies of the DiMarzio-Bishop model have been performed using the Clausius-Mossotti approximation.

4.3.1   Dimarzio & Bishop [1974]

Inserting the microscopic DiMarzio-Bishop model (equation 4.2.7) in the Clausius-Mossotti relation (equation 3.2.8) leads to

$$\frac{\varepsilon(\omega) - 1}{\varepsilon(\omega) + 2} = \frac{N}{3\varepsilon_0} \left(\alpha_i + \alpha_r(\omega) \right) = \frac{N}{3\varepsilon_0} \left[\alpha_i + \frac{\mu^2}{3k_B T \left(1 + \left(\frac{4\pi r^3}{k_B T} \right) G(\omega) \right)} \right]. \qquad (4.3.1)$$

This is how the macroscopic version of the model is first presented by Dimarzio and Bishop. In this formulation the model contains the microscopic DiMarzio-Bishop model and the Clausius-Mossotti relation, but no further assumptions.

The DiMarzio-Bishop model has three microscopic parameters μ, α_i and r. The dipole density N can trivially be lumped in with the microscopic parameter, making $N\mu^2$, $N\alpha_i$ and r the parameters.

In Dimarzio & Bishop [1974] two limiting equations are used, the high and the low frequency limit, to solve for two of the parameters leaving r as the only parameter to be fitted. If the limits are not determined with greater precision than the values at other frequencies, or if they are not reached by the measurements at all it is possible to handle them as new macroscopic fitting parameters.

The equation which is compared to data in Dimarzio & Bishop [1974] and the equation which is always cited (eg. in [Christensen & Olsen, 1994], [Díaz-Calleja et al., 1993], [Zorn et al., 1997], [Ferri & Castellani, 2001], and [Havriliak & Havriliak, 1995]) is a simplified version of the DiMarzio-Bishop model, in which an assumption of the limiting behavior of the shear modulus is introduced. The resulting equation is the classical Debye formula with the exception that η_0 is replaced by the frequency dependent viscosity $\eta(\omega)$,

$$\frac{\varepsilon(\omega) - \varepsilon_\infty}{\varepsilon_e - \varepsilon_\infty} = \frac{1}{\left(1 + \left(\frac{4\pi r^3}{k_B T} \right) \left(\frac{\varepsilon_e + 2}{\varepsilon_\infty + 2} \right) i\omega\eta(\omega) \right)} \qquad (4.3.2)$$

$$= \frac{1}{\left(1 + \left(\frac{4\pi r^3}{k_B T} \right) \left(\frac{\varepsilon_e + 2}{\varepsilon_\infty + 2} \right) G(\omega) \right)}. \qquad (4.3.3)$$

From the derivation of this equation in Dimarzio & Bishop [1974], it is seen that they by ε_∞ mean the quantity we refer to as ε_h.

DiMarzio and Bishop's derivation of this macroscopic formulation is the same as that of Debye. Debye, who models systems with a frequency independent viscosity η_0 makes

use of the fact that $i\omega\eta_0$ goes to respectively infinity and zero as ω does so. In order to generalize the derivation DiMarzio and Bishop make the assumption that this limiting behavior holds for the frequency dependent viscosity as well.

However, the assumption that $i\omega\eta(\omega) = G(\omega)$ goes to infinity as ω does so will in general be untrue because G is a limited function of frequency. Consequently an assumption is used which is in disagreement with the phenomenology the model tries to explain. The result of this assumption is that the macroscopic equation (4.3.3) cannot hold in the high frequency limit. In this limit the left hand side will approach zero whereas the right hand side will approach a positive finite value. This incorrect limiting behavior of equation 4.3.3 is pointed out by Christensen & Olsen [1994].

Another way of putting the same discrepancy is that it is an implicit assumption in the derivation by DiMarzio and Bishop of equation 4.3.3 that the induced molecular dielectric constant can be found as the high frequency plateau value measured by dielectric spectroscopy, that is they assume $\varepsilon_h = \varepsilon_i$. (See section 3.2.3 for the relation between ε_h and ε_i).

4.3.2 Christensen & Olsen [1994]

In a paper by Christensen & Olsen [1994] the model is re-proposed in a different formulation than that of Dimarzio & Bishop [1974].

The microscopic starting point of Christensen & Olsen [1994] is equation 4.2.7, it is the assumptions used when formulating the macroscopic model which differ. The difference lies in the fact that the macroscopic model is formulated in terms of the dielectric modulus, G_e, which they define as the inverse of the dielectric susceptibility[1]:

$$G_e(\omega) = \frac{1}{\chi(\omega)} = \frac{1}{\varepsilon(\omega) - 1}. \tag{4.3.4}$$

Solving for G_e in the Clausius-Mossotti equation and inserting the microscopic DiMarzio-Bishop model leads to

$$G_e(\omega) = \frac{\varepsilon_0}{N\alpha(\omega)} - \frac{1}{3} = \frac{\varepsilon_0}{N(\alpha_i + \alpha_r(\omega))} - \frac{1}{3} \tag{4.3.5}$$

$$= \frac{\varepsilon_0}{N\left(\alpha_i + \frac{\mu^2}{3k_BT\left(1 + \left(\frac{4\pi r^3}{k_BT}\right)G(\omega)\right)}\right)} - \frac{1}{3}. \tag{4.3.6}$$

Christensen and Olsen ignore the induced molecular polarization simplifying equation 4.3.6 to

$$G_e(\omega) = \frac{\varepsilon_0}{N\left(\frac{\mu^2}{3k_BT\left(1 + \left(\frac{4\pi r^3}{k_BT}\right)G(\omega)\right)}\right)} - \frac{1}{3} \tag{4.3.7}$$

$$= \left(3\frac{\varepsilon_0 k_BT}{N\mu^2} - \frac{1}{3}\right) + \left(12\frac{\varepsilon_0 \pi r^3}{N\mu^2}\right)G(\omega) \tag{4.3.8}$$

The neglection of the induced molecular polarization is very unphysical, because the squared refraction index $n^2 = \varepsilon_i$ generally is of the same order of magnitude as the high

---

[1]Note that $G_e(\omega)$ differes from the commonly used modulus, $M = \varepsilon^{-1}$.

frequency plateau value of the dielectric constant. This will be seen in our data present-ation in chapter 6 and in chapter 7, where the high frequency behavior is specifically discussed.

The simplified model in equation 4.3.8 connects the shear modulus to the dielectric mo-dulus through two parameters. This is one parameter less than the original DiMarzio-Bishop model, but the background for this difference is of course just that one parameter has been ignored.

The two moduli are normalized by their high an low frequency values (we here use C's as a shorthand notation for the two terms in the parentheses in equation 4.3.8)

$$G_{e,n}(\omega) = \frac{G_e(\omega) - G_{e,e}}{G_{e,h} - G_{e,e}} = \frac{C_1 + C_2 G(\omega) - (C_1 + C_2 G_0)}{C_1 + C_2 G_\infty - (C_1 + C_2 G_0)} \tag{4.3.9}$$

$$= \frac{G(\omega) - G_0}{G_\infty - G_0} = G_n(\omega). \tag{4.3.10}$$

[Christensen & Olsen, 1994]. The second subscript on G_e refers to equilibrium (e), high frequency plateau (h) and normalized (n).

This is how the model is finally presented and how it is compared to data by Christensen & Olsen [1994]. We shall return to their results in section 4.6.

4.4 A new macroscopic formulations, using the Clausius-Mossotti approximation

It is of course unsatisfactory to use unphysical assumptions about the high frequency plateau value of the dielectric data. It is therefor our objective to give a consistent treat-ment of the macroscopic model where unphysical assumptions are avoided. We will include both the induced polarization and the rotational contribution to ε_h contrary to the two earlier treatments which, as we have described in the preceding sections, ex-clude one of these, respectively.

In the following we will derive our result which looks the same as the original for-mulation by DiMarzio and Bishop (equation 4.3.3), but which has a different physical meaning.

Through the Clausius-Mossotti approximation the induced polarizability can be related to the induced molecular dielectric constant;

$$\frac{\varepsilon_i - 1}{\varepsilon_i + 2} = \frac{N}{3\varepsilon_0} \alpha_i \tag{4.4.1}$$

It is important to stress that equation 4.4.1 is *not* a high frequency limit of equation 4.3.1, because the second term in 4.3.1 does not go to zero as ω goes to infinity, as we have pointed out earlier. Equation 4.4.1 does hold at even higher frequencies where equation 4.3.1 becomes invalid because inertia starts effecting the rotation of the molecules. This means that ε_i can not be equated to the plateau value ε_h, which $\varepsilon(\omega)$ attains at the high frequency end of the dielectric spectroscopy spectrum.

In the zero frequency limit equation 4.3.1 reduces to

$$\frac{\varepsilon_e - 1}{\varepsilon_e + 2} = \frac{N}{3\varepsilon_0} \left[\alpha_i + \frac{\mu^2}{3k_B T} \right] \tag{4.4.2}$$

where $G(0) = 0$ has been used.

Using this and equation 4.4.1 gives

$$\frac{\varepsilon_e - 1}{\varepsilon_e + 2} - \frac{\varepsilon_i - 1}{\varepsilon_i + 2} = \frac{N}{3\varepsilon_0} \frac{\mu^2}{3k_B T}. \tag{4.4.3}$$

Inserting these results in the macroscopic DiMarzio-Bishop model (equation 4.3.1) yields

$$\frac{\varepsilon(\omega) - 1}{\varepsilon(\omega) + 2} = \frac{\varepsilon_i - 1}{\varepsilon_i + 2} + \left[\frac{\varepsilon_e - 1}{\varepsilon_e + 2} - \frac{\varepsilon_i - 1}{\varepsilon_i + 2} \right] \frac{1}{1 + \frac{4\pi r^3}{k_B T} G(\omega)}. \tag{4.4.4}$$

Finally some algebraic manipulation leads to:

$$\frac{\varepsilon(\omega) - \varepsilon_i}{\varepsilon_e - \varepsilon_i} = \frac{1}{\left(1 + \left(\frac{4\pi r^3}{k_B T} \right) \left(\frac{\varepsilon_e + 2}{\varepsilon_i + 2} \right) G(\omega) \right)}. \tag{4.4.5}$$

In deriving this equation we have used information about the zero frequency limit behavior (equation 4.4.2). It is valid to use this limit because the zero frequency behavior is the equilibrium situation for which data can be very well determined, and where the model reduces to a simple general Boltzmann distribution of the orientation of the molecules. ε_e can alternatively be regarded as a new macroscopic fitting parameter replacing the microscopic μ. By use of equation 4.4.1 the parameter α_i has been translated into a macroscopic physical quantity ε_i. By using the two macroscopic parameters ε_e and ε_i as fitting parameters rather than α_i and μ the dipole density N is lumped into the fitting parameters.

The last parameter r should of course be related to the size of the relaxing molecules. However, the agreement is not expected to be very precise, since the description of the molecules as spheres in most cases is very coarse. Further complications arise in the case of polymers because the relaxing entity will be a side chain instead of the entire molecule.

If the high frequency plateau values G_∞ and ε_h are known these can be used to determine the lumped parameter $K = \left(\frac{4\pi r^3}{k_B T} \right) \left(\frac{\varepsilon_e + 2}{\varepsilon_i + 2} \right)$, and r can of course be easily isolated herefrom.

If the high frequency plateau values are inserted in equation 4.4.5

$$\frac{\varepsilon_h - \varepsilon_i}{\varepsilon_e - \varepsilon_i} = \frac{1}{(1 + K G_\infty)}. \tag{4.4.6}$$

it is easily recognized that K controls how large the elastic contribution $(\varepsilon_h - \varepsilon_i)$ is compared to the whole rotational contribution $(\varepsilon_e - \varepsilon_i)$. Furthermore it is seen that a large K value (corresponding to a large r) will result in a small elastic contribution.

For a number of reasons, which hopefully will become clear we have chosen to test the model in the modulus formulation. In order to do so, we have isolated the shear modulus in equation 4.4.5

$$G(\omega) = \left(\frac{k_B T}{4\pi r^3} \right) \left(\frac{\varepsilon_i + 2}{\varepsilon_e + 2} \right) \left(\frac{\varepsilon_e - \varepsilon_i}{\varepsilon(\omega) - \varepsilon_i} - 1 \right). \tag{4.4.7}$$

This modulus formulation reveals no direct connection between the shear modulus and the dielectric modulus. The shear modulus is however related to the quantity $1/(\varepsilon(\omega) - \varepsilon_i)$, which is a modulus like quantity, though it only includes the rotational contribution.

4.5 The macroscopic DiMarzio-Bishop model with the Fatuzzo-Mason field

All the macroscopic versions of the DiMarzio-Bishop model described so far are based on the Clausius-Mossotti approximation for the local field, even though it is known that this does not hold.

In Fatuzzo & Mason [1967] a Debye (rotational diffusion) model with a more complicated field is presented. The field used in the model is derived by a generalization of the static Onsager approach, to the harmonic case. In Fatuzzo & Mason [1967] a frequency independent viscosity is used, but Díaz-Calleja et al. [1993] have combined the results with the DiMarzio-Bishop model by introducing a frequency dependent viscosity.

4.5.1 Essentials of the Fatuzzo-Mason model

In the static derivation of the Onsager approximation, it is a basic assumption that the part of the reaction field, which is due to the permanent dipole, always points in the direction of the dipole itself. This means that this part of the reaction field cannot give a torque on the dipole, and it is therefore left out of the directing field.

The problem is that in an oscillating field the reaction field will be out of phase with the movement of the dipole, and due to this it will give rise to a torque. In Fatuzzo & Mason [1967] this "lag of the reaction field" is modeled by introducing what they refer to as the "librating dipole method".

The basic equation in the Fatuzzo-Mason model is the Debye rotational diffusion differential equation (equation 4.1.5)

$$\frac{\partial f}{\partial t} = \frac{1}{\sin\theta}\frac{\partial}{\partial\theta}\left[\sin\theta\left(D_0\frac{\partial f}{\partial\theta} - \frac{M}{\zeta_0}f\right)\right].$$

In the original macroscopic Debye calculation the torque is taken to be

$$M = -\mu E_L\sin\theta = -\mu k E_m\sin\theta$$

where E_L is the Lorentz field, E_m the average macroscopic field and k is a proportionality constant (see equation 3.2.12). The contribution of Fatuzzo-Mason is to give an alternative calculation of this torque. The torque is still proportional to the macroscopic field but the dipole μ appears in a more complicated way.

It is assumed that the dipole is librating around an equilibrium position. It is further assumed that the libration of each molecule is small.

The permanent dipole is described by the following equation

$$\boldsymbol{\mu}_0 = \mu_e\boldsymbol{i} + \mu_1\boldsymbol{n}e^{i\omega t}$$

where $\boldsymbol{i}$ is a unit vector in the equilibrium direction, $\boldsymbol{n}$ is a unit vector perpendicular to $\boldsymbol{i}$, and where $\mu_1 \ll \mu_e$.

The first step in the determination of the torque is done by describing the field which acts on the dipole in an Onsager frame. The field is split into cavity and reaction fields: A time dependent cavity field which is parallel to, but out of phase with, the macroscopic field. A stationary reaction field which is parallel to $\boldsymbol{i}$. The reaction field of the time

dependent part of the dipole which is parallel to *n* but out of phase with the movement of the dipole. And finally the part of the reaction field, which stems from polarization by the reaction field itself.

The second step in finding the torque is to make an explicit crossproduct between the dipole and all the terms in the field. Counting torques from parallel components of field and dipole moment is hereby avoided in the most natural and straight forward way. The torque which Fatuzzo-Mason arrive at is simplified by using the assumption of small librations, in order to arrive at a term which is proportional to the macroscopic field and $\sin(\theta)$.

Finally Debyes first order solution is used to find the microscopic polarization and the macroscopic result is found by using the Onsager approximation and the standard Clausius-Mossotti result to relate α_i and ε_i (equation 4.4.1).

4.5.2   Final formulation of the model

The final result in Fatuzzo & Mason [1967] is

$$\frac{\varepsilon_e\left(\varepsilon(\omega)-\varepsilon_i\right)\left(2\varepsilon(\omega)+\varepsilon_i\right)}{\varepsilon(\omega)(\varepsilon_e-\varepsilon_i)(2\varepsilon_e+\varepsilon_i)} = \left(1+i\omega\tau_d + \frac{(\varepsilon_e-\varepsilon_i)(\varepsilon_e-\varepsilon(\omega))}{\varepsilon_e(2\varepsilon(\omega)+\varepsilon_i)}\right)^{-1} \qquad (4.5.1)$$

Where τ_d is the microscopic Debye relaxation time (equation 3.3.2). Díaz-Calleja et al. [1993] combines this result with the results from Dimarzio & Bishop [1974]. This is simply done by replacing the frequency independent viscosity with the frequency dependent viscosity. The result when expressed in terms of $G(\omega)$ is

$$\frac{\varepsilon_e\left(\varepsilon(\omega)-\varepsilon_i\right)\left(2\varepsilon(\omega)+\varepsilon_i\right)}{\varepsilon(\omega)(\varepsilon_e-\varepsilon_i)(2\varepsilon_e+\varepsilon_i)} = \left(1+\frac{4\pi r^3}{k_B T}G(\omega) + \frac{(\varepsilon_e-\varepsilon_i)(\varepsilon_e-\varepsilon(\omega))}{\varepsilon_e(2\varepsilon(\omega)+\varepsilon_i)}\right)^{-1}. \qquad (4.5.2)$$

We will later use this equation in a form where $G(\omega)$ is given as a function of $\varepsilon(\omega)$

$$G(\omega) = \frac{k_B T}{4\pi r^3}\left(\frac{-\varepsilon_e(\varepsilon(\omega))^2 + \varepsilon(\omega)\varepsilon_e^2 - \varepsilon_i(\varepsilon(\omega))^2 - \varepsilon_i\varepsilon_e^2}{\varepsilon_e(\varepsilon(\omega)-\varepsilon_i)(2\varepsilon(\omega)+\varepsilon_i)}\right) \qquad (4.5.3)$$

4.5.3   The high frequency limit

In the above section we presented the Fatuzzo-Mason model and the generalization by Díaz-Calleja et al. [1993] using our notation. The original versions use ε_∞ in the place of ε_i. This does not lead to ambiguity in the original Fatuzzo-Mason model because it uses a frequency independent viscosity and has $\varepsilon_i = \varepsilon_h$ just like the original Debye model. The meaning of ε_∞ is not discussed in Díaz-Calleja et al. [1993] when the result of DiMarzio-Bishop is combined with that of Fatuzzo-Mason, but here $\varepsilon_i \neq \varepsilon_h$ making a distinction necessary. The introduction of the macroscopic quantity ε_∞ is as mentioned above based on equation 4.4.1 and for this to hold ε_i has to be used in the place of ε_∞. Using $\varepsilon_\infty = \varepsilon_h$ would be erroneous, since the elastic contribution to the high frequency plateau ε_h has to be taken into account, just as in the Clausius-Mossotti version of the model.

4.6   Tests of the DiMarzio-Bishop model by others

The DiMarzio-Bishop model has been tested against data by several authors since it was proposed in Dimarzio & Bishop [1974]. In the following we give a review of how the testing has been performed and of the results which have been found in these previous works.

4.6.1   Dimarzio & Bishop [1974]

In the original paper [Dimarzio & Bishop, 1974], the model as formulated in equation 4.3.3, is compared to measurements on three different polymers. The raw data is not presented in the paper. For the dielectric data the best curve of a Havrilak and Negami fit is used. The shear data is taken from the book of Ferry [1961], and time temperature superposition is assumed in order to use them.

It is easily seen in figure 2 and 4 of Dimarzio & Bishop [1974] that there is a problem with the high frequency limit of equation 4.3.3, as the curves calculated on basis of the shear mechanical data have a high frequency plateau value considerably greater than the dielectric data. On top of this discrepancy the rest of the fit is also rather poor. The authors focus on the fact that the DiMarzio-Bishop model predicts the skewed arc shape of the Cole-Cole plot of the dielectric data.

The best fits are obtained with radii ranging from 0.95Å to 2.3Å depending on substance. These values might be reasonable as it is probably the sidechains rather than the whole polymer that is relaxing.

4.6.2   Díaz-Calleja et al. [1993]

The objective of this paper is to compare the significance of what is called "dielectric friction" and mechanical friction on the relaxation of the dipoles [Díaz-Calleja et al., 1993]. This is done by comparing the result of the original Lorentz field version of the DiMarzio-Bishop model to the version suggested by Díaz-Calleja et al. [1993] in which the Fatuzzo-Mason field is applied.

The DiMarzio-Bishop model is in both cases tested by using the value $r = 2$Å. This value is not fitted, but used because the size of relaxing entity is expected to be of that order. $n^2 = \varepsilon_\infty$ is additionally assumed. Consequently it is in fact equation 4.4.5, which is tested, rather than the original equation 4.3.3.

The comparison between dielectric data and model values calculated from shear data is displayed in a Cole-Cole plot and in a plot of the real part of the spectra. In the Cole-Cole plot the shape of the calculated dielectric constant has a clear resemblance to the measured dielectric constant. In the plot of the real part the calculated dielectric constant is shifted considerably towards lower frequencies, and possibly also lower plateau values, compared to the measured dielectric constant.

It is found that the Fatuzzo-Mason version of the DiMarzio-Bishop model gives slightly better agreement, though the difference is minor. It is concluded on this basis that the "dielectric friction" is of lesser importance than the mechanical friction.

4.6.3   Christensen & Olsen [1994]

The version of the DiMarzio-Bishop model which is formulated in equation 4.3.9 is tested against data from two molecular liquids.

The dielectric and shear mechanical data are not obtained at the same temperatures and therefore time temperature superposition is assumed in order to compare the two.

The frequency span (10Hz-60kHz) of the shear data is greater than that of any of the other data we have seen reported. In spite of this the high frequency plateau of the shear data is not reached by the measurements and its value is therefore fitted in such a way that the agreement of the Cole-Cole plots is optimized. By this procedure extremely good agreements are obtained in the Cole-Cole plots, yet the agreement between the positions of the loss peak frequencies, is quite poor.

The authors write that they can bring the loss peaks to coalesce by reintroducing the induced molecular polarization as a fitting parameter. However this alters the shape of the cole-cole-plots and in the case of 1,3-butandiol the fitted value of α_i becomes negative, which is highly unphysical.

4.6.4   Zorn et al. [1997]

In this paper Zorn et al. [1997] presents a general analysis of the dielectric behavior of different 1,2-1,4-polybutadienes[2]. A comparison with earlier shear mechanical data from Zorn et al. [1995] is also presented.

The comparison of shear data and dielectric data is partly done in terms of the model by DiMarzio-Bishop, as it is formulated in equation 4.3.3. In Zorn et al. [1997] the high and low frequency plateaus are not reached by the measurements, and ε_∞ is therefore handled as a fitting parameter. By using ε_∞ as a fitting parameter it is not assumed that it corresponds to the high frequency plateau value of the dielectric constant. This means that in the use of Zorn et al. [1997] there is effectively no difference between equation 4.3.3 and the correct equation 4.4.5.

ε_∞ is fitted along with r using the imaginary part of equation 4.3.3. The directly measured dielectric data is compared to those calculated from the shear data in a plot of the loss peak. The fits are quite poor, which is also the conclusion of the authors. Despite this conclusion they find that the values of r ($10\text{Å} - 20\text{Å}$) determined from the fitted value of r are reasonable compared to the expected size of the relaxating entity. Further they find that r has a dependence on the micro structure of the molecules which is in agreement with the expected.

4.6.5   Ferri & Castellani [2001]

In this paper the DiMarzio-Bishop model is tested on the segmental relaxation of two different polymers. The test is done by comparing the loss of the dielectric relaxation with model results found from shear data. The exact procedure is close to that of Zorn et al. [1997]. The agreement between the peak shapes is poor, the calculated peaks are too wide, but the loss peaks positions agree reasonably. The fitted values for r are 0.6Å and 1.1Å for the two polymers respectively. These values are too small compared to

---

[2]We have also made measurements on a polybutadien, but none of the molecules used by Zorn et al. [1997] agree in the composition of the two different monomers, with the one we study.

what the authors expect, but they argue by using the result of Zorn et al. [1997], that the difference found between the two values is due to an actual difference in the size of the relaxing entity.

In section 4.8 we will give a brief discussion of why further testing of the DiMarzio-Bishop model is needed and present the background for our tests. Before this we return to the question of the significance of the local field, as these consideration are of importance for our practical approach.

4.7   Influence of the local field when the dielectric relaxation strength is small

In section 3.2.2 we illustrated how the Lorentz field and the Onsager fields approach each other as α_r approaches zero. In this section we will continue this line of thought and show that the choice of local field is of little importance in the DiMarzio-Bishop model, when the dielectric strength of the liquid is small. This serves as the background for a systematic approach to studying the significance of the local field.

4.7.1   The dielectric strength as a measure of the rotational contribution

For some liquids the dielectric relaxation changes the total dielectric constant with just $1\% - 10\%$. It is the rotational polarization which gives rise to the relaxation process. This indicates that the rotational contribution to the dielectric constant is small compared to the induced polarization when the dielectric strength is small. A small relaxation would also be seen in the case of a large rotational polarization with very little frequency dependence, as would be found in the case of a large elastic contribution to the rotational polarization. This scenario would, however, lead to a much greater high frequency plateau value ε_h than the $\varepsilon_i = n^2$ value. In our study of liquids with small dielectric strength we find that the high frequency plateau value deviates from the squared refraction index by the same order of magnitude as the size of the dielectric strength itself (see chapter 6). This implies that the total contribution of the rotational polarization is of the same order of magnitude as the relaxation strength.

The frequency dependent, and the equilibrium dielectric constant, for liquids with small relaxation strength, can therefore be expressed as

$$\varepsilon(\omega) = \varepsilon_i + \delta(\omega) \ \text{ and } \ \varepsilon_e = \varepsilon_i + \delta_e, \tag{4.7.1}$$

where $\delta(\omega) \leq \delta_e \ll \varepsilon_i$, and where both delta values are due to the rotational contribution.

4.7.2   The DiMarzio-Bishop model with the Maxwell field

The following relation pops up immediately if the Maxwell field is used as both directing and inducing field in the relation between macroscopic and microscopic polarization (equation 3.2.5) and the microscopic DiMarzio-Bishop model (equation 4.2.7) is used for the description of α_r:

$$\chi(\omega) = \frac{N\mu^2}{3\varepsilon_0 k_B T} \frac{1}{\left(1 + \left(\frac{4\pi r^3}{k_B T}\right) G(\omega)\right)} + \frac{N}{\varepsilon_0} \alpha_i. \tag{4.7.2}$$

We introduce the equilibrium and the induced molecular dielectric constants

$$\varepsilon_e - 1 = \chi_e \quad = \quad \frac{N\mu^2}{3\varepsilon_0 k_B T} + \frac{N}{\varepsilon_0}\alpha_i \tag{4.7.3}$$

$$\varepsilon_i - 1 = \chi_i \quad = \quad \frac{N}{\varepsilon_0}\alpha_i, \tag{4.7.4}$$

which allows us to rewrite equation 4.7.2 as

$$\frac{\varepsilon(\omega) - \varepsilon_i}{\varepsilon_e - \varepsilon_i} = \frac{1}{\left(1 + \left(\frac{4\pi r^3}{k_B T}\right) G(\omega)\right)} \tag{4.7.5}$$

in total analogy with the procedure in section 4.4 where the Lorentz field was used.

Solving for the shear modulus $G(\omega)$ yields

$$G(\omega) = \left(\frac{k_B T}{4\pi r^3}\right) \left(\frac{\varepsilon_e - \varepsilon_i}{\varepsilon(\omega) - \varepsilon_i} - 1\right) \tag{4.7.6}$$

The equivalent result found in equation 4.4.7 by using the Lorentz field was

$$G(\omega) = \left(\frac{k_B T}{4\pi r^3}\right) \left(\frac{\varepsilon_i + 2}{\varepsilon_e + 2}\right) \left(\frac{\varepsilon_e - \varepsilon_i}{\varepsilon(\omega) - \varepsilon_i} - 1\right). \tag{4.7.7}$$

Both these equations can be posed as

$$G(\omega) = K_1 \frac{1}{\varepsilon(\omega) - \varepsilon_i} + K_2 \quad \text{or} \quad G(\omega) = K_3 \left(\frac{\varepsilon_e - \varepsilon_i}{\varepsilon(\omega) - \varepsilon_i} - 1\right). \tag{4.7.8}$$

where three independent parameters appear, as always.

This has the consequence that the Maxwell and the Lorentz versions of the DiMarzio-Bishop model field will yield fits of the same quality if all three parameters[3] are fitted with no additional constraints. The values of the lumped parameters can of course be used to solve for the "original" parameters ε_e and r, and the results found for r will depend on whether the Lorentz or the Maxwell field is used.

The difference between the two local fields is that when the Lorentz field is used a factor of $(\varepsilon_i+2)/(\varepsilon_e+2)$ is introduced. Liquids with a small strength, will have $\varepsilon_e \approx \varepsilon_i$, which signifies that the difference between using the Lorentz field and the Maxwell field is smaller the smaller the dielectric strength.

4.7.3   The Fatuzzo-Mason version of the DiMarzio-Bishop model when the dielectric strength is small

Inserting the expression of ε_e and $\varepsilon(\omega)$ from equation 4.7.1, in the Fatuzzo-Mason field version of the DiMarzio-Bishop model (equation 4.5.2) leads to

$$G(\omega) = \frac{k_B T}{4\pi r^3} \frac{\left(-3\varepsilon_i{}^2\delta(\omega) - 2\varepsilon_i(\delta(\omega))^2 + 3\delta_e\varepsilon_i{}^2 - 3\delta_e(\delta(\omega))^2 + 2\varepsilon_i\delta_e{}^2 + 3\delta(\omega)\delta_e{}^2\right)}{(\varepsilon_i + \delta_e)\delta(\omega)(3\varepsilon_i + 2\delta(\omega))}$$

---

[3]Which three parameters are chosen will not affect the fit within the precision of the fitting procedure, but posing the equation in this form makes it easy to see the equivalence between the two results.

If only the leading terms in the small quantities δ_i and $\delta(\omega)$ are kept in the denominator and numerator respectively the expression reduces to

$$G(\omega) = \left(\frac{k_B T}{4\pi r^3}\right)\left(\frac{\delta_e}{\delta(\omega)} - 1\right) = \left(\frac{k_B T}{4\pi r^3}\right)\left(\frac{\varepsilon_e - \varepsilon_i}{\varepsilon(\omega) - \varepsilon_i} - 1\right) \qquad (4.7.9)$$

which can be recognized as the expression obtained when the Maxwell field is used.

Excluding all other terms than the terms of lowest order in δ_e and/or $\delta(\omega)$ can only be justified if the two delta terms are of the same order of magnitude. This will always hold at the low frequency end of the spectrum, whereas it might not hold in the high frequency end of the spectrum. $\delta(\omega)$ goes to zero at high frequencies in the original Debye model making it unjustified to use the approximation above. $\delta(\omega)$ will approach a finite value in the case of the DiMarzio-Bishop model (if the high frequency plateau is properly treated). Thus the expression is better justified for testing this model. Anyhow the expression supports the assertion that the choice of local field is of lesser importance the smaller the dielectric strength is.

It is not surprising that the local field has less importance when the dielectric strength is small. Nevertheless it is an important result because it allows for a more systematic discussion of the influence of the local field on tests of the DiMarzio-Bishop model.

In Díaz-Calleja et al. [1993] the importance of the local field is as mentioned earlier discussed on the basis of a comparison between results from the DiMarzio-Bishop model with the Clausius-Mossotti approximation and the DiMarzio-Bishop model expressed in terms of the field developed in Fatuzzo & Mason [1967]. It is claimed that such a comparison is a probe on how important the lagging behind of the reaction field (referred to by Díaz-Calleja et al. [1993] as dielectric friction) is compared to the mechanical friction described by the DiMarzio-Bishop model.

The discussion above shows that even if the choice of local field is important, then it is very likely that this cannot be seen in liquids with small dielectric strength, and the importance is expected to be increasing with increasing dielectric strength. Hence the dielectric strength can have a major influence on the conclusions when studying the significance of the local field. It therefore clear that such a study should not be made without testing on liquids with different dielectric strength.

4.8   Our experimental goals

In section 4.6 we summarized the earlier tests which have been made of the DiMarzio-Bishop model by others. It is difficult to draw any final conclusions from these tests.

One problem is that a lot of different procedures are used in the testing, regarding the fitting or determination of parameters in other ways. Some of these procedures are erroneous[4] others are just difficult to compare and to conclude upon. It is specifically a problem that there is no consensus on how r should be interpreted, hence what values should be expected. Most of the tests are made in the susceptibility formulation with the Clausius-Mossotti approximation, making all three parameters (r, ε_e and ε_i (or ε_h)) influence on both loss peak shape and position. Another problem is the local field, which has not been discussed systematically, in connection with any of the earlier tests.

---

[4]We refer here to the earlier discussed problem in Dimarzio & Bishop [1974] where $G_\infty = \infty$ is assumed and Christensen & Olsen [1994] where $\chi_i = \varepsilon_i - 1 = 0$ is assumed.

It is consequently difficult to know if the explanation of poor fits lies in the choice of local field or in inadequateness of the DiMarzio-Bishop model itself.

We have there performed comparable shear mechanical and dielectric measurements on a series of liquids, which have been specifically chosen, in order to enable a broad and systematic test of the DiMarzio-Bishop model.

4.8.1   Requirements to the series of liquids

We have aimed at finding molecular liquids which differ in dielectric strength and to include liquids both with and without a beta relaxation.

Molecular liquids are chosen rather than polymers because we want to avoid extra degrees of freedom due to movement of side chains. The approximation by spherical molecules which is the starting point of the DiMarzio-Bishop model also seems more appropriate for a smaller molecule.

Testing whether the DiMarzio-Bishop model's predictions holds better for small dielectric strength than for large dielectric strength can give an indication of whether disagreements are due to the local field problem. It is additionally possible that the DiMarzio-Bishop model's assumption of no correlation of the direction of the molecules might hold better if the dipoles are small.

Since all alpha relaxations look much alike, the demands, on what the model should predict for different liquids, are limited. By including liquids with a beta relaxation we achieve a variation of the relaxation spectrum and we hereby obtain a stronger quantitative as well as qualitative test of the DiMarzio-Bishop model. The beta relaxation is also interesting because shear mechanical beta relaxations are very rarely studied. It is thus interesting to make even simple phenomenological assertions about the shear mechanical beta relaxation and its relation to the dielectric beta relaxation.

4.8.2   The actual choice of liquids

Nature has unfortunately made it difficult for us to fulfill all the requirements. We will in this section give a short presentation of the liquids we have choose, and the compromises that lead to some of the choices.

We refer to the liquids by the abbreviations given in table 4.1. Relevant information about the substances is also shown in table 4.1.

TPE, DC704 and PPE are liquids without a visible beta relaxation, and the dielectric strength varies from very small to rather large.

Squalane, PB20, DHIQ and TPG have a visible beta relaxation, and have dielectric strength varying from extremely small to very large.

The main problem has been finding a molecular liquid with a small dielectric strength and a beta relaxation (with its peak in the frequency span where we can access it). We have chosen squalane, but the dielectric strength is so small that we hardly get a dielectric signal (see chapter 6). Polybutadiene is a polymer[5] but complies with the other demands, and we have therefore chosen to include it in the study.

---

[5]The polybutadiene (PB20) is composed of chains with an average of 80% 1, 4- and 20% 1, 2- butadiene monomers. The monomer molecular weight is 54.09g/mol and the average molecular weight of a chain is 5.000g/mol.

By this choice of liquids we have a series of liquids that allows us to perform detailed testing of the DiMarzio-Bishop model.

All liquids are used as acquired, see section 5.4 for a discussion of chemical stability and handling of the liquids. We will in the next chapter present details about the experimental equipment, procedures and uncertainties.

DC704 is very chemically stable [Olsen, 2003], [*Sigma-Aldrich*, n.d.]. It is used as a standard liquid in our laboratory and it has been found to have a pure alpha relaxation which obeys TTS [Olsen, 2003]. We have therefore used DC704 as a reference liquid for testing reproducibility and noise level on our data.

	n^2	M	T_g	m	γ	$\Delta\varepsilon$	ε_h	$\nu_{\beta,lp}$
TPE Triphenylethylene	–	256.3 g/mol	249K	73	3.5	0.05	2.71	–
DC704 Tetramethyltetraphenyl- trisiloxane	2.430	484 g/mol	211K	83	3.9	0.2	2.63	–
PPE Polyphenyl Ether	2.659	454 g/mol	244K	80	3.9	1.5	2.95	–
Squalane Perhydrosqualene	2.105	422.8 g/mol	167K	64	2.9	0.015	2.15	$10^{4.5}$Hz
PB20 Polybutadiene	2.310	5000 g/mol	176K	79	3.7	0.15	2.35	$10^{4.5}$Hz
DHIQ Decahydroisoquinoline	2.221	139.2 g/mol	179K	154	8.3	1.5	2.2	$10^{2.7}$Hz
TPG Tripropylene glycol	2.085	192.3 g/mol	190K	65	3.0	20	2.8	$10^{4.0}$Hz

Table 4.1 Data on the chosen substances.
Refraction index (n), molecular weight (M), glass temperature (T_g), Angell fragility index (m), Olsen index (γ), dielectric relaxation strength ($\Delta\varepsilon$), dielectric high frequency plateau value (ε_h), and position of the beta loss peak ($\log_{10}(\nu_{\beta,lp})$).

The refraction index (taken at 25°C) and molecular weight of PPE is from *Scientific Instrument Services, Inc.* [n.d.]. The refraction index of PB20 was measured on a PZO RL3 refractometer at approximately 28°C. No refraction index is given for TPE because it is a solid at room temperature. The refraction index (taken at 20°C) and molecular weight of other liquids are from *Sigma-Aldrich* [n.d.].
$\Delta\varepsilon = \varepsilon_e - \varepsilon_h$, ε_h, and the position of the beta loss peaks are rough numbers found from our dielectric data, the precise value is temperature dependent.
T_g and fragility indices are also based on our dielectric data, (see section 13.3 for details on how they are found).

5 Experimentals

In this chapter we present the two measuring methods that we use, along with a presentation of our general experimental setup, and procedures.

We present a thorough analysis of the uncertainties and systematic errors involved. This analysis is crucial because we aim to compare data from two different methods, and therefore some of the uncertainties which normally are disregarded (e.g. absolute values) need to be accounted for.

5.1 Measuring a capacitance

Common to the two methods we use, is that a frequency dependent capacitance needs to be determined with great accuracy. In this section, we will describe the capacitance measuring setup and its accuracy.

5.1.1 The setup

Our setup consists of a HP3458A multimeter in conjunction with a Keithley AWFG used at frequencies in the range $10^{-3} - 10^2$Hz, and a HP 4284A LCR-meter used at $10^2 - 10^6$Hz.

The two different setups are connected to the measuring cell through a relay, giving the opportunity of automatic switching between the two frequency ranges. Everything is controlled from a computer enabling automatic measurements.

LCR-meter method

The 4284A LCR-meter is a commercial LCR-meter and is used directly to measure the complex capacitance of the sample.

Multimeter method

The multimeter measurements are performed on a homebuilt setup which is based on a voltage divider. The total input voltage is known, and the output voltage is measured over a known component, C_i, consisting of a 10nF capacitor in parallel with a 100MΩ resistor (see figure 5.1).

The unknown capacitance, C_x is found from the ratio between input and output voltage:

$$\frac{U_{out}}{U_{in}} = \frac{U_{out}}{U_x + U_{out}} = \frac{C_x}{C_i + C_x} \Leftrightarrow C_x = \frac{U_{out}}{U_{in} - U_{out}} C_i \qquad (5.1.1)$$

Figure 5.1 Schematic illustration of the multimeter method. See the text for details.

where U_x is the voltage over the unknown capacitance C_x.

In order to use the above equation, the exact value of C_i has to be known at all frequencies. This is obtained by a calibration in which C_x is interchanged with a known capacitor of about the same order of magnitude as the real part of C_i. The leaking current, which inevitably is in the system, is modeled by a $1 \cdot 10^{16}\,\Omega$ resistance in parallel with this capacitor. The frequency dependent C_i is found by making a measurement on this system. The calibration of C_i is done for each specific measuringcell holder, which means that resistance and capacitance of all[1] the wiring is included in C_i.

Typical spectrum

Figure 5.2 Real and imaginary part of capacitance of the empty dielectric cell, measured at approximately 200K, in vacuum.

A measurement on the dielectric measurement cell (a 22 layer platen capacitor with capacitance of approximately 68pF) is show on figure 5.2 to give an overview of the systems performance.

---

[1]Except the final connection between the measuring cell and the holder.

The ideal spectrum in figure 5.2 would be a constant real part and a zero imaginary part. It is seen that the spectrum deviates somewhat from this ideal spectrum. The deviations are due to systematic errors in the LCR-meter and noise.

5.1.2   Systematic errors in the LCR-meter frequency range

In this section we describe the systematic errors of the LCR-meter and account for how we have dealt with them.

The errors seen in the right plot in figure 5.2 are systematic[2], but changes slowly with time, and they change abrupt if the LCR meter is restarted. There is a problem at low frequencies ($100Hz$ to roughly $10kHz$) mostly seen as a negative imaginary part, a high frequency anomaly seen as a increase in the imaginary part, and finally there are reproducible nicks in both the imaginary and real part. These features are not related to the dielectric cell but are found in all our measurements.

The high and low frequency problems in the imaginary part are partly additive, which make it possible to eliminate them to some extend. This also has the consequence that the artifacts are seen less in measurements of bigger capacitances. The nicks in the spectrum, however, are not additive, and show up in most of our measurements at the same frequencies. We believe that the non-additivity of the nicks is due to changes of internal modes in the LCR-meter.

Dielectric measurements

The artifacts from the LCR-meter show up directly in the dielectric measurements, and are handled in the following way.

The systematic errors are of minor importance in the real part of the signal (notice the axis in figure 5.2) as they are in general of much smaller scale than the variation in capacitance, which we wish to observe, however this is not the case regarding the imaginary part. The simplest way to deal with the problem in the dielectric measurements is to subtract an imaginary part of a measurement on a pure capacitor from our raw data.

The problem with this procedure is, as described, that the errors changes with time, and therefore a complete removal of the artifacts is not possible. In the measurements on substances with a small dielectric strength, the problem becomes fatal because they have small imaginary parts.

Shear mechanical measurements

The systematic errors of the LCR-meter have a minor influence on the shear mechanical measurement. This is due to two things: Firstly the calculations of the shear modulus limits the problem, since a reference spectrum is subtracted from the measurement (see section 5.3.2), and secondly the capacitance of the shear transducer is somewhat larger than the errors (real parts are typically 10nF and imaginary parts are typically 0.1nF). However, the high frequency nicks are seen in our shear data.

---

[2]The high frequency artifacts could also be due to the inductance and resistance of the wiring. This would give a negative capacitance at the high frequencies, but that is not what we see.

5.2 Dielectric measurements

In this section the dielectric measuring method is presented. The noise due to the limits of the equipment is evaluated, and we analyze systematic errors that occur due to improper filling of the measuring cell and thermal contraction.

5.2.1 The dielectric cell

The dielectric measuring cell is a multilayered golden platen capacitor with an empty capacitance of $C_{\text{empty}} \approx 70\text{pF}$. We use two capacitors which differ slightly in value. The capacitance of the empty capacitor is regarded as frequency independent, and this holds with an accuracy of approximately 0.1% (see figure 5.2).

The dielectric constant of a liquid is found by placing the liquid between the plates in the capacitor, and measuring the capacitance. From this capacitance of the full cell the dielectric constant (ε) of the liquid can be found by using the equation:

$$C = \frac{\varepsilon_0 A}{d_0} \varepsilon = C_{\text{empty}} \varepsilon. \tag{5.2.1}$$

5.2.2 Accuracy

We have estimated the noise over signal ratio, by looking at the measurement on the empty capacitor, which was shown in figure 5.2. It is seen that the absolute level of noise on the real part is about 0.1pF on a capacitor with a capacitance of approximately 68pF. Leading to a relative accuracy $\Delta C_{\text{noise}}/C$ of approximately 0.1%.

Since we have found that our worst problem is with measuring the imaginary part of the dielectric constant of substances with a small strength, we have studied this situation in more detail. This is done by estimating where noise starts to dominate over signal in the imaginary part of a dielectric spectrum taken on the substance DC704. The spectra is shown in figure 5.3.

We present the limits of the data resolution as levels of dielectric constants because this is what we mostly will need, but if raw capacitances are needed they can be obtained by multiplying with the geometric capacitance $68 \cdot 10^{-12}\text{F}$ (corresponding to a shift of approximately 10 decades on the logarithmic scale).

It is seen that below $-\varepsilon'' = 10^{-3}\text{F}$ noise is dominant in the high frequency end (in agreement with the noise seen on the imaginary part in figure 5.2). As a rough procedure we choose to only use data from the $-\varepsilon'' > 10^{-3}\text{F}$ range, but in special cases this range can be extended if care is taken. Above $-\varepsilon'' = 10^{-2}\text{F}$ the signal dominates over noise (except for a small deviation seen in some data sets just below 10^6Hz apparently due to the sharp rise seen in the high frequency end of the spectrum of the empty cell).

In the interval $10^{-3}\text{F} < -\varepsilon'' < 10^{-2}\text{F}$ the accuracy becomes highly frequency dependent. In the high frequency end the errors from the LCR meter are seen. Due to this we choose to exclude this frequency range when dealing with small dielectric losses. At the crossover between the two measuring methods some noise is seen, but it is also seen that the curves generally pass through the crossover and return to the same slope as before. Care should of course be taken if data sets end right at the crossover or if the loss peak position is at the crossover.
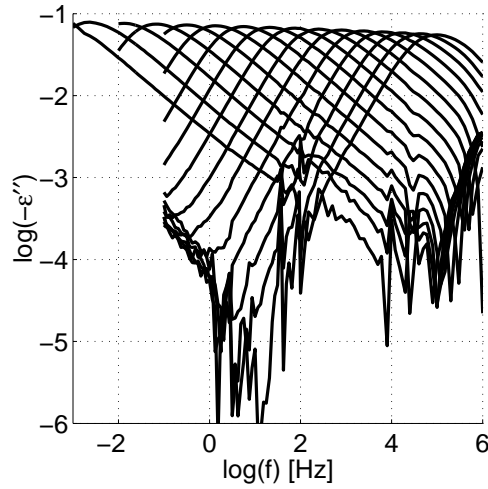
Figure 5.3 A dielectric spectrum of DC704. 209.4K to 239,7K in steps of approximately 2K per curve. A background was subtracted before dividing with the geometric capacitance (see section 5.1.2).

In conclusion we generally exclude the following data

$$-\varepsilon'' < 10^{-3}\text{F} \tag{5.2.2}$$

$$f > 10^5\text{Hz and } -\varepsilon'' < 10^{-2}\text{F} \tag{5.2.3}$$

5.2.3   Systematic errors

There are a number of problems regarding the determination of the absolute value of the dielectric constant.

Firstly it is impossible to determine the exact value of the empty capacitance of the cell. This is because the distance between the capacitor plates varies as the temperature is decreased. When we determine the empty capacitance at some desired temperature (typically 100K below room temperature) the cell has been contracting from room temperature *empty* whereas it contracts *with* the liquid, when we measure the capacitance of the cell with liquid. The contraction in the first case is determined by the expansivity of the spacers in the cell, while it is the expansivity of the liquid that dominates the contraction in the latter case. Thus the empty capacitance we need is that of an empty capacitor, which has a spacing between the plates as if it had been contracting full, however this value is not known.

A related problem is that the capacitor, due to thermal contraction of the liquid, might not be totally filled and this further complicates the question of what empty capacitance should be used.

An additional problem is that it is difficult to fill the capacitor properly. This problem has been revealed by reproduction measurements, where we have found that different degrees of filling can explain differences in results from liquids, which we believe are chemically stable.

The measured capacitance is given by

$$C_m = \frac{\varepsilon_0 A}{d}b\varepsilon + \frac{\varepsilon_0 A}{d}(1-b) \tag{5.2.4}$$

where A is the area of the capacitor plates, d is the spacing between the plates, b is the fraction of the capacitor which is filled with the liquid and ε is the dielectric constant of the liquid.

We divide the measured capacitance by the capacitance of the empty cell to obtain the measured dielectric constant. The capacitance of the empty cell is:

$$C_{\text{empty}} = \frac{\varepsilon_0 A}{d_0}, \tag{5.2.5}$$

where d_0 is the spacing between the plates when the capacitance of the empty capacitor is measured.

Assuming that $d = d_0(1 + \Delta d)$, where $\Delta d \ll 1$, and that $b = 1 - \Delta b$ where $\Delta b \ll 1$ and keeping track of first order terms in Δb and Δd leads to the following relation between the measured dielectric constant ε_m and the actual dielectric constant

$$\begin{aligned} \varepsilon_m &= \varepsilon(1 - \Delta b - \Delta d) + \Delta b \tag{5.2.6} \\ &= \varepsilon - \Delta d \varepsilon + \Delta b(1 - \varepsilon). \tag{5.2.7} \end{aligned}$$

This shows that the measured dielectric constant will be smaller than the actual dielectric constant for $\Delta b > 0$ (unfilled capacitor) and $\Delta d > 0$ (a greater distance between the plates in the full than empty cell). The typical situation is $\Delta b > 0$ and $\Delta d < 0$, and the two effects will therefore counteract each other. We return to this problem in section 7.2, where we study the temperature dependence of the high frequency dielectric constant.

The error described above will not effect the frequency dependence, but only the measured absolute value.

5.2.4 The effect of uncertainties on reproduction of experiments

When we want to check if our results are reproducible we compare two different measurements taken on the same liquid using the same dielectric cell. This means that the degree to which the capacitor is filled may vary. The distance between the plates will approximately be the same in the two experiments since it is the same liquid that is contracting in the two cases, and the (small) difference in filling will not influence the degree of contraction significantly.

The two measured dielectric constants (designated ε_{m1} and ε_{m1}), will thus be described by two equations of the same type as 5.2.6 in which the filling degree parameters Δb_1 and Δb_2 are different whereas the distance between the plates is the same. Assuming that the dielectric constant of the liquid is unchanged the relationship between the two measured dielectric constants will, to first order, be:

$$\begin{aligned} \varepsilon_{m1} &= (1 - \Delta b_1 + \Delta b_2)\varepsilon_{m2} + \Delta b_1 - \Delta b_2 = f \varepsilon_{m2} + (1 - f) \tag{5.2.8} \\ \text{with} \quad & f = 1 - \Delta b_1 + \Delta b_2 \approx 1 \tag{5.2.9} \end{aligned}$$

This equation should hold at all frequencies with the same factor f, and this factor should not have any significant temperature dependence. (The contraction in the plane can lead to a smaller filling degree, but this will happen at the same rate in the two experiments as it is the same liquid in the two cases).
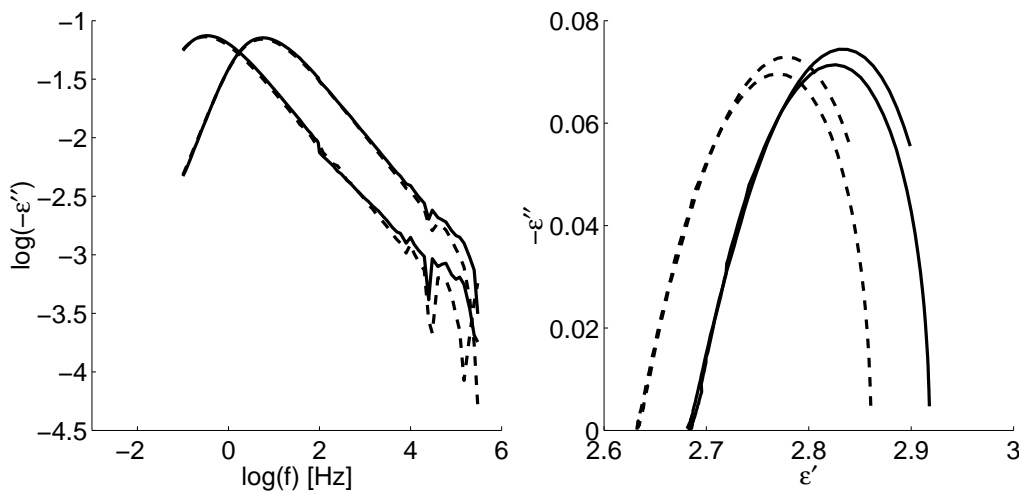
Figure 5.4 Raw data from two different dielectric measurement taken on DC704. Dashed lines from one measurement, solid lines from a measurement taken several months later. The temperatures are 221.5K and 223.5K in both cases.

5.2.5   A dielectric measurement of reproducibility

Figure 5.4 shows data from two different dielectric measurements under the same physical conditions on the silicone oil DC704. DC704 is as mentioned in the presentation of the substances (see section 4.8) very chemically stable and therefore we consider these curves a measure of how well we can reproduce dielectric results. These curves show that the shape of the relaxation peak is reproduced with high accuracy whereas there is a deviation of approximately 2% on the absolute value. The difference in absolute value can be explained by an un-perfect filling of the measuring cell. By use of equation 5.2.8 with $f = 1.03$ the absolute values are brought to agree. This is depicted in figure 5.5, and we regard this plot as a measure of the quality of our dielectric measurements.

5.3   The piezoelectric shear modulus gauge (PSG)

The shear measurements are performed with a piezoelectric shear modulus gauge (PSG). The PSG has been developed at IMFUFA by T. Christensen and N. B. Olsen. The principle of the PSG and the full analysis leading to the shear data is reported in Christensen & Olsen [1995].

In the following section we will give a review of the physical principle behind the method and report some of the practical problems that are important for the routines and precautions that have to be taken when using the PSG. We also present an analysis, which has not been performed earlier, of how the uncertainties involved affect the results, especially regarding the influence on the position and shape of the loss peak.

5.3.1   General principle and construction

The PSG is a sandwich construction of three piezoceramic discs, each coated with a thin conducting layer at the top and bottom. There is a 0.5mm gap between the discs, and
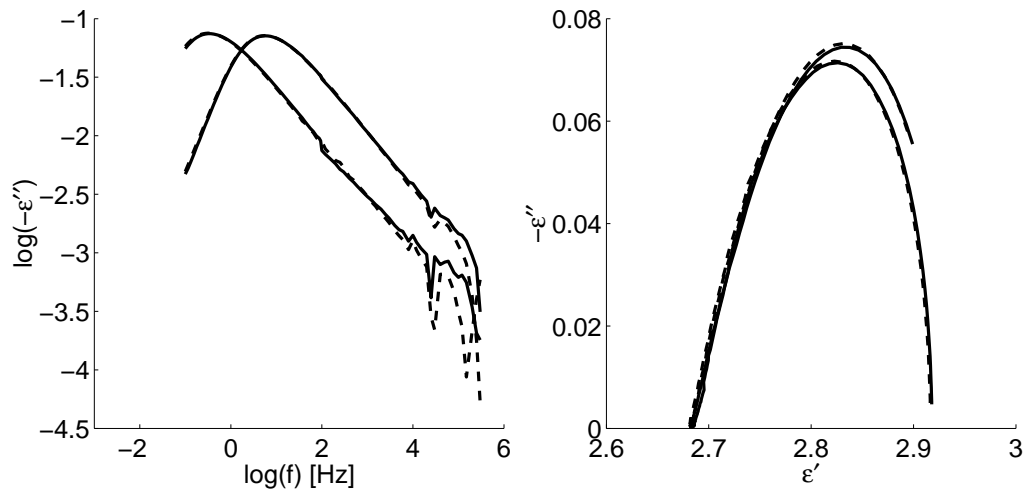
Figure 5.5 Data from two different dielectric measurements taken on DC704. The data are the same as in figure 5.4. Agreement in the absolute values is obtained by using equation 5.2.8 with $f = 1.03$. Dashed lines from one measurement, solid lines from a measurement taken several months later. The temperatures are 221.5K and 223.5K in both cases.

the liquid to be studied is loaded in these gaps.

When an electric field is applied over the discs they expand (or contract depending on the direction of the field compared to the polarization of the disc) in the radial direction. The measurements are performed by measuring the capacitance of the combination of the three discs. The disc are electrically connected as illustrated in figure 5.6, which means that there is a field over each of the discs, but none over the gaps between them.

Figure 5.6 The electric connections of the discs in the PSG. The dot illustrates the polarization direction of the pierzoceramics. [Christensen & Olsen, 1995]

The capacitance of the piezoceramic disc depends on the strain of the ceramics, and the strain depends on how free the ceramics are to move. The shear modulus of the liquid between the plates in the PSG hinders the movement of the plates, making the measured capacitance dependent on the shear modulus of the liquid, and this is the central idea of the PSG.

One of the problems which usually appear when measuring the shear modulus on glass forming liquids close to the glass transition is that the rigidity of the liquid becomes

comparable to that of the rheometer, leading to an undesired deformation of the rheometer. This problem does not appear in the PSG because the deformation of the measuring gauge is an integrated part of the method. Another great advantage of the PSG when doing linear experiments is that the strain is approximately 10^{-6}, which is an extremely low value, making nonlinearity no problem. [Christensen & Olsen, 1995]

5.3.2   Technical details and complications

In order to obtain shear mechanical data, it is of course necessary to calculate the exact connection between the shear modulus and the measured capacitance. This is possible in the case of the PSG due to a very convenient construction and geometry.

The voltage over the central disc is twice that of the outer discs and opposite directed, while the discs are all directed with the polarity in the same direction (parallel to the field). This means that the middle disc moves inward while the outer ones move outward and vise versa. The middle disc is also subjected to twice the mechanical tension of the outer discs, because the net tension on each liquid layer is zero and because the inner disc is in contact with two layers of liquid. The double tension and double voltage on the middle disc leads to double charge and double displacement compared to the outer discs, since the displacement and charge are given by the mechanical tension and the electric voltage via the elastoelectric matrix[3]. Therefore the middle disc has the same capacitance (double charge and double voltage) as the outer ones, making the total measured capacitance $^3/_2$ of this, due to the electrical connection. The movements of the discs result in neutral planes in the liquid displacement fields $^1/_3 d$ from the outer discs, where d is the distance between the plates. The neutral plane can be regarded as an infinitively rigid support, because the points in this plane do not move.

By combining all this it can be realized that the mathematical problem of finding the capacitance of the PSG as a function of the shear modulus of the liquid is equivalent to finding ($^3/_2$ of) the capacitance of one piezoceramic disc with a liquid layer of thickness $^1/_3 d$ clamped between the disc and an infinitively rigid support. From this stage the calculation of the capacitance is done in two steps. First the capacitance of the disc is found as a function of the outer radius of the disc by using the elastoelectric matrix of the piezodisc, and an integration of the charge. Second the outer radius of the disc is found as a function of the liquid shear modulus by solving the equation of motion for a differential element of the piezodisc. This is done by using the boundary condition that the disc does not move in the center, it is free to move at the edges and on one side, and that it has a no slip connection to the liquid on the other side. The tangential stress is assumed to decrease linearly from the liquid to the free side of the plate and the displacement of the plate is assumed to be strictly radial. The stress applied by the liquid is found by assuming that the liquid deformation is pure shear and that the liquid does not change its thickness. In practice there will be a small volume change. However, the relative volume change is of the order of magnitude $\Delta R / R_0$, while the shear deformation is approximately $\Delta R / d$, where R_0 is the radius of the transducer and ΔR is the change in radius. Hence the ratio between relative volume change and shear deformation is approximately given by d / R_0, which in the PSG is 3%.

The liquid is loaded in to the transducer at room temperature, and it is hereafter cooled down to a little above the glass temperature, typically at $150 - 250$K. It is attempted to fill the transducer such that the liquid is in line with the edge of the piezo discs, but

---

[3]The elastoelectric matrix is assumed to be the same for all three discs.

the cooling of the liquid will make it contract. The effective radius of the liquid will therefore be smaller than the radius of the disc at the time of the measurement. This has to be included in the calculation of the displacement of the edge of the disc. A measure of the filling degree, is introduced in order to do this.

$$x_l = \frac{R_l}{R_0} \tag{5.3.1}$$

R_l being the radius of the liquid, and R_0 the radius of the transducer disc. The motion of the piezodisc is therefore solved by using two domains, the outer rim which has no contact to the liquid and the inner part of the disc which has contact to the liquid. The boundary conditions are as before, except for the outer rim which is subjected to zero stress on both sides and the additional condition of continuity of displacement and stress at the boundary between the domains.

The characteristic shear modulus, G_c, and the characteristic inertance, M_c, which define a characteristic frequency $\omega_c^2 = G_c/M_c$ are introduced in order to make the problem dimensionless. The characteristic inertance is given by the physical dimensions of the PSG, $M_c = \rho dh$, where ρ, h are the density and thickness of the piezoceramic disc. The characteristic frequency is found from determining the first and second resonance frequency of the empty transducer (see Christensen & Olsen [1995] p. 5023-5024 for details). The absolute uncertainties on the characteristics of the PSG lead to absolute uncertainties on the measured modulus.

The frequency and shear modulus of the liquid are both normalized by these characteristic quantities of the PSG

$$S = \left(\frac{\omega}{\omega_c}\right)^2 \quad V = \frac{G(\omega)}{G_c}. \tag{5.3.2}$$

The result which is used to find the shear modulus is a dimensionless quantity, describing the measured capacitance as a function of frequency, shear modulus of the liquid and x_l

$$F(S, V, x_l) = \frac{C_m - C_{cl}}{C_f - C_{cl}} \tag{5.3.3}$$

where C_m is the measured capacitance, C_{cl} is the capacitance of the transducer as measured if the transducer is clamped, and C_f is the capacitance of the transducer when the piezoelectric discs are free to move.

A final complication is that C_f and C_{cl} are frequency dependent due to dispersion in the ceramics, but it is assumed that C_f/C_{cl} is frequency independent. To cope with this frequency dependence a new normalized capacitance Φ is introduced. It relates to the measured and theoretical quantities by:

$$\Phi(S, V, x_l) = \frac{C_m - C_{cl}}{C_r - C_{cl}} = \frac{F(S, V, x_l)}{F(S, 0, 1)} \tag{5.3.4}$$

where C_r is a reference spectrum, of the empty transducer. This reference measurement has to be made under the same physical conditions, including same temperature history, due to thermal memory of the ceramics (see section 5.3.4), as the actual measurement.

The last step is to invert the equation in order to obtain $G(\omega)$ as function of Φ, x_l and S. The approximative inversion formula applied in the data analysis program, which we have used is given by

$$G(\omega) = G_c \frac{a - b\Phi + \sqrt{(a - b\Phi)^2 - 4\Phi c(\Phi - 1)}}{2\Phi c} \tag{5.3.5}$$

where a, b, c are functions of x_l and S. Details can be found in Christensen & Olsen [1995].

The validity of the inversion is also tested in Christensen & Olsen [1995], and the accuracy is reported as 5% for $0.95 < x_l < 1.0$ at frequencies below the first resonance of the free transducer.

5.3.3   Precision

The more a relative change in modulus of the liquid changes the measured capacitance the greater is the precision of a measurement. In Christensen & Olsen [1995] the sensitivity defined as

$$\Psi = G \frac{\partial F}{\partial G} \tag{5.3.6}$$

where F is the dimensionless capacitance defined in equation 5.3.3. Ψ depends on the rigidity of the liquid and the characteristic modulus of the transducer G_c.

A measurement on a capacitor of same order of magnitude as the PSG capacitance, 10nF, gives $C_{\text{noise}} \approx 0.002$nF corresponding to a relative accuracy of approximately 0.05% on the measured capacitance.

A relative change in capacity is approximately equal to the change in F, hence it possible to calculate the relative accuracy of the shear measurements if Ψ is known. We have determined Ψ from figure 18 in Christensen & Olsen [1995] and found that at shear moduli around 10MPa the relative accuracy on the shear measurements becomes approximately 2%, and at moduli at 100MPa the relative accuracy becomes 0.5%.

For practical purposes we mainly focus on the imaginary part of the shear modulus. Here we cut of data which lies below 10MPa, and we believe that the uncertainty on the loss peak shape above 10MPa, due to our electrical noise, is of minor importance compared to the problem discussed in the next section.

5.3.4   Relaxation of the piezoceramics

The properties of the piezoceramics are strongly temperature dependent and have extremely long relaxation time. This is why it is necessary to make the reference spectrum (C_r) at each desired temperature, and to do this with the same thermal history as the actual measurement. However it is impossible to obtain the same mechanical conditions for the thermal relaxation of the piezoceramics in the reference measurement and the actual measurement. The reference spectrum is taken on an empty transducer, where the ceramic is free to move. In the actual measurement there is (of course) liquid in the transducer and this influences the relaxation, especially at low temperatures, where the liquid is very rigid.

The difference in relaxation can be seen at very low frequencies in the raw data. In the ideal case there should be no difference between the capacitance of the empty and the full transducer in the low frequency limit, because the shear modulus of the liquid approaches zero. We do however often see a small difference, and this is handled by scaling the curves to agree. In practice the factor is chosen such that the measured shear modulus actually approaches zero, as is expected. Usually the scaling factor is around 1.005.

5.3.5   Errors due to uncertainties in the degree of filling

The greatest problem regarding our shear measurements stems from not knowing the degree of filling, x_l. x_l is not a quantity which is easily determined, and uncertainties in its value can give uncertainties in the loss peak position and in the shape of the relaxation spectrum.

In the calculation of the shear modulus in the data analysis program, the following expression is used to determine x_l:

$$x_l(T) = \frac{R_l(T_0)}{R_0} \left(1 + \frac{\alpha \Delta T}{2} \right) \tag{5.3.7}$$

where α is the thermal expansion coefficient which is assumed to be temperature independent, T_0 is room temperature, and $\Delta T = (T - T_0)$. In the data analysis program (that calculates our shear data from the measured capacitances) the ratio $\frac{R_l(T_0)}{R_0}$ is assumed to be equal to one, that is it is assumed that the transducer is perfectly filled at T_0.

If the filling of the PSG is not perfect or the expansion coefficient is poorly determined an error will be introduced on the x_l used in the inversion algorithm. We will first give en estimate of the magnitude of these errors, and subsequently analyze what changes they introduce on the calculated shear modulus.

Uncertainty due to unknown coefficient of expansion

The expansion coefficient is often difficult to find in the literature or on chemical databases. We have therefore assumed that all the liquids have expansion coefficients in the interval[4] $50 \cdot 10^{-5} - 90 \cdot 10^{-5} \mathrm{K}^{-1}$. And we generally use $\alpha = 70 \cdot 10^{-5} \mathrm{K}^{-1}$, except of the case of DC704 where we use $\alpha = 80 \cdot 10^{-5} \mathrm{K}^{-1}$. This value has been measured by the resonance method by Olsen [2003], and corresponds to a value given on an old data sheet (which seems to be unavailable from the manufacturer).

To distinguish between the real physical degree of filling and the one assumed in the inversion we introduce the following notation; $x_{l,r}$ for the real physical value of the ratio of filling and $x_{l,u}$ for the one used in the inversion algorithm.

Typical values of the temperature jump are $\Delta T = -100K$ This gives an uncertainty on the real $x_{l,r}$ of the oder of magnitude $\Delta x_{l,r} \approx \frac{20 \cdot 10^{-5} \mathrm{K}^{-1} \cdot 100\mathrm{K}}{2} = 0.01$. A typical value of the used fraction of filling is $x_{l,u} = 1 - \frac{70 \cdot 10^{-5} \mathrm{K}^{-1} 100\mathrm{K}}{2} = 0.965$.

Uncertainty due to different filling

The absolute precision of the filling is estimated to be ± 0.2mm, and the radius of the transducer is 1cm, giving a relative error of $\pm 2\%$ It might be argued that we should be able to fill the transducer more precisely (especially given that the distance between the discs is 0.5mm) but the problem is that we have to compare fillings made at different times, and this increases the uncertainty. This leads to an uncertainty in $x_{l,r}$ of approximately ± 0.02, that is a larger uncertainty than the one due to the approximative values of the expansion coefficients.

The uncertainty in determining the filling of the transducer and in determining the expansion coefficient leads to approximately $\pm 3\%$ uncertainty on $x_{l,r}$.

---

[4]Typical expansions coefficients for liquids are given in Ferry [1961] as $60 \cdot 10^{-5} - 100 \cdot 10^{-5} \mathrm{K}^{-1}$. The expansion coefficient of glycerol is known to be $50 \cdot 10^{-5} \mathrm{K}^{-1}$.

Estimation of uncertainty in the shear spectrum

We have performed model calculations to estimate how the uncertainties in the degree of filling affects the final shear mechanical spectrum obtained from a measurements. The tests were generally performed the following way: A simulated shear modulus (G_s) was calculated from a shear modulus model, from this Φ was found using the exact equations (with a given $x_{l,r}$), and finally a calculated shear modulus, G_{ca}, was found from the approximative inversion formula (this time using a different degree of filling, $x_{l,u} \neq x_{l,r}$). Because we generally use the same $x_{l,u}$ in our calculation of the shear modulus on a given substance, we choose to fix this and let $x_{l,r}$ change.

A realistic shear signal was constructed using the extended Maxwell model (see appendix B) with parameter values $G_\infty = 2\mathrm{GPa}$, $q = 1.5$ and $\alpha = 0.5$. The data for the PSG were set as $M_c = 6.4 \cdot 10^{-4}$ and $G_c = 6 \cdot 10^7 \mathrm{Pa}$ [Christensen & Olsen, 1995] placing the first resonance at approximately $10^{5.8} \mathrm{Hz}$.

In figure 5.7 it can be seen that errors in the degree of filling leads to shifts in the loss peak position. It is generally seen that $x_{l,u} < x_{l,r}$ leads to a shift of the found loss peak to a higher frequency. It is also seen that there is a systematic error in the inversion algorithm, if $x_{l,r} = x_{l,u}$ the found loss peak becomes approximately 0.05 decade too high. The consequence of this is that the symmetric uncertainty on $x_{l,r}$ leads to an asymmetric uncertainty on the loss peak. It becomes more likely to find too high a loss peak frequency than one which is too low.

The shape of the imaginary part of the shear modulus, is generally affected very little by the differences in the filling factor. By close inspection it is found that an increase

Figure 5.7 Change in loss peak position calculated as $\log G_{ca,lpf} - \log G_{s,lpf}$ (that is the loss peak in the calculated shear modulus minus the loss peak of the real shear modulus), as a function of the real filling factor $x_{l,r}$. The filling factors used in the inversion algorithm, $x_{l,u}$, are 0.94 (circles), 0.96 (crosses) and 0.98 (squares).
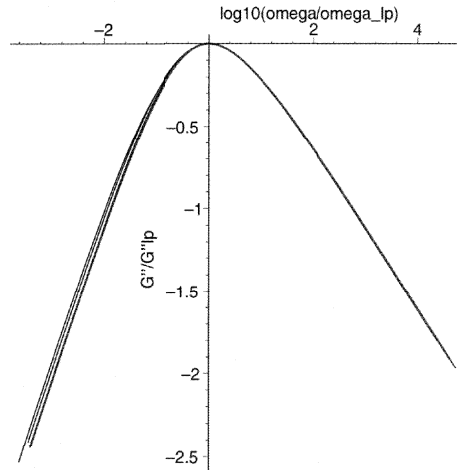
Figure 5.8 The bold line is the real shear modulus (calculated from the extended Maxwell model). The thin lines are the calculated shear modulus using $x_{l,u} = 0.96$ and $x_{l,r} = 0.93$, $x_{l,r} = 0.96$, and $x_{l,r} = 0.99$. The curves are scaled to make the peak positions coalesce in order to make a direct comparison of shape possible.

in $x_{l,r}$ (with fixed $x_{l,u}$) leads to an increase in the width of the curve. At approximately $x_{l,r} = x_{l,u} - 0.03$ the calculated curve gets the right shape, and at lower $x_{l,r}$ the calculated curve becomes too narrow. The change in shape is most pronounced at the left side of the peak. Figure 5.8 shows the deviation in shape from ± 0.03 error on x_l.

The absolute values of the shear modulus are also influenced by differences in the filling factor. To analyze this we have made Cole-Cole plots of the calculated shear modulus for different values of $x_{l,r}$. The result is shown in figure 5.9. It is seen that the uncertainty on the absolute values is approximately 50%. This is a very large error, but we hardly ever use the real part of the shear data in our further work, thus it has little or no influence on our conclusions.

Summary of uncertainties in the shear modulus due to uncertainties in the degree of filling

If the degree of filling assumed when calculating the shear modulus is smaller than the actual degree of filling $(x_{l,u} < x_{l,r})$, it has the following consequences; the calculated loss peak is shifted to a higher frequency than the actual shear loss peak of the liquid, and the absolute level of the real part of the calculated shear modulus becomes too high. Finally the shape of the calculated shear loss peak becomes slightly too wide compared to the real shear peak.

The total uncertainty on $x_{l,r}$ is approximately ± 0.03, and there is a 0.05 decade systematic error on the loss peak position, this gives a total measured loss peak position in between $\nu_{\text{real},lp} + 0.2$ and $\nu_{\text{real},lp} - 0.1$, where $\nu_{\text{real},lp}$ is the physical loss peak position.

5.3.6 The effect of uncertainties on reproductions measurements

When comparing experiments on the same liquid the same expansion coefficient is used. The difference between the measurements should therefore be explained by the uncertainty in the initial filling alone.
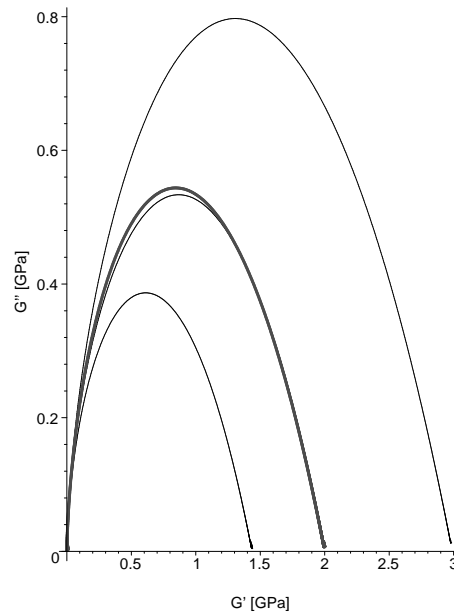
Figure 5.9 The bold line is the real shear modulus (calculated from the extended Maxwell model). The thin lines are the calculated shear modulus using $x_{l,u} = 0.96$ and $x_{l,r} = 0.93$, $x_{l,r} = 0.96$, and $x_{l,r} = 0.99$, with 0.93 being the inner curve with lowest absolute values and 0.99 the curve with highest absolute values.

This uncertainty in $x_{l,r}$ was estimated to be ± 0.02 leading to a maximum difference in $x_{l,r}$ of 0.04 between measurements. From figure 5.7 it is seen that a difference of 0.04 in $x_{l,r}$ leads to a 0.2 decade difference in loss peak position, which thus is the largest difference that we will expect as a result of differences in the degree of filling.

5.3.7 A shear mechanical reproduction measurement

The quality of our shear mechanical measurements is tested by comparing three different measurements on DC704. In the following we report only the results of the two sets that deviate the most (the last set lies between these two in all aspects), it should be noted that the deviation seen in this test is the largest we have seen in any of our measurements, normally we see better agreement between shear mechanical measurement. The measurements are at the same temperatures. The results from the two different measurements are shown in figure 5.10. The absolute values deviate with approximately 50% and the loss peak position differs by almost 0.2 decade. These discrepancies are quite big but within the error that we expect from uncertainty in the degree of filling of the transducer, and consistent with the type of discrepancies we expect. The largest absolute values are found for the measurement which has the loss peak position at the highest frequency. Figure 5.11 shows the same data, but now the loss peak is scaled in order to make a comparison of the shape of the relaxation. The agreement is seen to be good, which is also expected from our analysis, in the preceding sections.

Based on these measurements we asses that the main uncertainty on the shear measurements is due to the problems with determining x_l, and hence that the precession is determined by the model calculations in section 5.3.5.
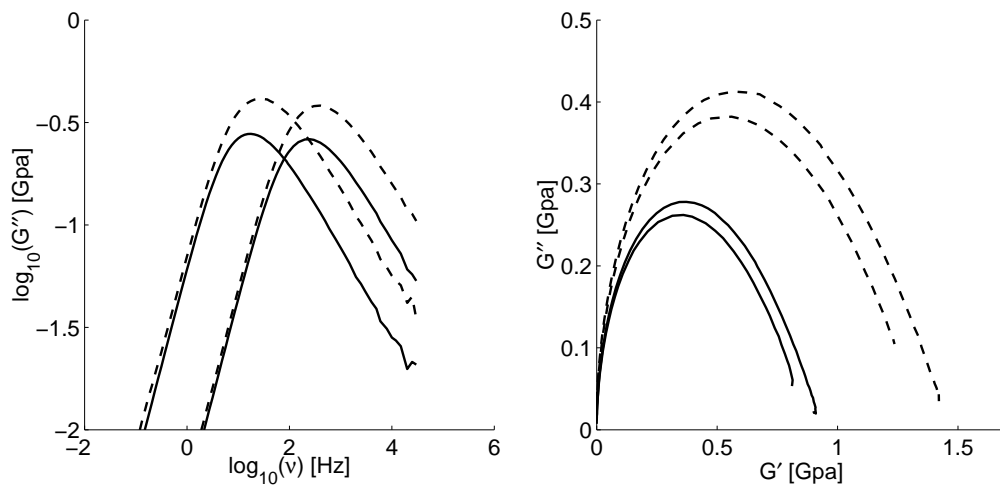
Figure 5.10 Reproduction test of shear mechanical measurement taken on DC704. Dashed lines from one measurement, solid lines from a measurement taken several months later (using a different shear transducer). The temperatures are 225.5K and 223.5K.
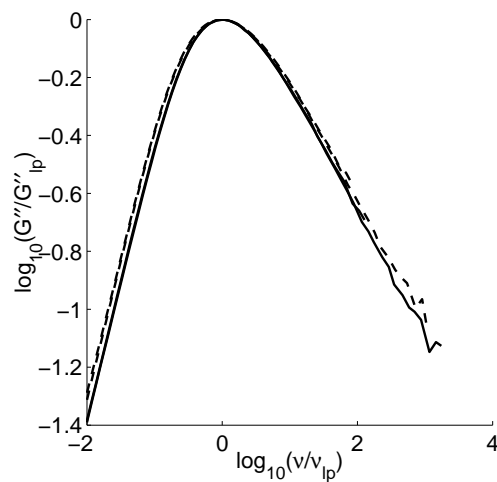

Figure 5.11 Reproduction test of shear mechanical measurement taken on DC704. Dashed lines from one measurement, solid lines from a measurement taken several months later (using a different shear transducer). The temperatures are 225.5K and 223.5K, and the data are the same as in figure 5.10. The peaks are scaled so that the shape of the measured relaxation can be directly compared. (There are really two dashed and two full curves, though this is difficult to see, due to the large degree of TTS).

5.3.8   Possible improvements of the determination of x_l

The PSG itself offers a possibility of determining the value of x_l [Christensen & Olsen, 1995], which we have not applied.

Besides the quasi-static method we have used and described, the PSG can also be used in a resonance method. The principle is that the resonance of the measured capacitance shifts when there is liquid in the transducer, and this shift is dependent on the shear modulus. The method gives the shear modulus at the frequency of the resonance which in practice means at around $1 \cdot 10^5$Hz. The result of this measurement is also dependent on x_l but in a different way than the quasi-static method. [Christensen & Olsen, 1995]

If the high frequency plateau value of the shear modules G_∞ is reached by the quasi-static method (that is below $1 \cdot 10^{4.5}$Hz) the same value should be found by the resonance method. The values will only agree if the proper x_l is used due to the different dependence on x_l. Thus a comparison can be used to determine the right value of x_l.

The method described above does not work on DHIQ, TPG, squalane nor PB20 because the beta process will lead to a frequency dependence of G in the relevant frequency interval. The method could in principle have been used on DC704, TPE and PPE.

Our electrical setup has not been in a condition to use this method because the number of frequencies monitored by the LCR-meter in the vicinity of the resonance is much too scarce to determine the exact position of the resonance. This could of course be handled by using a different instrument, but this would have required a considerable change of the setup and it would (with the available equipment) have led to a large uncertainty on the value of the measured capacitance.

5.4   The liquids; handling and chemical stability

As mentioned in the beginning of this chapter, chemical instability is always a problem because it makes i difficult to compare measurement. With our focus on comparing results from two different types of measurements it becomes critical to know if, and how fast the substances we work with change due to chemical reactions. A solution could be to make the dielectric and shear mechanical measurements simultaneously. However, this has not been possible, except in a few cases, because we had full time access to only one cryostat. In this section we will describe how we treated the substances, and show tests of their chemical stability.

All liquids are used as acquired, that is no further purification was performed. The PPE used is the Santovac®5P Vacuum Pump Fluid, and DC704 is the Dow Corning® Diffusion Pump Fluid DC704. Everything else is acquired from Sigma-Aldrich.

DC704, PPE, squalane, PB20 and TPG are stored as liquids and are not very reactive. They are loaded into the measuring cells at normal atmospheric conditions.

DHIQ is known to react very much with oxygen. The measurements we report on DHIQ are therefore obtained from samples taken from a bottle right after the sealing was broken. The breaking of the sealing as well as the loading of the gauge was performed in a container with an atmosphere of a very high nitrogen (N_2) concentration. The nitrogen atmosphere was obtained by boiling 1L liquid nitrogen per 15min at the bottom of the $0.2m^3$ container from half an hour before and during the loading.

TPE was obtained as a solid and it recrystallizes after melting when kept at room temperature. We therefore melted TPE at about 370K and loaded it immediately after by a glass syringe or a glass pipette into preheated measuring cells.

5.4.1 Tests of chemical stability

In the following we present comparison of different measurements on the substances. We use dielectric data for these tests, because there are fewer experimental problems with the dielectric measurements than with shear measurements.

The chemical changes can have very different time scales, from slow changes in the bottle to changes during filling and measuring.

We generally find that we are able to reproduce the dielectric experiments, showing that chemical changes of the liquids does not influence the results.

TPE Test of reproducibility on TPE is shown in figure 5.12. It is seen that all features are well reproduced. It seems as there is a small problem with the real part, it was impossible to scale all the curves onto each other. Some crystallization was observe after the measurement (especially in the first measurement), and it is not possible to determine if this crystallization only happened after the measurement or it has happened before or during measurement.

PPE Test of reproducibility on PPE is shown on figure 5.13. It is seen all features in the accepted data range are well reproduced. Further investigation show that the high frequency behavior described in section 7 is also reproduced.

Squalane Dielectric data was compared to the data from Richert et al. [2003] which was kindly provide in an electronic form by R. Richert. These data span a greater frequency range ($10^0 - 10^6$Hz) than the data by R. Richert which are presented together
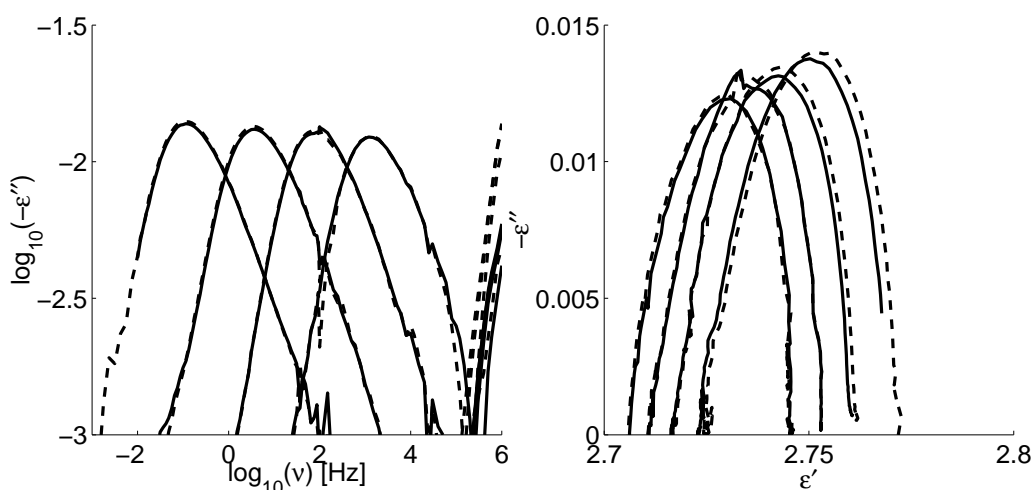

Figure 5.12 Reproduction test of dielectric measurement taken on TPE. Dashed lines from one measurement, solid lines from a measurement taken three months later. The temperatures are 256K, 262K, 268K and 274K in both cases. Values of the first data set is corrected according to equation 5.2.8 with $f = 1.006$.
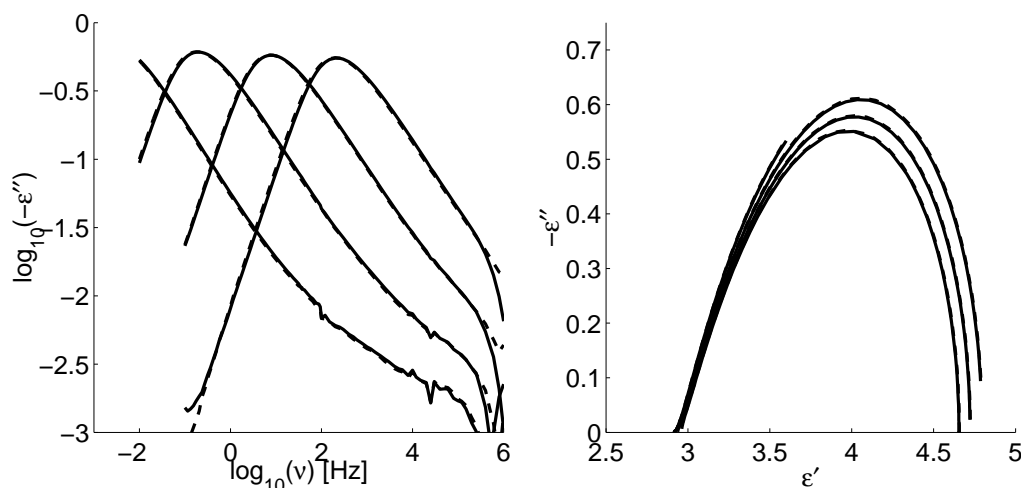
Figure 5.13 Reproduction test of dielectric measurement taken on PPE. Dashed lines from one measurement, solid lines from a measurement taken one and a half months later. The temperatures are 246.0K, 252.0K, 258.0K and 264.0K, in both cases. The data is shown raw.

with our data in chapter 6. Good agreement between our data and the data from R. Richert was found.

PB20   Test of reproducibility on PB20 is shown in figure 5.14. It is seen that the main features are well reproduced, but that the strength is so small that the LCR meter problems become pronounced.

DHIQ   DHIQ is as mentioned earlier known to be chemically unstable. To test if DHIQ changes in the bottle two measurements from the same bottle are compared in figure 5.15. A minor change in the loss peak frequencies can be seen, but the overall spectrums are reproduced.

To test the consequence of exposing DHIQ directly to air, we performed a test in which the dielectric cell was filled and measured, after this initial measurement, the cell was exposed to air for some hours and a second measurement was taken, and it was found that there was a significant change in the spectrum.

This all together shows that our way of handling DHIQ is sufficient to prevent chemical reaction between the sample and the air.

TPG   TPG is the only of the substance we work with that has a large conductance. This is seen as a large signal in the imaginary part of the dielectric constant. The amount of conductance is not reproducible from measurement to measurement but this does not seem to give rise to any change in the other parts of the spectrum. In figure 5.16 two measurements are shown, the samples are taken from the same bottle with a month separating the two measurements. It is seen that there is a good agreement between the two spectra, except for the conductance contribution.
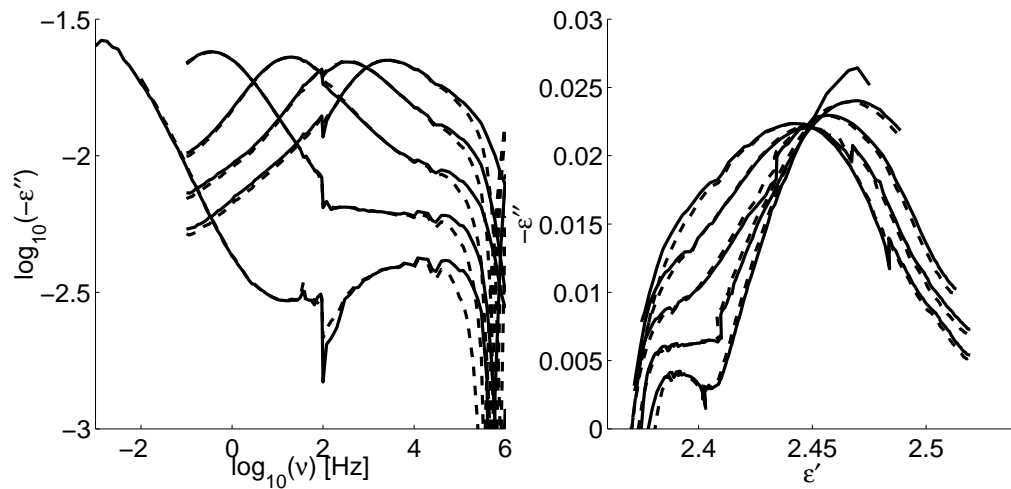
Figure 5.14 Reproduction test of dielectric measurement taken on PB20. Dashed lines from one measurement, solid lines from a measurement taken two weeks later. The temperatures are 176.0K, 182.0K, 188.0K, 194.0K, and 200.0K, in both cases. Values of the first data set is corrected according to equation 5.2.8 with $f = 1.016$.
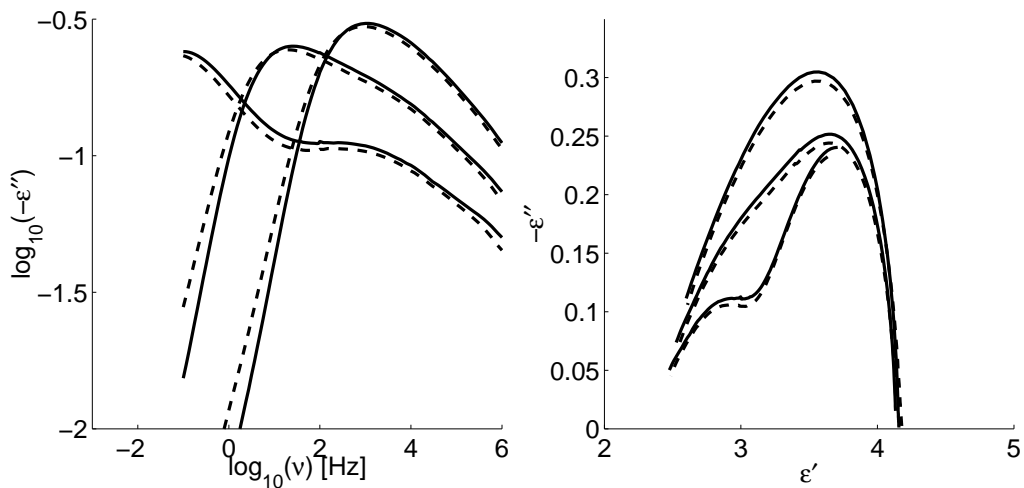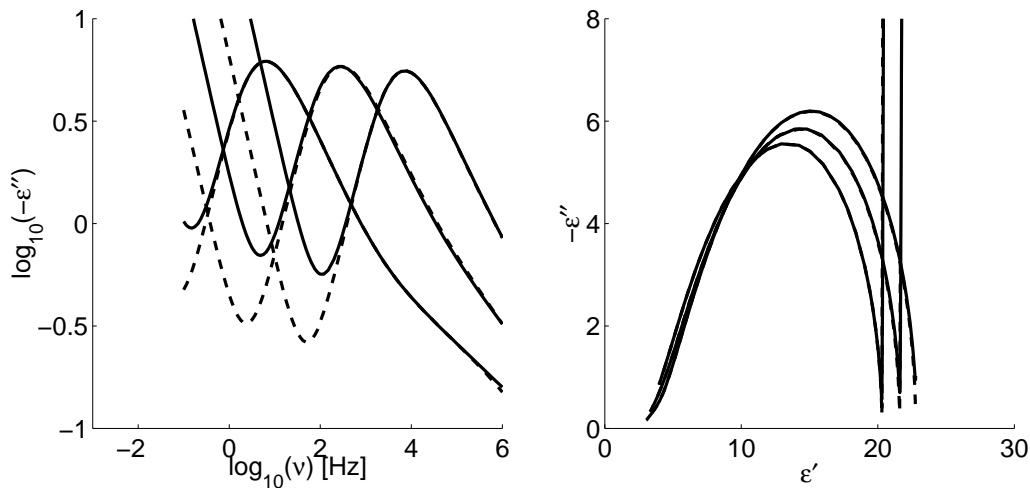

Figure 5.15 Reproduction test of dielectric measurement taken on DHIQ. Dashed lines from one measurement, solid lines from a measurement taken one months later. The temperatures are 181.2K, 185.2K, and 189.2K in both cases. Values of the first data set is corrected according to equation 5.2.8 with $f = 1.19$.

Figure 5.16 Reproduction test of dielectric measurement taken on TPG. Dashed lines from one measurement, solid lines from a measurement taken two months later. The temperatures are 201.3K, 209.3.0K, and 219.5K, in both cases. No correction for different filling was performed.

5.5 The experiments

In this section we give a description of how the experiments were performed, and of the equipment that we used beside that, which has already been described.

The liquids are loaded into the measuring gauges via a syringe and (in the case of the shear measurements) a metal needle. The measuring gauge is mounted in a measuring cell holder and placed in a cryostat.

The measurement are generally performed in the following way:

- The measurements are taken in the temperature interval where the loss peak position is within the frequency span we cover. The relevant temperature interval is estimated from preliminary dielectric measurements.

- The system is cooled to the highest temperature where measurement are to be taken.

- The system is left to equilibrate at this temperature for 5 hours (thermal equilibrium is reached much faster, giving the liquid plenty of time to reach thermodynamic equilibrium).

- The system is further cooled by stepping down through the desired temperatures (normally the steps are 2K) and two measurements are taken at each temperature.

- At each temperate the liquid is left for 30 minutes to equilibrate before the first measurement is taken, and then left for 30 minutes again before the second measurement.

By having two measurements at each temperature we are able to determine if we are in thermodynamic equilibrium at each temperature, simply by comparing the first and second measurement. Hence, if the liquid is out of equilibrium the two spectra will differ due to annealing. By this procedure it was found that, at the used cooling rate, we generally fall out of equilibrium when the loss peak of the measured quantity is at approximately 10^{-3}Hz.

The cryostat

The cryostat is a liquid nitrogen cooled cryostat homebuilt at IMFUFA, RUC. The temperature is controlled by having a constant flow of nitrogen giving a constant cooling, and a variable heating produced by a heating coil.

The cryostat setup has an absolute certainty on the temperature better than 0.2K, and a temperature stability better than 20mK Rasmussen [2003]. This uncertainty will influence the loss peak position and also the shape of the relaxation curve. However, the effect is minor, especially compared to the uncertainty on the shear loss peak position.

A temperature calibration of the cryostat was performed during our work. We have after this calibration recalculated the temperatures of the measurements, which were performed before the calibration. This is why some of our measurements are taken at unevenly spaced temperatures.

6 Raw data

The aim of this section is to give a complete overview of the data we have taken.

The raw data are shown on 6.2 to figure 6.8. There is a figure per substance, showing imaginary part and Cole-Cole plot for both the shear modulus and the dielectric constant. We only show a subset of the temperatures we have measured at, 3 or 4 temperatures for each liquid, and generally with a step of 4 degrees between each measurement. All data shown are measured at thermodynamic equilibrium and the shear and the dielectric data shown are (except for the case of DHIQ) obtained at the same temperatures.

Many of the curves appear similar, but the scaling on the axes of the dielectric data is dramatically different from substance to substance, due to the big difference in strength. We have plotted dielectric data from some of the substances together in figure 6.1 to illustrate how different they are.

Figure 6.1 Cole-Cole plots illustrating the difference in dielectric relaxation strength. The substances shown are (listed in order of decreasing strength) TPG, PPE, DC704 and TPE. The right plot is a zoomed version og the left plot (notice the axis). We have only included some of the substances in order to make the figure readable. DHIQ has a strength comparable to PPE, the strength of PB20 is close to that of DC704 and the strength of squalane is about 5 timed smaller than that of TPE.

TPE and DC704   (figure 6.2 and 6.3) Both liquids are without any visible beta relaxation, and have small dielectric strength. TPE has such a small strength that noise is seen in the dielectric signal.

PPE   (figure 6.4) No beta relaxation is seen in the shear modulus or dielectric constant of PPE. A deviation from power law behavior is seen in the high frequency tail of the dielectric spectrum, but not in the shear data.

Squalane   (figure 6.5) Squalane has an extremely small dielectric strength and it is very difficult for us to get any decent data, with the available equipment. The alpha peak can be seen in the low frequencies, but the high frequencies are heavily dominated by noise and the systematic error of the LCR-mete. We have subtracted a loss from a measurement deep in the glass (162K) to get rid of as much of the systematic error as possible. The beta peak is still present in the glass, and this means that the beta peak is not visible after this procedure.

We have been very fortunate that R. Richert has provided us with unpublished dielectric data on squalane [Richert, 2003] which are obtained with a AH2700A "Andeen-Hagerling ultra-precision capacitance bridge". The data from R. Richert are in a very limited frequency range (50Hz to 2000Hz), but have much less noise. The results agree well with our data and we have been able to patch together [1] two of the measurements with our own data. This all in all leads to a reasonable amount of dielectric data on squalane.

PB20   (figure 6.6) A pronounced beta relaxation is seen in the shear mechanics and a less pronounced dielectric beta relaxation is seen. The strength of PB20 is small and the beta relaxation in the dielectric constant is unfortunately heavily disturbed, by the LCR-meter artifacts, due to its even smaller strength.

At the low frequency side of the alpha peak, a pronounced deviation from power law behavior is seen in the dielectric constant.

Similar[2] polybutadienes have been investigated by dielectric spectroscopy by Deegan & Nagel [1995] and Zorn et al. [1997]. Both groups find a behavior similarly to what we see. In Deegan & Nagel [1995] the low frequency dielectric tail is attributed to what is known as an alpha prime relaxation, which is commonly seen in polymeric systems.

DHIQ   (figure 6.7) A very pronounced beta relaxation is seen in both the shear mechanical and dielectric signal. The beta is positioned at such a low frequencies that we are able to see the actual *peak* in the shear data.

The data on DHIQ are not obtained at the exact same temperature. This is because the dielectric measurement used is from before a temperature calibration and the shear data are from after. Our conclusions regarding DHIQ are not affected by the small deviations in temperature because the quantitative agreement with the model is very poor in the case of DHIQ, see section 9.3.

TPG   (figure 6.8) The most prominent fact about TPG is the large strength. Conductance exist in TPG giving a raise in the imaginary part at the low frequency side of the alpha peak. We are not interested in comparing the conductance to the shear behavior and we have therefore limited the data range on the left side of the alpha peak – in the plots of raw data as well as in the further investigations.

---

[1]A calculation equivalent to the one in section 5.2 shows that if the dielectric constant is measured (on the same substance) using two capacitors with different filling and different ability to contract, the two measured dielectric constants (ε_1 and ε_2) will (to first order) be connected as $\varepsilon_1 = a\varepsilon_2 + b$, where a and b are temperature dependent uncorrelated constants.

[2]Deegan & Nagel [1995] use a polybutadiene with the same composition as the one we study, but with a molecular weight of 6000g/mol. Zorn et al. [1997] investigate a series of polybutadiene with different compostion.

A beta relaxation is again seen in both the shear modulus and the dielectric constant. It is most pronounced in the shear modulus, which can be clearly seen by comparing the two Cole-Cole plots.
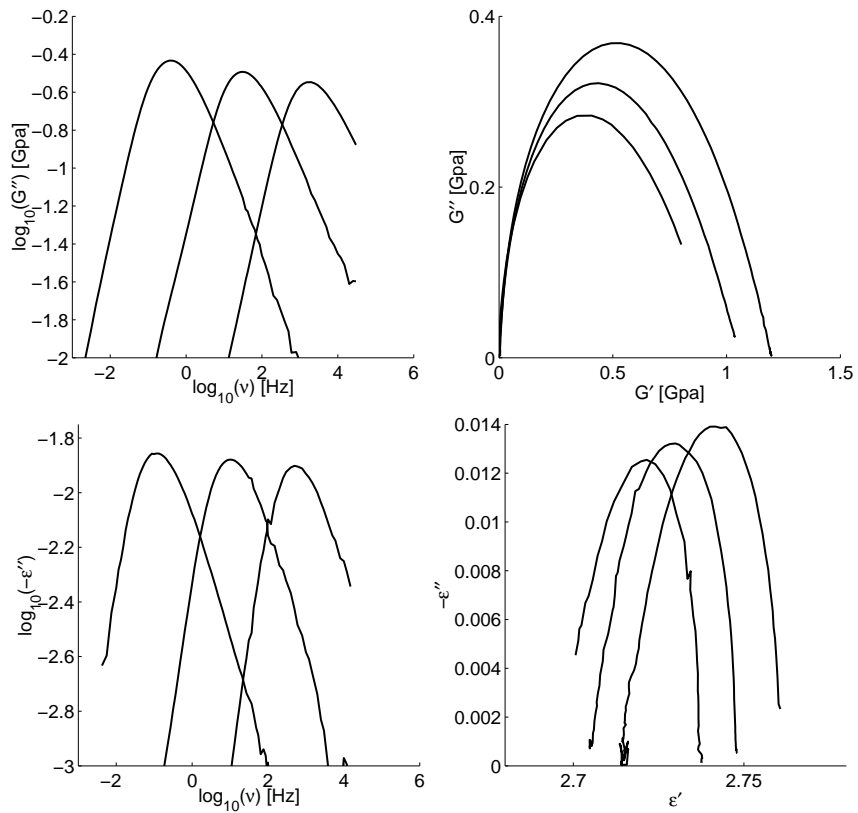

Figure 6.2 TPE shear and dielectric data. 256.0K, 264.0K, and 272.0K.

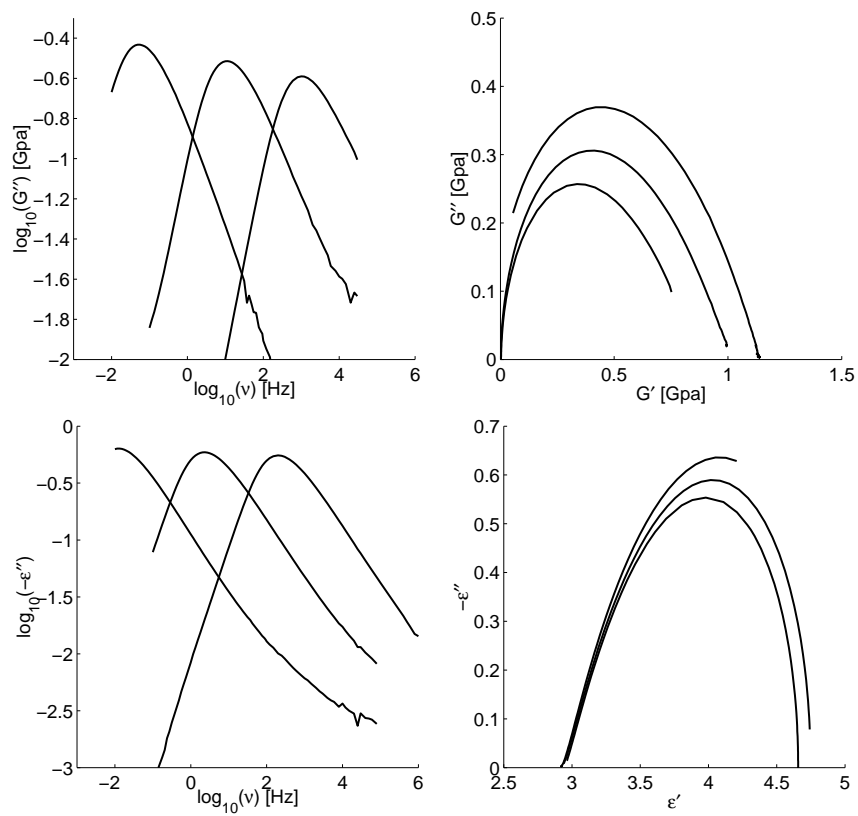**Figure 6.3** DC704 shear and dielectric data. 215.5K, 223.5K, and 231.6K.

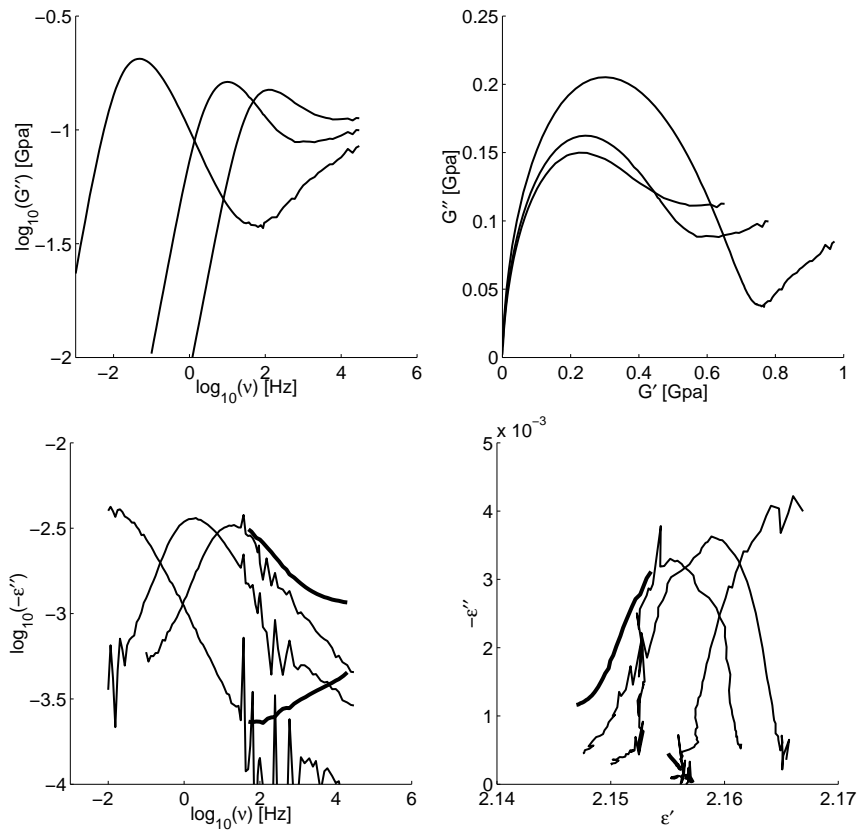**Figure 6.4** PPE shear and dielectric data. 248.0K, 256.0K, and 264.0K.

Figure 6.5 Squalane shear and dielectric data. 170.0K, 176.0K, and 180.0K. Bold line shows dielectric data from Richert [2003].

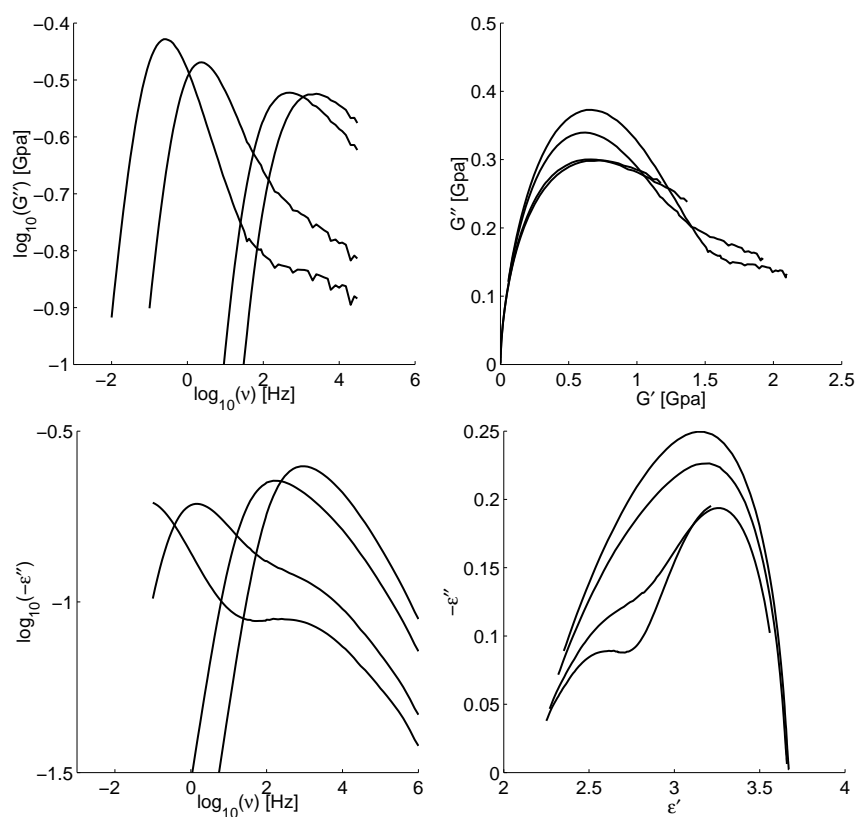**Figure 6.6** PB20 shear and dielectric data. 178.0K, 186.0K, and 194.0K.

Figure 6.7 DHIQ shear data taken at 181.5K, 183.0K, 187.5K, and 189.5K, and DHIQ dielectric data taken at 181.2K, 183.2K, 187.2K, and 189.2K.
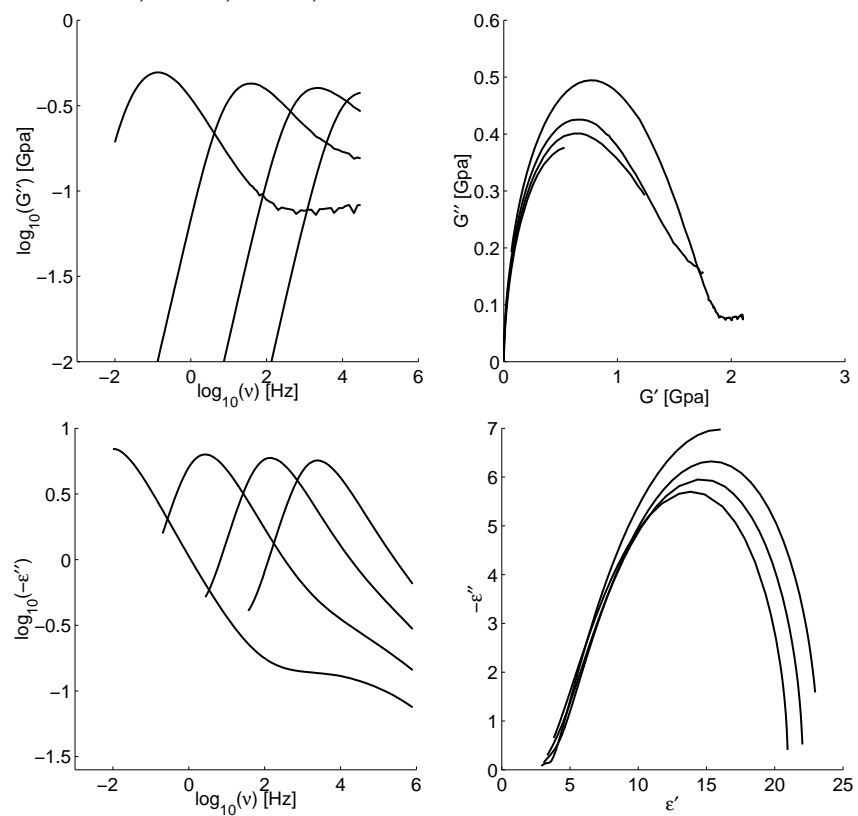

Figure 6.8 TPG shear and dielectric data. 192.0K, 200.0K, 208.0K, and 216.0K.

7 Elastic contribution to the high frequency dielectric constant

In this chapter we look closer at the high frequency plateau values of the dielectric constant, in order to establish if it behaves qualitatively in accordance with the DiMarzio-Bishop model.

7.1 The DiMarzio-Bishop model in the high frequency limit

The high frequency limit of the dielectric spectra is according to the DiMarzio-Bishop model (equation 4.7.2) given by[1]

$$
\chi_h = \varepsilon_h - 1 = \frac{N}{\varepsilon_0} \left(\alpha_i + \frac{\mu^2}{3k_B T \left(1 + \left(\frac{4\pi r^3}{k_B T} \right) G_\infty \right)} \right) ,
$$

indicating that there is an elastic contribution to the high frequency limit of the dielectric constant. The elastic contribution cannot be detected directly from our measurements due to the uncertainties on absolute values of the dielectric constant. However, we have performed an analysis which enables us to detect the elastic contribution via its temperature dependence.

7.2 Possible effects of expansion

Taking the experimental problems, described in section 5.2.1, into account it is found that the following effects control the change in the measured ε_h as the temperature is increased.

- Model predictions
  Effect giving increasing ε_h

    - G_∞ decreases

  Effects giving decreasing ε_h

    - N decreases due to thermal expansion
    - T increases

---

[1]We here use the model in the Maxwell field approximation, but the conclusions are general because ε always is a monotonic growing function of α.

- Experimental problems
  Effect giving increasing ε_h

    – Liquid expands in the radial direction

  Effects giving decreasing ε_h

    – Spacing between capacitor plates increases due to the thermal expansion

We assume that the microscopic molecular induced polarizability, α_i is temperature independent[2]. This assumption implies that ε_i only is temperature dependent via the density.

It can be seen that there are two effects giving a increase in the measured dielectric constant: The elastic contribution and the contribution from radial expansion. We will however show that an actual increase in the measured ε_h with temperature is a fingerprint of an elastic contribution, because it can not be due to the expansion of the liquid alone.

To analyze this we look at the hypothetic situation where the liquid only expands in the radial direction and no elastic contribution exist. This means that the microsopic polarization is considered temperature independent leading to $\varepsilon_h = N\alpha_i/(\varepsilon_0) + 1$.

We start with a situation where the capacitor is not necessarily completely filled. The measured dielectric constant ε_m can, in this situation, be described by an equation of the same type as equation 5.2.6.

The measured capacitance becomes

$$C_m = \frac{\varepsilon\varepsilon_0 A_0(1 - \Delta b)}{d} + \frac{\varepsilon_0 A_0 \Delta b}{d} + \frac{\varepsilon_0(A_g - A_0)}{d},$$

where A_0 is the area that is filled at T_0. A_g is the total area of the capacitor plates, and d is the fixed distance between the capacitor plates. Δb is redefined to describe the difference between the actual temperature dependent filling and A_0.

Dividing with the geometric capacitance $\frac{\varepsilon_0 A_g}{d}$ yields the measured dielectric constant

$$\varepsilon_m = A_r\varepsilon(1 - \Delta b) + A_r\Delta b + 1 - A_r \qquad (7.2.1)$$
$$= A_r\Delta b(1 - \varepsilon) + A_r\varepsilon + 1 - A_r, \qquad (7.2.2)$$

where $A_r = \frac{A_0}{A_G}$. It is seen that at the initial situation (corresponding to $\Delta b = 0$) the measured capacitance is given as $\varepsilon_m = A_r\varepsilon + 1 - A_r$.

We would like to know how a differential change in the temperature, changes the measured dielectric constant. Given an initial temperature T_0 with a corresponding A_0, we want to find $\varepsilon_m(T_0 + \Delta T)$. This can be achieved by looking at a first order expansions in temperature of the controlling parameters ε_h and Δb, as the relevant change in temperature is differential.

Expanding the change in ε_h and Δb to first order around T_0 gives (recalling that $\varepsilon_h(T_0) = 1 + \frac{N(T_0)}{\varepsilon_0}\alpha_i$)

$$\varepsilon_h(T_0 + \Delta T) = \varepsilon_h(T_0) - \frac{\alpha_i}{\varepsilon_0}\alpha N(T_0)\Delta T$$
$$\Delta b(T_0 + \Delta T) = -\alpha\Delta T,$$

---

[2]This assumption is standard [Böttcher, 1973], [Jonscher, 1983] and it is for example applied to determine expansion coefficients of glass forming liquids from dielectric measurements in Bauer et. al. [2000] and Bauer et. al. [2001].

where α is the thermal expansion rate.

Using these approximations in equation 7.2.1 and only keeping first order terms in ΔT leads to

$$
\begin{aligned}
\varepsilon_m(T_0 + \Delta T) &= A_r \left(-\alpha\Delta T \left(1 - \left(\varepsilon_h(T_0) - \frac{\alpha_i}{\varepsilon_0}\alpha N(T_0)\Delta T \right) \right) \right) + \\
&\quad A_r \left(\varepsilon_h(T_0) - \frac{\alpha_i}{\varepsilon_0}\alpha N(T_0)\Delta T \right) + 1 - A_r \\
&= A_r \left(-\alpha\Delta T \left(-\frac{N(T_0)}{\varepsilon_0}\alpha_i + \frac{\alpha_i}{\varepsilon_0}\alpha N(T_0)\Delta T \right) \right) + \\
&\quad A_r \left(\varepsilon_h(T_0) - \frac{\alpha_i}{\varepsilon_0}\alpha N(T_0)\Delta T \right) + 1 - A_r \\
&= A_r\varepsilon_h(T_0) + 1 - A_r = \varepsilon_m(T_0). \qquad (7.2.3)
\end{aligned}
$$

The final equality is seen from the equation describing the measured capacitance, and by remembering that $\Delta b = 0$ at T_0.

The result shows that a pure radial expansion and a temperature independent microscopic polarizability yields a temperature independent measured ε_h, because two counteracting effects cancel out each other. Radial expansion is expected to dominate at high temperatures where the liquid easily will flow between the plates in the transducer.

A decrease in the measured ε_h can occur if the liquid expands in the direction perpendicular to the capacitor plates whereby the distance between the plates grows. Expansion perpendicular to the plates is expected at temperatures close to T_g, because the rigid liquid will be clamped to the plates.

The conclusion of this calculation is that an increase in the measured ε_h value with increasing temperature *has* to be due to an increase in the microscopic polarizability itself.

7.3 High frequency data

In order to study the temperature dependence of the high frequency dielectric limit it is necessary to have a number of temperatures, at which this limit is well determined. In practice this means that the liquid has to be well relaxed at about 100kHz because our maximum frequency is 1MHz. The three liquids without beta relaxation (TPE, DC704 and PPE) fulfill this requirement. We have used Havriliak-Negami fits to get ε_h values which were unaffected by noise on the curve. The fits were good for TPE and DC704, while the PPE fits were less convincing due to the deviation from power law behavior. The values found in the fit might underestimate the temperature dependence. However, the tendencies of the temperature dependence found is indisputable. This can be seen directly from the raw data in figure 7.1.

The temperature dependencies of ε_h are shown explicitly in figure 7.2. TPE shows a decrease in ε_h with temperature. The tendency is the same for DC704 but the temperature dependence is not as strong. PPE, on the other hand, shows an incraese in ε_h with increasing temperature.
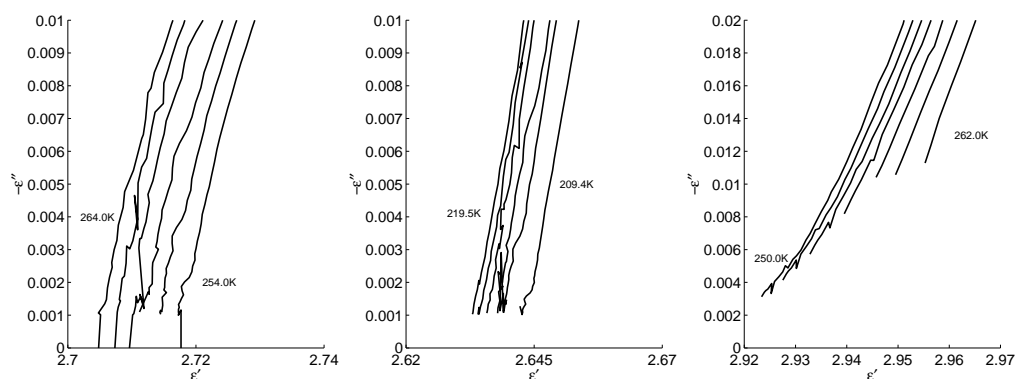
Figure 7.1 Dielectric data from TPE, DC704 and PPE (shown in this order from left to right). The figure shows zooms of the high frequency end of the Cole-Cole plot.
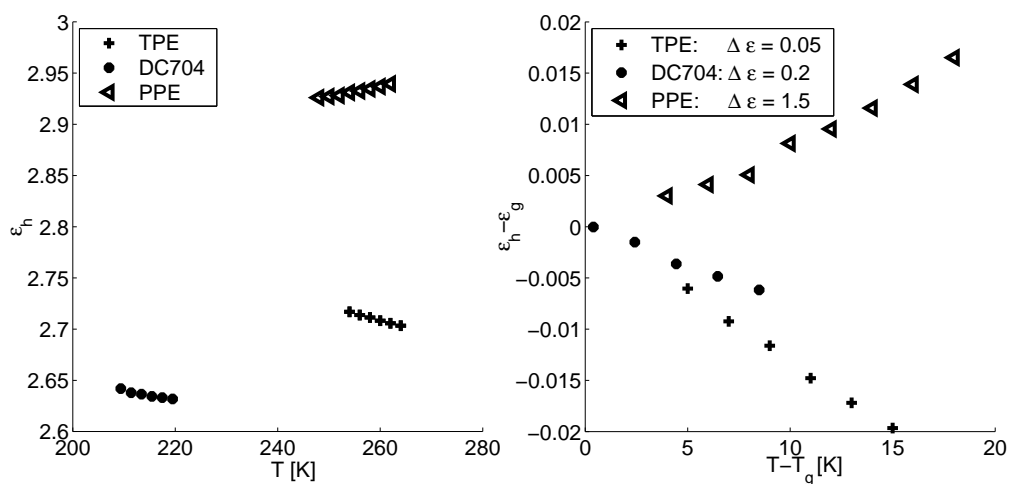

Figure 7.2 High frequence dielectric behavior. The left figure shows absolute values. In the right figure the data has been translated (not scaled) in order to facilitate comparison.

7.4   Interpretation

The increasing value of ε_h of PPE with increasing temperature is an inevitable sign of an increase in the microscopic high frequency polarizability with temperature. Returning to equation 4.3.1, we see that the microscopic polarizability in terms of the DiMarzio-Bishop model is given by:

$$\alpha_h = \alpha_i + \frac{\mu^2}{3k_B T + 12\pi r^3 G_\infty}. \tag{7.4.1}$$

All our data show that G_∞ decreases with increasing temperature (see chapter 6), corresponding to a softening of the elasticity as the liquid becomes warmer. This means that the DiMarzio-Bishop model predicts an increase in α_h if the following relation holds

$$3k_B \Delta T < \left| 12\pi r^3 \Delta G_\infty \right|, \tag{7.4.2}$$

where ΔG_∞ is the change in G_∞ which corresponds to ΔT. A comparison of the orders of magnitudes show that the above relation holds if r is greater than approximately 0.5Å. Thus, an increase of α_h with temperature is consistent with the DiMarzio-Bishop model. We noted in section 4.4 that the elastic contribution to ε_h is larger for smaller values of r. The above inequality shows us that the temperature dependence of the elastic contribution is stronger if r is large.

The physical interpretation of an increasing α_h is simply that the elastic forces which determine how much the dipoles can turn get weaker as temperature is increased. This interpretation is not dependent on the DiMarzio-Bishop model, in the sense that any "elastic contribution" to the polarizability is expected to show this behavior. Hence it could also be an elastic contribution which is coupled to the shear modulus in a different way, or a contribution which is also (or only) related to the bulk modulus.

The decreasing ε_h values which are seen for TPE and DC704 do not necessarily mean that α_h decreases with temperature, because a decrease of the measured ε_h can be due to expansion of the liquid in the direction perpendicular to the capacitor plates.

In the following we suggest a consistent interpretation of the different behaviors of the three liquids in terms of their in dielectric strength.

The difference between the high frequency and the low frequency values of the dielectric constant for TPE is approximately 1%, indicating that the dipoles contribution to the total dielectric constant is very small. In the notation of section 3.2.1 it can be put as $\alpha_r \ll \alpha_i$. This means that a relative change of the high frequency limit of α_r has little relative effect on the total α_h, making the latter virtually temperature independent. It is therefore the expansion which controls the temperature dependence of the total measured high frequency dielectric constant. DC704 has a relative strength of approximately 10%. This implies that the less pronounced decrease of ε_h with increasing temperature can be attributed to a greater significance of α_r on the total temperature dependence. PPE has a relative strength of approximately 50%, and this is why the high frequency value of α_r dominates over the other effects, which influence the total temperature dependence of ε_h.

It is reasonable to assume that PPE expands in the direction perpendicular to the capacitor plates just as the other liquids. The increase in ε_h is therefore a sign of a larger increase in α_h than what is seen directly. If the expansion coefficient under the given circumstances was well determined then it would be possible to make a quantitative comparison of the temperature dependence of ε_h and G_∞. However with our uncertainties

it is not possible to neither prove nor falsify the DiMarzio-Bishop models quantitative predictions regarding the relation between the temperature dependencies of ε_h and G_∞.

8 Shear mechanical and dielectric loss peak shape and position

After focusing on merely the high frequency behavior in last chapter, we will consider the entire relaxation spectrum, in terms of the DiMarzio-Bishop model, in this and the following two chapters.

The objective of this chapter is to establish whether the DiMarzio-Bishop model provides qualitatively correct predictions regarding the relationship between the actual dielectric and shear mechanical relaxation spectra. We consider the results of this chapter cardinal to our discussion of the DiMarzio-Bishop model's quality as a tool for understanding the fundamental mechanisms of dielectric relaxation.

8.1 Predictions from the DiMarzio-Bishop model

When characterizing relaxation spectra it is often done in terms of the loss peak width, shape and position. The relation between the shear and dielectric behavior with respect to these features is therefore central for a qualitative comparison between the two relaxations. Therefore, we examine what the DiMarzio-Bishop model predicts regarding the differences between the shear mechanical loss peaks and the dielectric loss peaks, and compare these predictions to our data.

Our general procedure for determining predictions of the DiMarzio-Bishop model is to calculate a fictive shear mechanical spectrum using a realistic phenomenological model, and to subsequently use this shear spectrum as input to calculate the corresponding dielectric spectrum, from the DiMarzio-Bishop model.

We start by rewriting the model expression (see section 4.4), to a form where the normalized elastic contribution $a = \frac{\varepsilon_h - \varepsilon_i}{\varepsilon_e - \varepsilon_i}$ is explicitly uses as a parameter

$$\frac{\varepsilon(\omega) - \varepsilon_i}{\varepsilon_e - \varepsilon_i} = \frac{1}{1 + \frac{1/a - 1}{G_\infty} G(\omega)}. \tag{8.1.1}$$

The parameter a is a measure of how big the high frequency rotational polarization $(\varepsilon_h - \varepsilon_i)$ is compared to the total equilibrium rotational polarization $(\varepsilon_e - \varepsilon_i)$. From this formulation it also becomes clear that a controls how the relaxation shape and position changes when going from shear modulus to dielectric constant.

8.1.1 Alpha peak

We start by considering a simple spectrum with an alpha peak, but no beta peak, and we analyze the connection between the shear modulus, the dielectric constant, and the dielectric modulus.

The shear spectrum was calculated using an extended Maxwell model (see equation B.2), and the dielectric constant and modulus were calculated from this, using the DiMarzio-Bishop model in the formulation above. The results are illustrated on figure 8.1 (see the caption on the figure for details about the parameters used). It can be
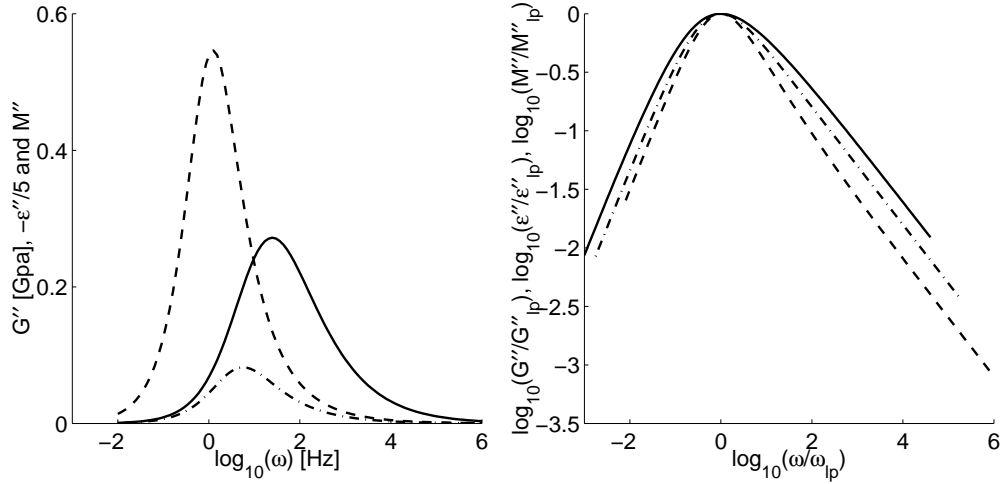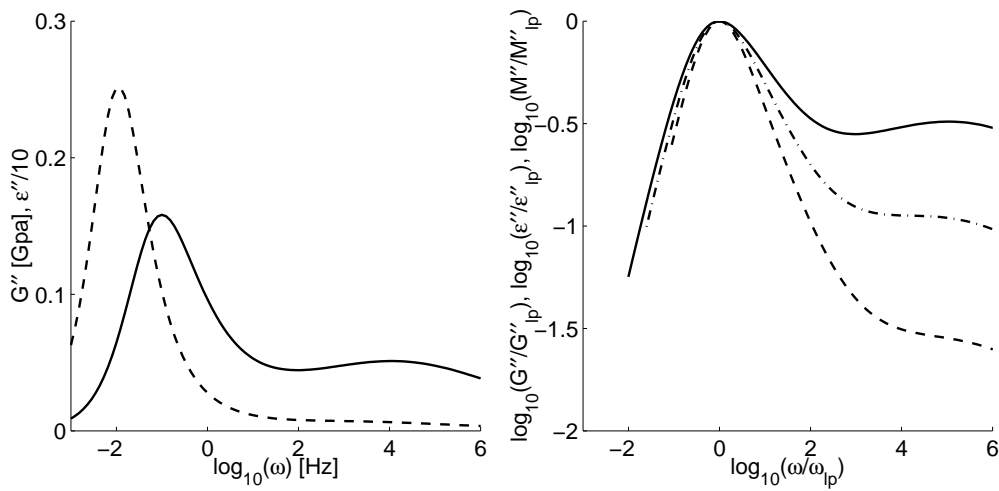

Figure 8.1 Simulated shear modulus (full lines), dielectric constant (dashed lines), and dielectric modulus (dash-dotted line). The shear data is calculated according to an extended Maxwell model (equation B.2) with $G_\infty = 1.0$GPa, $\alpha = 0.5$, $q = 1.5$ and $\tau_M = 0.1$s. The dielectric data is found from these shear data by using the DiMarzio-Bishop model (equation 8.1.1) and $\varepsilon_e = 10.0$, $\varepsilon_i = 2.0$ and $a = 0.1$ (corresponding to $\varepsilon_h = 2.8$). The left plot shows the raw loss peaks illustrating the difference in loss peak position. The right plot shows a comparison of the shape of the relaxation plots. This is done in a log-log plot, and the data have been scaled by the maximum loss and plotted against a reduced frequency in order to make the peak positions coalesce.

seen that the dielectric loss peak frequency attains a lower value than the shear mechanical loss peak frequency. Moreover, it can be seen that the loss peak in the dielectric signal is narrow compared to the loss peak in the shear modulus.

This is of course only an example and care must be taken not to make conclusions, which would be altered if another set of parameters was used. By looking at the DiMarzio-Bishop model (e.g. equation 8.1.1), it can be seen that the choice of ε_i and ε_e cannot change the shape of the imaginary part of the dielectric constant nor the dielectric loss peak position. A complete analysis of the DiMarzio-Bishop model's predictions can consequently be performed merely by letting a vary through values between 0 and 1. It is found by inspection that the qualitative findings are universal. However, the dielectric constant approaches the shear modulus in both shape and position as a is increased. The limiting behavior, corresponding to $a \approx 1$, is thus perfect agreement between the two relaxations.

The dielectric modulus will always have a higher loss peak frequency than the dielectric constant[1]. The DiMarzio-Bishop model predicts that the dielectric modulus lies between the dielectric constant and the shear modulus, both regarding loss peak position and curve width. This predicted relation between shear modulus and dielectric modulus, is contrary to the predicted relation between shear modulus and dielectric constant, dependent on the dielectric relaxation strength. The DiMarzio-Bishop model predicts

---

[1] $M'' = -\frac{\varepsilon''}{|\varepsilon|^2}$ where $|\varepsilon|$ is the absolute value of ε, which is a monotonic decreasing function of frequency.

that the dielectric modulus approaches the shear modulus as the dielectric strength is increased (keeping *a* constant).

8.1.2   Beta peak

To analyze what the DiMarzio-Bishop model predicts about a case with a beta relaxation, a shear mechanical signal with a beta relaxation was constructed using the "mechanical alpha-beta-model" (equation B.3) choosing the same shape of the alpha peak as above, and a rather pronounced beta peak. The results can be seen in figure 8.2 along with details about the simulation.

Figure 8.2 Simulated shear (full lines), dielectric constant (dashed lines) and dielectric modulus (dash-dotted line). The shear data is calculated according to an extended Maxwell model with a beta contribution (equation B.3) with $G_\infty = 1.0$GPa, $\alpha = 0.5$, $q = 1.5$, $\tau_\alpha = 10$s, $G_f = 1$, $\tau_\beta = 1 \cdot 10^{-3}$s and $\beta = 0.25$. The dielectric data is found from these shear data by using the DiMarzio-Bishop model (equation 8.1.1) and $\varepsilon_e = 10.0$, $\varepsilon_i = 2.0$ and $a = 0.1$.

It is seen that the DiMarzio-Bishop model predicts that the beta relaxation becomes much less pronounced in the dielectric signal. By close inspection it is additionally seen that the dielectric beta peak is predicted at a lower frequency than the mechanical beta peak, as it was seen for the alpha peaks. In the plot where the shapes of relaxation curves are shown it is again seen that the dielectric modulus, according to the DiMarzio-Bishop model, lies between the dielectric constant and shear mechanical modulus, which is broadest of the three.

8.2   Comparisons on our data

In this section a qualitative comparison of the dielectric and shear mechanical data is presented. The focus is of course on testing whether the model predictions made in last section hold.

8.2.1 Position of loss peak

Looking at the raw data (see section 6), it is seen that the loss peak of the dielectric constant is shifted to lower frequencies compared to the loss peak in the shear modulus. This is in perfect agreement with the prediction of the DiMarzio-Bishop model. To substantiate this, and to test how the two loss peaks changes with temperature, a loss peak decoupling plot is presented on figure 8.3. This type of plot has been introduced by Zorn et al. [1997].

It was in section 5.3.5 found that we measure the loss peak position in the shear mechanics with an uncertainty of maximum 0.2 decade, and it was argued that there is a systematic error which makes it more likely to measure a too high loss peak frequency. However, the differences between the ε and G loss peaks (ranging from 0.4 to 1.2 decade), are significantly greater than experimental uncertainties.

The difference between the loss peak position of shear modulus and dielectric modulus are also shown for the substances with large dielectric strength (PPE and TPG). The dielectric modulus of PPE lies at lower frequencies than the shear mechanical modulus as predicted from the DiMarzio-Bishop model, but this does not hold for TPG. The difference between the shear loss peak and the dielectric modulus loss peak of TPG is, according to the DiMarzio-Bishop model, expected to be small due to the very large dielectric strength of TPG, and the difference between the two is not much bigger than our uncertainty on the shear loss peak position. We do however believe the difference is significant and indicates a genuine deviation from the model predictions.

For the substances with only an alpha peak, it is seen that the shift in loss peak is fairly temperature independent. On the contrary for the substances with a beta relaxation, it is generally seen that the shift becomes very temperature dependent (TPG being a counter example).

We have used the simple maximum loss peak as a substitute for the alpha loss peak position, because it is impossible to perform a reliable separation of the beta and the alpha peak, especially in the case of the shear data, where the shear loss peak is not reached by our measurements. The merging with the beta peak will alter the behavior of the maximum loss frequency compared to a situation with a pure alpha peak. The decoupling between the loss peaks for the substances with a beta relaxation can therefore be interpreted as a difference in how the alpha and beta relaxation merges in the shear mechanical and dielectric relaxation.

8.2.2 Shape of the relaxation curve

We have showed that, if the DiMarzio-Bishop model is correct, then the alpha loss peak of the dielectric constant will be narrower than the peak of the shear modulus. This is generally consistent with what we see on figure 8.4 (the figure only shows one temperature for each substance, but we will in section 13.1 show that the shape is nearly temperature independent). For DC704, PPE, and TPG it is easily seen that the shear peak is wider than the dielectric peak, though the difference is small.

For squalane no clear difference between the two curves can be seen around the alpha peak. TPE exhibits a very small difference between the two relaxation curves, but the difference seen is in contrast to the model prediction because the dielectric peak is wider than the shear peak. The widening of the dielectric curve on the left side of the peak seen
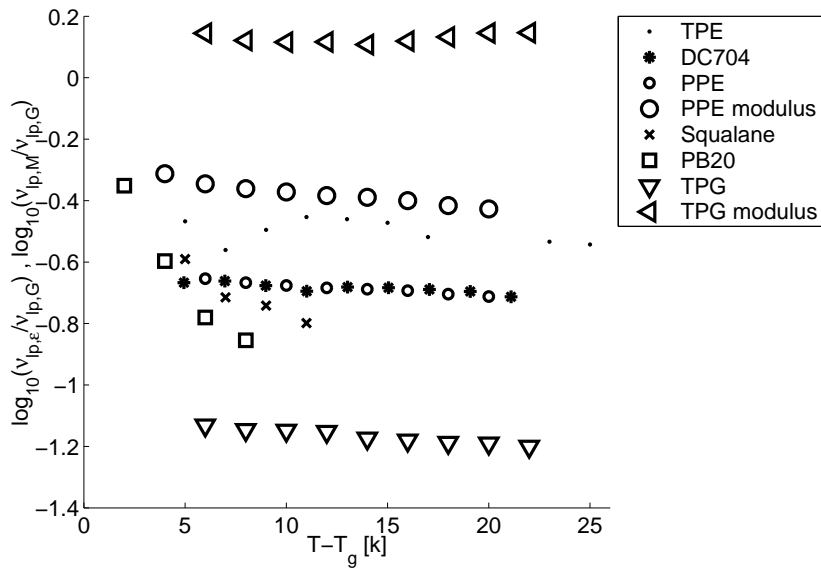
Figure 8.3 The logarithmic shift in shear loss peak compared to the dielectric loss peak at the same temperature. This is sometimes referred to as the decoupling index between dielectric and shear mechanical relaxation. The dielectric constant is generally used for the dielectric data. The loss peak of the dielectric constant and the dielectric modulus coalesce for liquids of small strength (TPE, DC704, squalane and PB20); for PPE and TPG both the M and ε loss peaks are compared to G loss peaks.

in PB20 is possibly due to the alpha prime relaxation, which is only seen in the dielectric spectrum.

The position of the dielectric modulus of TPG deviated from the prediction of the DiMarzio-Bishop model, and the same is found for the shape of the curve. This is illustrated in figure 8.5

The last qualitative prediction we showed was that the beta peak, according to the DiMarzio-Bishop model, becomes less pronounced in the dielectric constant than in the shear modulus. This is also found in our data, and seen in figure 8.4, or perhaps more convincing in the raw data in chapter 6. Notice for example the beta peak of TPG, which can hardly be seen in the dielectric Cole-Cole plot, while it is clearly seen in the shear data (figure 6.8).

DHIQ was not included in the analysis in this chapter, because we do not have proper shear and dielectric data, which are obtained at the same temperature. The raw data in figure 6.7 do however indicate that the findings hold for DHIQ as well. An exception is the beta peak of DHIQ, which is very pronounced in both response functions.

8.3   Summary

The qualitative predictions from the DiMarzio-Bishop model were generally found to be true for all the substances we have instigated.

The shear and dielectric loss peak positions has been compared several times before. The main focus is usually on the differences in temperature dependence sometimes referred to as the decoupling, because, as it is in phrased in Zorn et al. [1997]: "there is
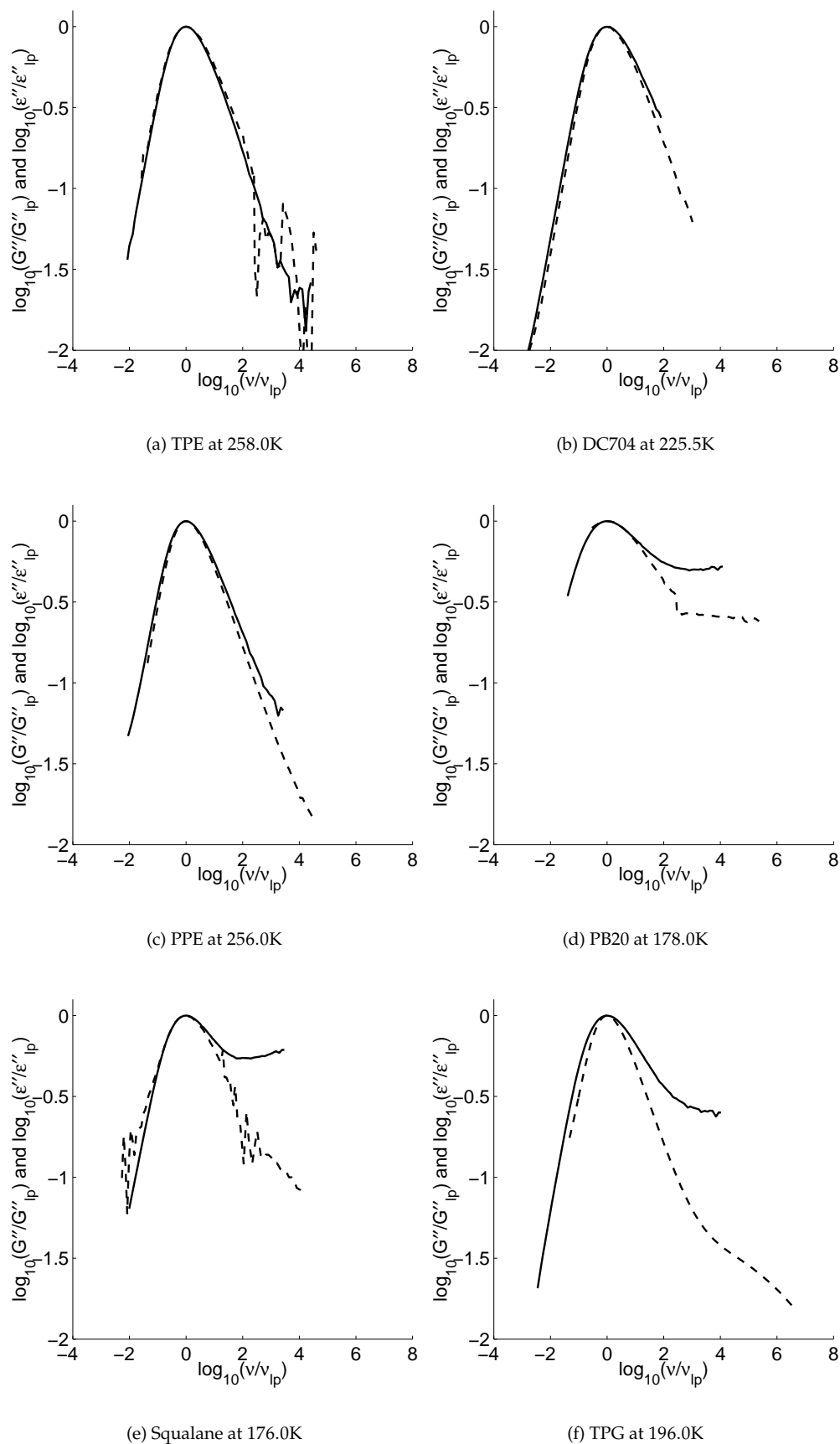
(a) TPE at 258.0K

(b) DC704 at 225.5K

(c) PPE at 256.0K

(d) PB20 at 178.0K

(e) Squalane at 176.0K

(f) TPG at 196.0K

Figure 8.4 Comparison of the dielectric and shear mechanical loss peak shape. Dashed line is dielectric constant, full line is shear modulus.
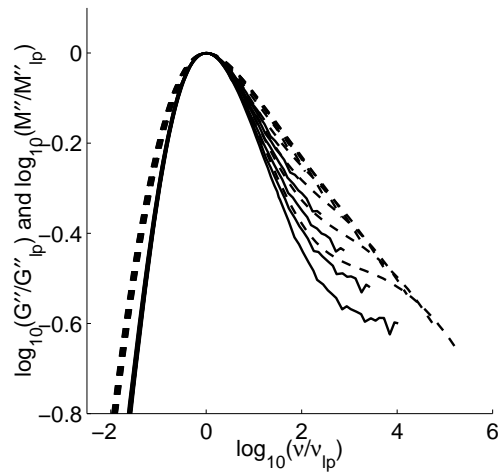
Figure 8.5 TPG. Comparison of the dielectric and shear mechanical modulus. Dashed line is dielectric modulus, full line is shear modulus. Temperatures are 196.0K to 212.0K in steps of 2K.

no reason why an arbitrarily chosen characteristic time $1/\omega_{max}$ should be identical for dielectric and rheological measurements". The general finding is that there is little or no decoupling between the two characteristic times. [Menon et al., 1994], [Christensen & Olsen, 1994], [Donth et al., 1996], [Deegan et al., 1999], [Ferri & Castellani, 2001] [Paluch, 2000], [Schröter & Donth, 2000], [Schröter & Donth, 2002], [Ribierre et al., 2003].

We have found that the DiMarzio-Bishop model predicts the shear loss peak at higher frequencies than the loss peak of the dielectric constant. This model based prediction makes it interesting to look at the absolute difference between the two loss peak positions rather than just their different temperature dependence. It is not always possible to extract the absolute difference in loss peak position from the reported data, but where it is possible, it is seen that the predictions regarding dielectric constant and shear modulus holds. Shear loss peaks are found at a higher frequency than dielectric loss peaks, with differences ranging from 0.1 to 2 decades. [Menon et al., 1994],[Christensen & Olsen, 1994], [Donth et al., 1996], [Deegan et al., 1999], [Schröter & Donth, 2000], [Schröter & Donth, 2002].

In Paluch [2000] the loss peak frequency of the dielectric modulus is found to be higher than the shear loss peak frequency. This is in contrast to the predictions of the DiMarzio-Bishop model but consistent with our experimental findings on TPG, which has a large dielectric strength. The dielectric relaxation strength is not reported in Paluch [2000] but a dielectric loss peak plot of the data from one of the two studied substances, reveals that the strengths also is large in this case, ($\Delta\varepsilon \approx 20$).

The width of the shear mechanical and dielectric relaxations have not been compared as often. Deegan et al. [1999] reports a difference in the temperature dependence of the width, but the width itself is not compared.

It is in Suchanski et al. [2000] found that the shape of the dielectric response is narrower than the shear mechanical response in agreement with the predictions of the DiMarzio-Bishop model. It is in Suchanski et al. [2000] suggested that this is because the dielectric response only couples to the charged modes, and that slow modes might not carry any dipole moments. This is discussed without any model saying that the two shapes ought to be the same.

Our analysis of the DiMarzio-Bishop model offers a simple framework for understand-

ing a lot of the differences between shear and dielectric relaxation which have been re-
ported. This agreement between model and data supports the DiMarzio-Bishop model
as a qualitative model for understanding the connection between the dielectric and
shear mechanical relaxation.

9 One parameter test of the DiMarzio-Bishop model

Our objective with this chapter is to formulate and test the model in a simple version, where only one macroscopic parameter controls both shape and position of the loss peak. An analysis on how known possible errors in the measurements affect the results is also presented.

We have earlier showed (see section 4.7) that the local field question is of lesser importance if the dielectric strength is small. We exploit this result by using a simple field and testing the model on substances with different dielectric strength (approximately 1% to 50%). This will lead to a systematic greater deviation with greater strength, if the deviations seen, are due to local field problems.

9.1 Formulation of the one parameter test

Most of the earlier test on the DiMarzio-Bishop model have been performed in the susceptibility formalism. The essence of our one parameter model test is the modulus formulation of the model in the version where the Maxwell or Lorentz field is used, as we have already presented it in equation 4.7.8:

$$G(\omega) = K_1 \frac{1}{\varepsilon(\omega) - \varepsilon_i} + K_2 \qquad (9.1.1)$$

Taking the imaginary part leads to

$$G''(\omega) = K_1 \left(\frac{1}{\varepsilon(\omega) - \varepsilon_i} \right)'' , \qquad (9.1.2)$$

because K_1 and K_2 are real.

In this formulation it is easily seen that ε_i controls both the position and the shape of the loss peak when shear behavior is predicted from dielectric data by using the DiMarzio-Bishop model. K_1 only gives a scaling, which corresponds to a simple vertical translation in a log-log plot of the loss.

ε_i has a great advantage over r, which is the main parameter in the susceptibility formulation, because it is a macroscopic quantity and its expected values can be given with much higher precision. ε_i relates to the easily measurable refraction index through $\varepsilon_i = n^2$. n^2 is generally known at room temperature, and will increase with decreasing temperature, making the room temperature value a lower boundary of ε_i values at low temperatures. Moreover, ε_i is bounded from above by the plateau value ε_h as the latter is a sum of ε_i and a contribution from rotational polarization.

The quantity $(\varepsilon(\omega) - \varepsilon_i)$ is the frequency dependent rotational contribution to the susceptibility. In the last chapter we used the elastic contribution $(\varepsilon_h - \varepsilon_i)$ normalized by

the total rotational contribution $(\varepsilon_e - \varepsilon_i)$ as a controlling parameter in theoretical studies of the model. In this section we have data as a starting point and ε_h and ε_e are therefore a given (even if they are not always known). This means that there is a one to one connection between ε_i and the elastic contribution $(\varepsilon_h - \varepsilon_i)/(\varepsilon_e - \varepsilon_i)$.

A complication in finding ε_i is introduced due to the absolute errors on the $\varepsilon(\omega)$ data used in the test of the model. We will discuss this in the next section.

9.2 The implications of data with absolute errors

In the chapter on experimentals we showed that systematic absolute errors can sometimes appear, especially on the absolute values of the dielectric constant. The absolute errors can be expressed in the following way

$$G_m(\omega) = b_1 G(\omega) \quad \varepsilon_m(\omega) = b_2 \varepsilon(\omega) + b_3 \qquad (9.2.1)$$

where $b_1 \approx 1$, $b_2 \approx 1$, $b_3 \approx 0$ and where the subscript m refers to the *measured* value as opposed to the actual physical value.

Inserting this in the model (equation 9.1.1) gives

$$G_m(\omega) = b_1 \left(\frac{K_1}{\left(\frac{\varepsilon_m(\omega) - b_3}{b_2} - \varepsilon_i \right)} + K_2 \right) = \frac{b_1 b_2 K_1}{\varepsilon_m(\omega) - (b_2 \varepsilon_i + b_3)} + b_1 K_2, \qquad (9.2.2)$$

which shows that the absolute errors can be absorbed in the three fitting parameters. Hence, the predicted relation between shear modulus and dielectric constant holds for the values we measure in spite of the absolute errors. This result is quite important, because the best we can do is of course to test the model with our data.

Another way of phrasing the above result is that the errors on the dielectric experiments will have no influence on the agreement between model and data; it is only the values found for the parameter ε_i which is affected. The ε_i value which should be used in the one parameter model test is really $(b_2 \varepsilon_i + b_3)$. That is the value of ε_i encumbered with the same errors as the measured $\varepsilon(\omega)$ data.

Our analysis of the shear measurements revealed that the shear loss peak position might be determined with an error of up to 0.2 decade. This will effect the agreement found between the model and data in a more direct way. We return to the implications of this in the next chapter.

9.3 Test on data

In the following section we present tests of the DiMarzio-Bishop model on all the substances we made shear and dielectric measurements on, by using the one parameter formulation presented above.

We have just argued that the ε_i value which should be used is the hypothetical ε_i, which would be measured if it was possible to reach the ε_i limit with the applied method. This has the consequence that the analysis from section 7.2, regarding the T dependence of the measured ε_h, applies to the ε_i, which is to be used. Thus it is only possible to have an ε_i which decreases or is constant with increasing temperature. This means that the room

temperature n^2 is a true lower bound for the ε_i values to be used. The only exception for this is the case where the capacitor is poorly filled. This would lead to an error on our "room temperature" ε_i which would make it smaller than the table value of n^2. The very lowest possible ε_i value is 1 ($\chi_i = 0$) as this is the value corresponding to no induced polarization at all.

Our starting point was to fit ε_i values by using equation 9.1.2, but the fits of ε_i are always quite poor at the high and low temperatures where we only have measured part of the relaxation curves. We have therefore restricted the fitting of the ε_i value to one appropriate temperature, where the whole relaxation was obtained in both shear and dielectric measurements, and where the loss peak of the shear data is in the center of the measured frequency range.

We expect the measured ε_i to decrease with increasing temperature, because this is the temperature dependence we have seen in our measurements on TPE and squalane, which have very small rotational contributions, making the measured ε_h value close to ε_i. We have used the temperature dependence of ε_h of TPE as a reference for estimating the temperature dependencies of all the liquids, by assuming an equivalent[1] temperature dependence in ε_i for all liquids. Hence, ε_i is found by fitting at one temperature (T_0), and this ε_i value is extrapolated to other temperatures by a decreasing first order function of temperature

$$\varepsilon_i(T) = \varepsilon_i' - \gamma(T - T_0). \tag{9.3.1}$$

where ε_i' is the fitted value at T_0.

When ε_i values have been determined in this way G data are calculated from the dielectric data at all temperatures using equation 9.1.2. This means that the shear relaxation at the different temperatures are predicted from just one fit of ε_i and the estimated temperature dependence given by γ.

The parameter K_1 (which only changes the scale of G'') has been chosen subsequently such that the loss peak of the calculated and real shear modulus are at same level. Different values of K_1 correspond to vertical translations of the loss peak in the log-log plot. We have chosen K_1 as described, because it is simple and unbiased. A better overall agreement between the model and the data, could in most cases be found by using a different K_1 value.

For some of our substances the model predictions are so poor that it is impossible to carry out the above described procedure, because the ε_i values found from fitting were way out of the physically reasonable range. In these cases we chose a reasonable value of ε_i for the model calculation. To confirm that the tendencies are general we changed ε_i over the physical reasonable range and observed that no qualitative changes in the results were seen.

All graphs are collected at the end of this section and the results are discussed in section 9.4.

---

[1]By equivalent we mean the same relative change in the actual χ_i value, and the same contraction of the liquid in the vertical direction.

TPE

Data from $T = 262.0$K was fitted treating ε_i as a fitting parameter ($\varepsilon_i = 2.6611$), the fit is show on figure 9.1. The fitted value is within the reasonable range ($\varepsilon_h \approx 2.71$ and $\Delta\varepsilon \approx 0.05$).

Using this fitted ε_i and an γ value of $\gamma = 0.0013$ (the value is estimated from the change in ε_h) in equation 9.3.1 the temperature dependent G was calculated from the model, the result is shown in figure 9.1.

DC704

The value $\varepsilon_i = 2.50$ was found by fitting to the data at 221.5K This value of ε_i is in the reasonable range, between $\varepsilon_h \approx 2.63$ and $n^2 = 2.42$ (see table 4.1). $\gamma = 0.0012$ was used to extrapolate ε_i.

As for TPE we see that the fits are reasonable but not extremely convincing.

PPE

Data from $T = 256.0$K was fitted treating ε_i as a fitting parameter, and it was found that the optimal value was $\varepsilon_i = 1.946$. Given that $n^2 = 2.659$ and $\varepsilon_h \approx 2.95$ the fitted value of ε_i is totally out of the physical range, and it is not possible to use this value for the test over more temperatures. Choosing a $\varepsilon_i = 2.7$ and $\gamma = 0.0013$, the model was tested over a temperature range as shown in figure 9.5. It is seen that the loss peak frequency of the calculated shear modulus is too high.

Choosing a different value of γ in equation 9.3.1 does not change the overall picture, and changing ε_i in the physical range does not change the picture of a to high loss peak frequency either.

Squalane

Data from $T = 172.0$K was fitted treating ε_i as a fitting parameter, the frequency range was chosen around the alpha peak, the fit is show in figure 9.6. Because of the very noisy data above 50Hz a rather low temperature was chosen. The fitted $\varepsilon_i = 2.144$ is within the reasonable range, for squalane ($\varepsilon_h \approx 2.15$ and $n^2 = 2.105$).

The model was tested on the two data sets where we have high frequency data from Richert [2003] (see figure 9.7) using this value for ε_i. The γ value in equation 9.3.1 was estimated from the temperature change in the ε_h value of squalane itself.

PB20

Data from $T = 182.0$K was fitted treating ε_i as a fitting parameter, the frequency range was chosen around the alpha peak, the fit is show in figure 9.8.

The fitted $\varepsilon_i = 2.308$ is within the reasonable range, for Pb20 ($\varepsilon_h \approx 2.35$ and $n^2 = 2.304$). The model was tested on a number of data sets (see figure 9.9) using this value for ε_i, and $\gamma = 0.0011$ in equation 9.3.1.

DHIQ

Data from $T = 178.5$K (a temperature where alpha and beta relaxation are well separated) were fitted using the automatic procedure treating ε_i as a fitting parameter. However it was not possible to get physical reasonable ε_i values from the fitting procedure (the returned values of the fitting procedure were large negative numbers).

To get a qualitative comparison, a model calculation was performed on a dielectric data set using $\varepsilon_i = 1.8$. The result is shown in figure 9.10 together with shear mechanical data taken at comparable temperatures. It is seen that the beta peak is far too big in the calculated shear modulus. The chosen value of ε_i is rather low ($n^2 = 2.221$), but raising it only increases the seen discrepancy between the model and experiment.

TPG

We attempted to fit data from $T = 192.0$K (a temperature where alpha and beta relaxation are well separated) by using the automatic procedure treating ε_i as a fitting parameter. However, it was not possible to get physical reasonable ε_i values from the fitting procedure (the returned values were approximately -1).

We have used $\varepsilon_i = 2.1$ in testing the model, while $n^2 = 2.085$ and $\varepsilon_h \approx 2.8$. The used ε_i value is rather low, however raising it to a higher value only makes the agreement between model and data worse.

In figure 9.11 the result from $\varepsilon_i = 2.1$ is shown. It is seen that the beta relaxation in the calculated shear modulus are too big, and that the loss peaks found from the model are shifted relative to the data.
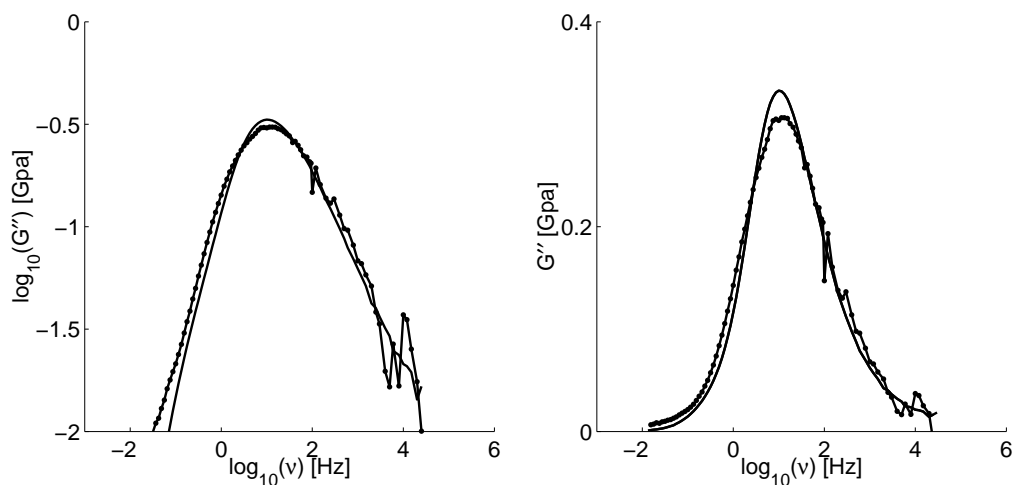
Figure 9.1 Test of the DiMarzio-Bishop model. TPE shear data (solid line), and shear spectrum calculated from TPE dielectric data using equation 9.1.2 (solid dotted line). Data taken at 262.0K. The result of the fit is $\varepsilon_i = 2.6611$.
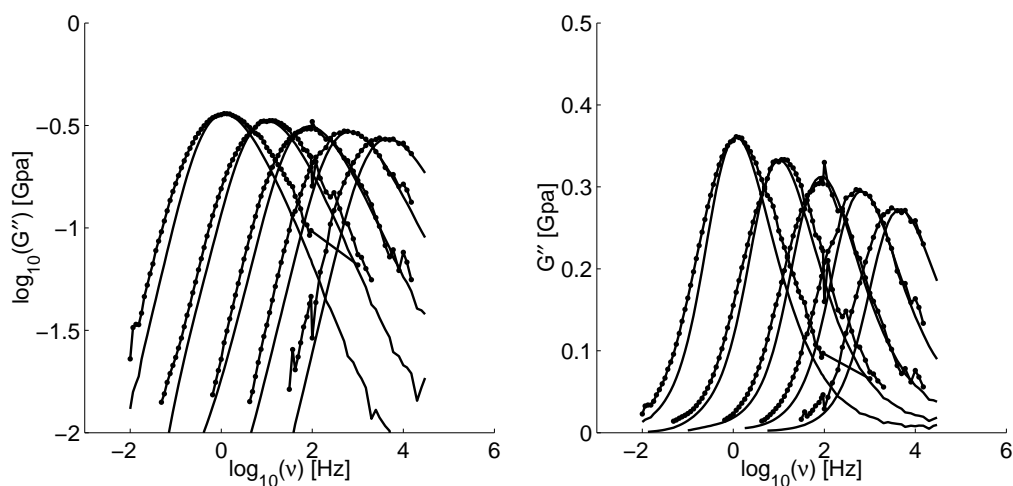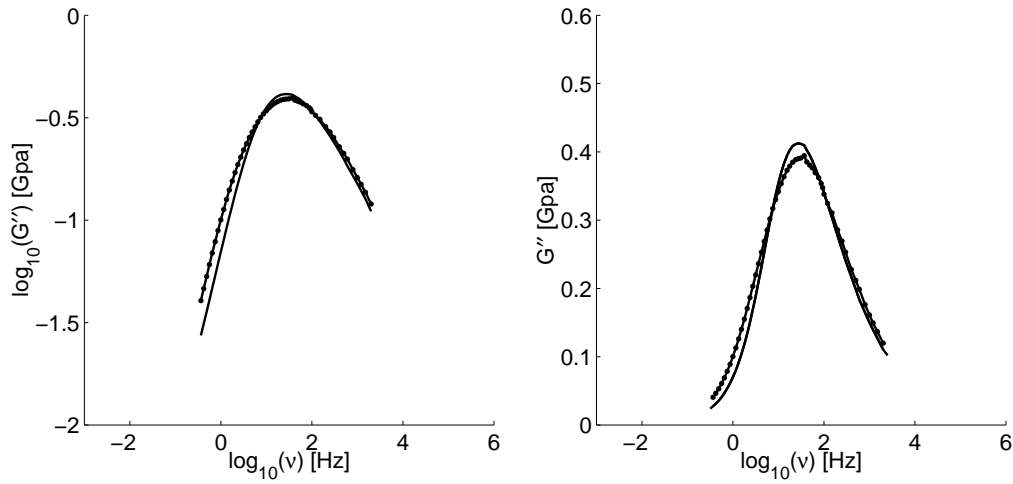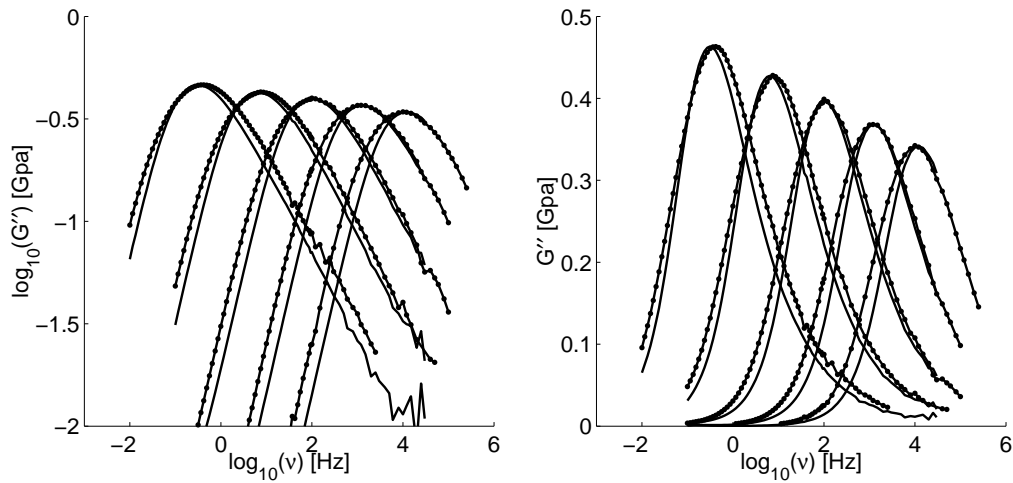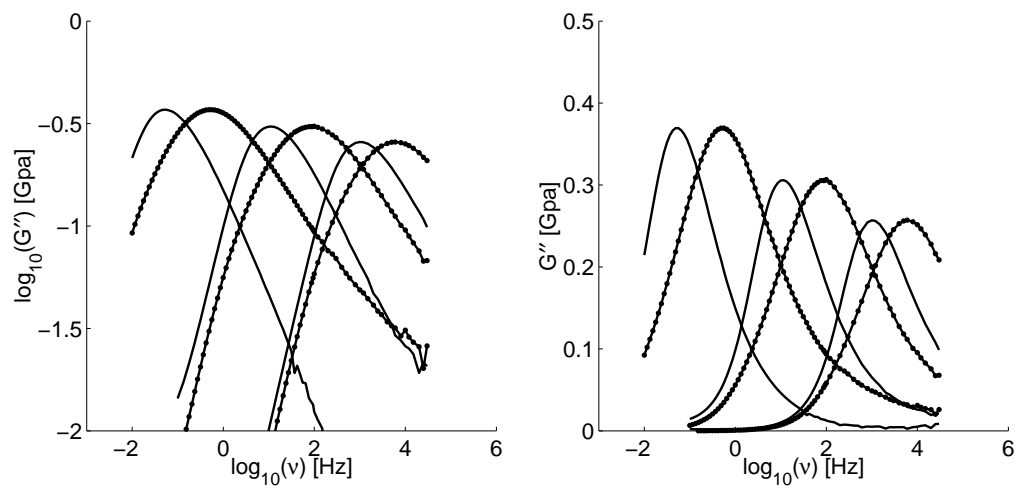

Figure 9.2 Test of the DiMarzio-Bishop model. TPE shear data (solid line), and shear spectrum calculated from TPE dielectric data using equation 9.1.2 (solid dotted line). Temperatures are 258.0K to 274K in steps of 4K. ε_i calculate according to 9.3.1, with $\varepsilon_i' = 2.6611$, $T_0 = 262.0$K, and $\gamma = 0.0013$.

Figure 9.3 Test of the DiMarzio-Bishop model. DC704 shear data (solid line), and shear spectrum calculated from DC704 dielectric data using equation 9.1.2 (solid dotted line). Data taken at 221.5K. The result of the fit is $\varepsilon_i = 2.500$.

Figure 9.4 Test of the DiMarzio-Bishop model. DC704 shear data (solid line), and shear spectrum calculated from DC704 dielectric data using equation 9.1.2 (solid dotted line). Temperatures from 215.4K to 231.6K in steps of approximately 2K. ε_i calculate according to equation 9.3.1, with $\varepsilon_i' = 2.5$, $T_0 = 221.5$, and $\gamma = 0.0012$.

Figure 9.5 Test of the DiMarzio-Bishop model. PPE shear data (solid line), and shear spectrum calculated from PPE dielectric data using equation 9.1.2 (solid dotted line). Temperatures are 248.0K 256.0K and 264.0K with ε_i calculate according to equation 9.3.1, with $\varepsilon_i' = 2.7$, $T_0 = 256.0$, and $\gamma = 0.0013$.
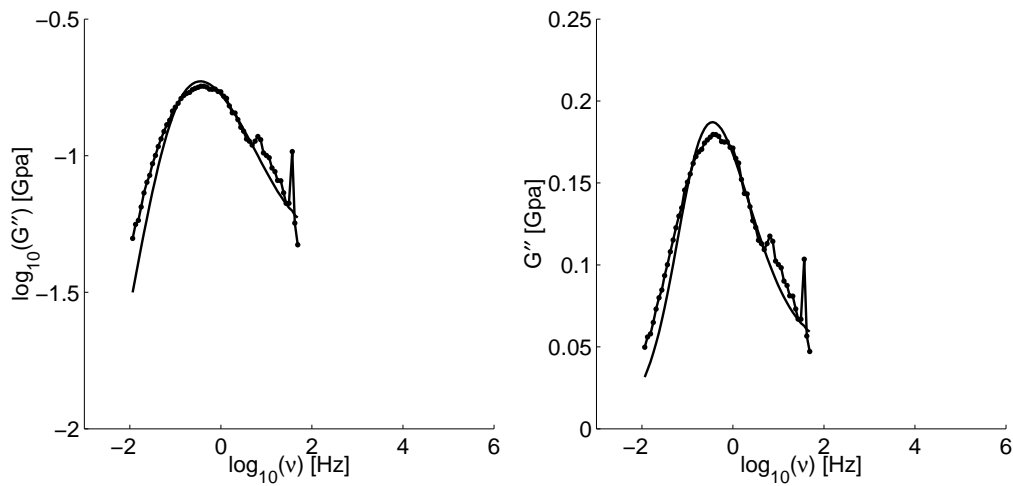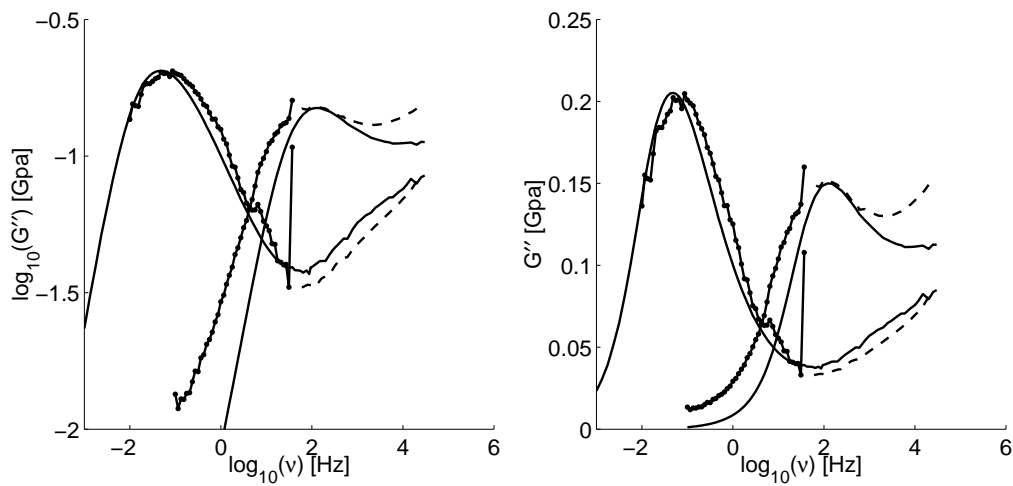
Figure 9.6 Test of the DiMarzio-Bishop model. Squalane shear data (solid line), and shear spectrum calculated from squalane dielectric data using equation 9.1.2 (solid dotted line). Data taken at 172.0K. The result of the fit is $\varepsilon_i = 2.144$.

Figure 9.7 Test of the DiMarzio-Bishop model. Squalane shear data (solid line), shear spectrum calculated from squalane dielectric data using equation 9.1.2 (solid dotted line), and shear spectrum calculated by using equation 9.1.2 and squalane dielectric data from Richert [2003] (dashed line). Temperatures are at 170.0K and 180.0K. ε_i calculate according to 9.3.1, with $\varepsilon_i' = 2.144$, $T_0 = 172.0$K, and $\gamma = 0.0009$.
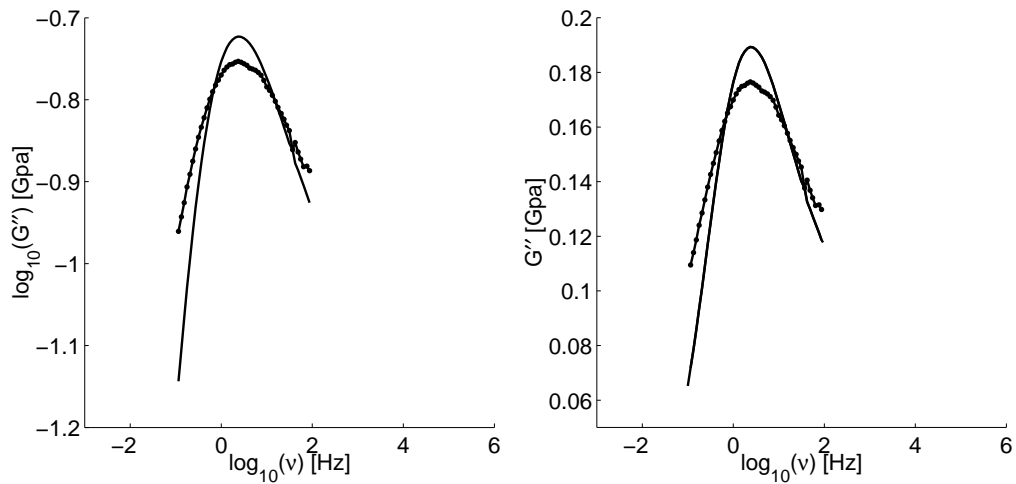
Figure 9.8 Test of the DiMarzio-Bishop model. PB20 shear data (solid line), and shear spectrum calculated from PB20 dielectric data using equation 9.1.2 (solid dotted line). Data taken at 182.0K. The result of the fit is $\varepsilon_i = 2.308$.
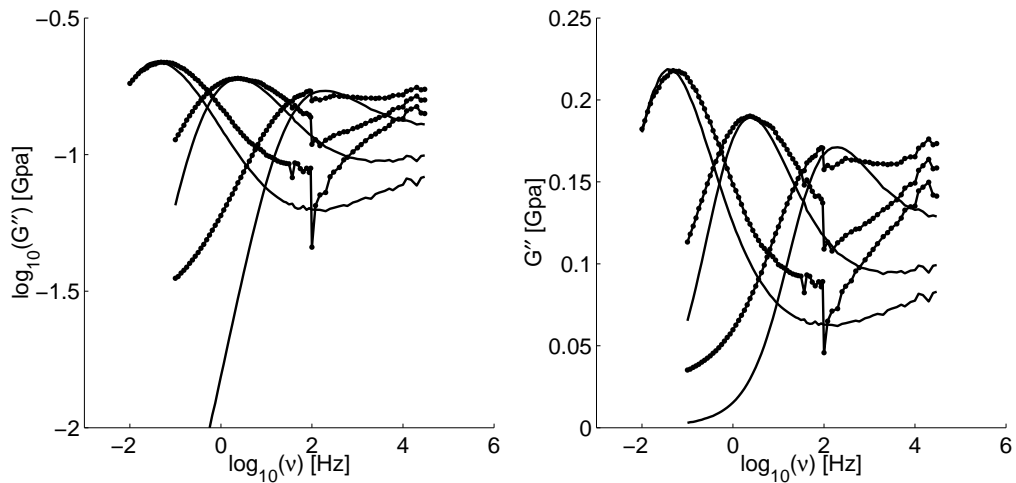

Figure 9.9 Test of the DiMarzio-Bishop model. PB20 shear data (solid line), and shear spectrum calculated from PB20 dielectric data using equation 9.1.2 (solid dotted line). Temperatures are 178.0K, 182K and 188K. ε_i calculate according to equation 9.3.1, with $\varepsilon_i' = 2.308$, $T_0 = 182.0$, and $\gamma = 0.0011$.
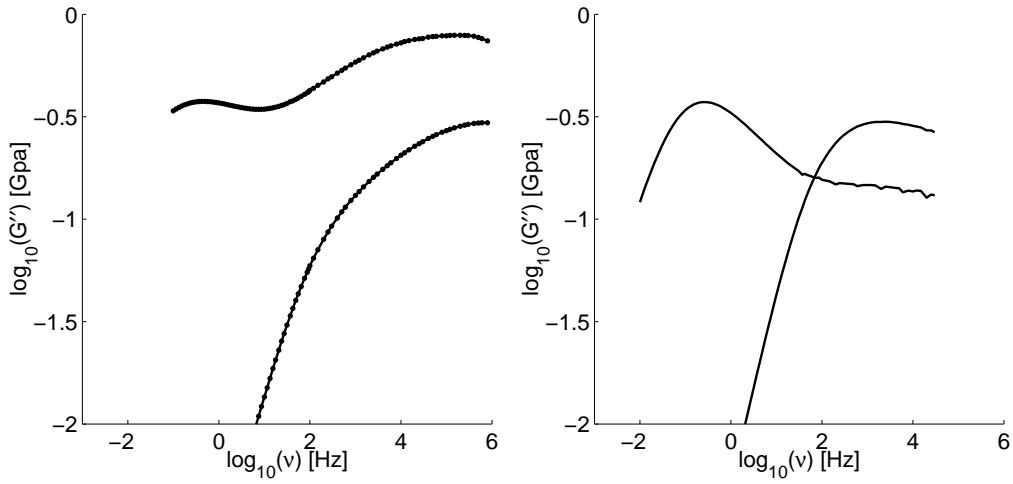
Figure 9.10 Test of the DiMarzio-Bishop model. DHIQ shear data (solid line), and shear spectrum calculated from DHIQ dielectric data using equation 9.1.2 (solid dotted line). Dielectric data taken at 181.2K and 189.2K shear mechanical data taken at 181.5K and 189.0K. Used $\varepsilon_i = 1.8$.
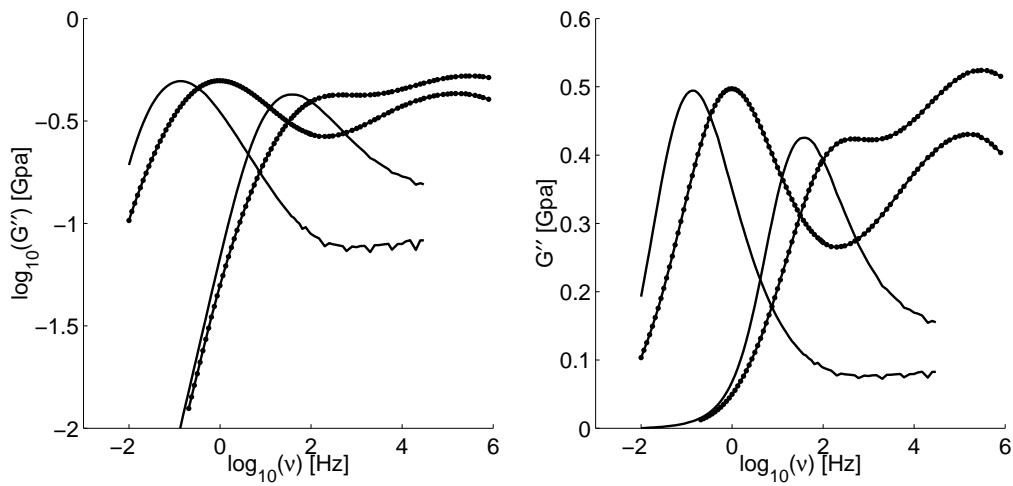

Figure 9.11 Test of the DiMarzio-Bishop model. TPG shear data (solid line), and shear spectrum calculated from TPG dielectric data using equation 9.1.2 (solid dotted line). Data taken at 192.0K and 200.0K. Used $\varepsilon_i = 2.1$.

9.4   Discussion of the results

We see the following pattern in the data presented above. The model fits reasonably on data with a simple alpha relaxation and a small dielectric strength. It fits very poorly on substances with great dielectric strength, and it fits moderately well on substances with small dielectric strength and a beta relaxation.

The model always predicts too broad a relaxation peak, even in the case of TPE and DC704 where the results of the model have the best resemblance with the data. On the substances with great dielectric strength this broadening is dramatic, and the loss peak position becomes overestimated at the same time. The greater strength might lead to a bad agreement due to the field or due to the stronger interactions between the molecules in the liquid. We elaborate on these points in chapter 11 and chapter 12. A third possibility is that the difference between big and small strength arises from our different limits when fitting ε_i. The freedom to fit ε_i is always limited by ε_h and n^2 (or the extreme minimum 1). For the liquids of small strength this leaves room for a large elastic contribution ($\varepsilon_h - \varepsilon_i$) when compared to the total rotational contribution ($\varepsilon_e - \varepsilon_i$). Expressed in terms of the parameter $a = (\varepsilon_h - \varepsilon_i)/(\varepsilon_e - \varepsilon_i)$, which we have introduced in section 8.1, this means that a can attain values ranging from 0 to at least 0.5. This is not the case for liquids with great strength because the interval between ε_h and n^2 is relatively smaller. For TPG the minimal physically realistic ε_i corresponds to an a value of approximately 0.05.

The model strongly overestimates the beta peak. This is very dramatic in the case of liquids with great dielectric strength, where we also saw a strong overestimation of the width of the alpha peak.

On the substances with small dielectric strength and a beta relaxation the pattern is that the position, and to some extend the shape of the alpha peak is well determined, whereas the beta peak is somewhat overestimated. This seems to indicate that the model is less appropriate for the beta relaxation than for the alpha relaxation. This possibility was also suggested in Zorn et al. [1997] on the basis of data from polybutadienes, even though the mechanical beta relaxation was not reached by their measurements.

We do not have much data where the beta and alpha relaxations are well separated, but the lowest temperature on squalane show such a situation. It is, a little surprisingly, seen that the model seems to hold better in this case. This raises the possibility that the model holds for both relaxations but captures the merging poorly, though we find this conjecture difficult to interpret from a physical point of view. It should also be recalled that the squalane data are obtained by patching together measurements from two different laboratories, via two parameters to adjust for absolute differences, why we do not want to draw very strong conclusions based on these data alone.

10 Possible quantitative agreement

In this chapter we will focus on the situations were the DiMarzio-Bishop model gives reasonable results, in order to establish to which degree these results support a quantitative agreement between the model and data.

The chapter has two objectives. To analyze whether the discrepancies that do appear between model and data are due to experimental uncertainties, and to discuss whether the DiMarzio-Bishop model provides a good method to estimate shear behavior from dielectric behavior.

10.1 Dependence on the parameter ε_i

We start by analyzing how sensitive the results are on the value of the parameter ε_i. The results are used in the next section to evaluate how the uncertainty on measuring the shear loss peak position affect the determination of ε_i and the predicted shape of the curve.

The question we pose is how ε_i controls the position of the loss peak and the shape of the imaginary part of the calculated shear modulus. To do so, we analyze the simulated data we used in section 8.1, in this frame. The data was produced by calculating a shear modulus from the extended Maxwell model (with reasonable parameters), and from this shear modulus a dielectric constant was calculated using the DiMarzio-Bishop model (equation 8.1.1), choosing, among other parameters, the molecular induced dielectric constant ($\varepsilon_{i,r}$). The dielectric spectrum calculated in this way corresponds to the fictive shear data *if* the DiMarzio-Bishop model is correct. We subsequently calculate shear spectra from these dielectric data via the DiMarzio-Bishop model using different values of the parameter ε_i. This gives us a measure of how sensitive the test of the DiMarzio-Bishop is on a correct determination of ε_i.

Notice that $\varepsilon_{i,r}$ is the induced dielectric constant used when calculating the fictive dielectric spectra, whereas ε_i is the parameter value used when going from these dielectric spectra to shear spectra as we do it when testing the DiMarzio-Bishop model.

The first test is on the alpha system presented in figure 8.1. The simulated dielectric signal is used as input in the simple formulation of the DiMarzio-Bishop model (equation 9.1.2), choosing different values of ε_i. The found imaginary part of the shear modulus is naturally a perfect match to the input shear modulus when the ε_i value is chosen to be the one that was used in calculating the dielectric signal ($\varepsilon_{i,r}$).

In figure 10.1 it is seen that if the chosen ε_i parameter value is close to ε_h, the loss peak changes fast with ε_i. It is also seen that if the ε_i value is low compared to $\varepsilon_{i,r}$, then the loss peak positions becomes less dependent on the precise value of ε_i.

To get an impression on how the shape changes with ε_i, values on both sides of the actual value ($\varepsilon_{i,r}$) were chosen. In figure 10.2 the shapes from these calculations are shown

together with the shape of the imaginary part of the shear modulus. It is seen that if a too small molecular induced dielectric constant is used ($\varepsilon_i < \varepsilon_{i,r}$), the model predicted loss peak becomes too narrow. The opposite ($\varepsilon_i > \varepsilon_{i,r}$) leads to a model predicted loss peak which is too wide and too asymmetric with a pronounced change of shape in the low frequency side of the peak.
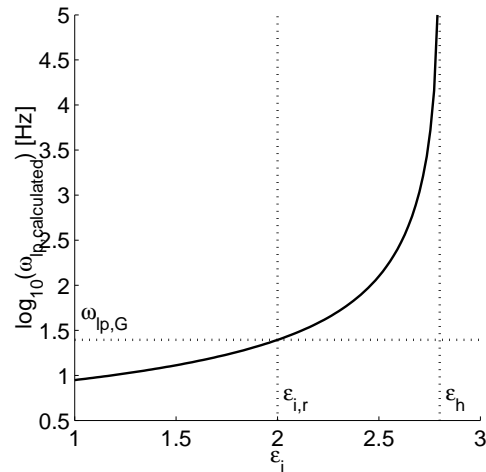

Figure 10.1 Loss peak frequency of the shear modulus calculated from the DiMarzio-Bishop model and simulated dielectric data (using equation 9.1.2), as a function of the parameter ε_i. The two vertical lines gives the position of the real molecular induced dielectric constant ($\varepsilon_{i,r}$) and the high frequency limit of the dielectric constant (ε_h), the horizontal line indicates the loss peak of the real shear signal. See caption of figure 8.1 for details on the simulated data.
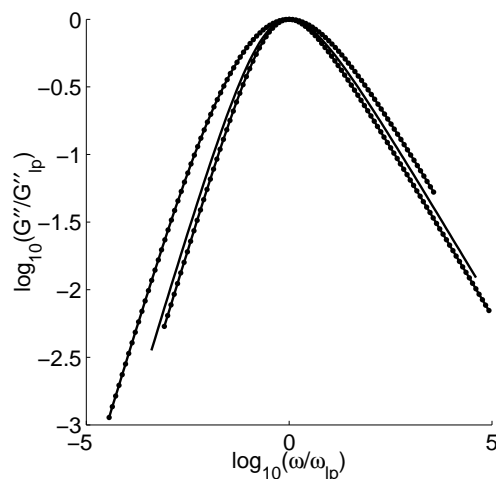

Figure 10.2 Imaginary part of the shear modulus. Original simulated shear data (solid line) and shear data calculated using simulated dielectric data ($\varepsilon_{i,r} = 2.0$) and equation 9.1.2 (solid dotted lines), the inner curve is with $\varepsilon_i = 1.4$, the outer curve is with $\varepsilon_i = 2.6$. See caption of figure 8.1 for details on the simulated data.

10.2   Details of shape and position found from data

The figures shown in the last chapter smear the deviation in loss peak with the deviation in shape of the relaxation curve. In the following analysis we separate the discrepancies in loss peak position and the shape of the relaxation curve in order to get a clearer picture.

We include comparisons between the shear modulus, the DiMarzio-Bishop model and the raw dielectric data, represented by the dielectric modulus M. The reason for choosing M instead of ε is that it generally resembles the shear spectra more. Albeit, the choice of M makes very little difference for the substances with small dielectric strength, as it is illustrated in figure 13.7.

The substances with small strength, pure alpha relaxations and reasonable fits were DC704 and TPE.

DC704

The loss peak position as a function of temperature is shown in figure 10.3. It is seen that the loss peak position of the shear modulus calculated from the DiMarzio-Bishop model, agrees well with the the real shear mechanical loss peak position. The temperature dependence of the loss peak position is predicted with a quite small error. However, it is a systematic error, which is clearly seen in the right part of figure 10.3.

In figure 10.4 we have zoomed in on a loss peak from the fit which was earlier shown in figure 9.4. Two temperatures, respectively above and below the 221.5K, which was used to fit an ε_i starting point, are depicted to illustrate that there is little temperature dependence in the shape predicted by the DiMarzio-Bishop model. All the data are scaled to make the loss peaks coalesce in order to make a pure comparison on the shape of the relaxation. It is clear that the DiMarzio-Bishop model predicts too wide a relaxation curve, as has been seen already.

The loss peak positions given by the model can be brought to agree perfectly with the measured shear loss peaks without altering the shape of the model loss peak significantly. The problem with such a fit is that it leads to an increase in ε_i with temperature, of about the same magnitude as the decrease we expect.

The analysis of the model's dependence on ε_i, which was reported in last section, indicates that a too wide relaxation corresponds to an overestimation of ε_i. The analysis also shows that if ε_i is overestimated, then the loss peak predicted by the model will be too large. The loss peaks were seen to agree quite well, but the discrepancy could be due to an error on the measured shear loss peak. Our analysis of the shear measurements showed that we have up to $+0.2, -0.1$ decade error on the position of the loss peak (see section 5.3.5).

The model data in the right plot of figure 10.4 is obtained by using the lowest physically reasonable value of ε_i, which is the square of the room temperature refraction index. The corresponding loss peak position is 0.21 smaller than the measured shear loss peak, thus not quite within the uncertainty of the determination of the shear loss peak position.

The agreement on the relaxation shape is seen to be extremely good on the right hand side of the peak. The left hand side is still estimated too wide, though the fit is better than the original fit. The overestimated width can not be due to errors in our measurements, because the width of the shear peek is measured with high accuracy and
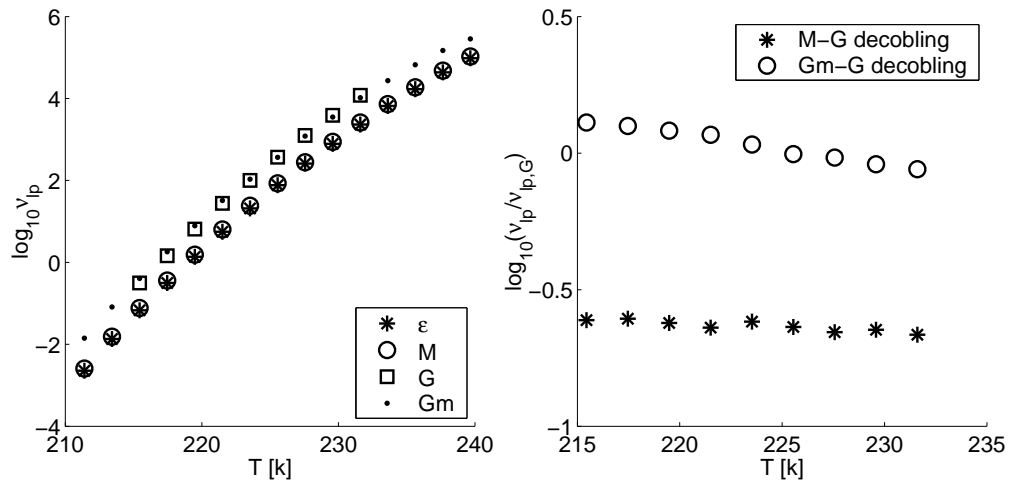
Figure 10.3 DC704. The loss peak position predicted by the DiMarzio-Bishop model, G_m, shear data and pure dielectric data. The model data are the same as in figure 9.4. This means that ε_i is found from an overall fit at 221.5K and extrapolated to other temperatures. The right figure shows $\log_{10}$ of the decoupling index between the shear modulus, G, and the dielectric modulus, M, and the $\log_{10}$ of the decoupling index between the shear modulus, G, and the shear modulus given by the DiMarzio-Bishop model, G_m. The latter is simply the residual of the shear and model data in the left figure, hence the slope reveals a systematic error in the determination of loss peak as a function of temperature.
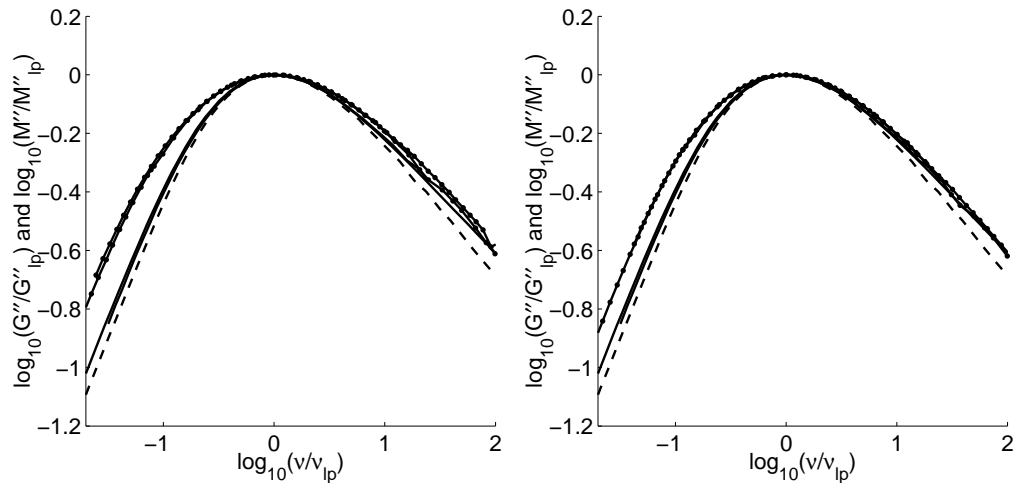

Figure 10.4 DC704. The shape of the relaxation peak found from the DiMarzio-Bishop model (solid dotted line), shear data (solid line) (both at 215.5K and 227.6K) and pure dielectric modulus (dashed line) (221.5K). All curves are scaled by peak position, to allow for a comparison of the shape alone. In the left figure the model data are the same as in figure 9.4. This means that ε_i is found from an overall fit at 221.5K and extrapolated to other temperatures. In the right figure ε_i used in the DiMarzio-Bishop model is chosen as the smallest physically possible value $\varepsilon_i = n^2 = 2.43$.

deviations, if present, will tend to make the measured relaxation wider than the real relaxation, while there is virtually no error on the measured dielectric loss peak position and relaxation shape.

The raw dielectric modulus (M) is depicted along with the shear modulus and the model shear peak in figure 10.4. The shape of the dielectric relaxation curve agrees quite well with the shear data, but it is slightly too narrow. In figure 10.3 it is seen that the loss peak position of the dielectric modulus evolves very close to the same way as that of the shear modulus, that is virtually no *decoupling* is seen. The pure dielectric modulus gives a better quantitative estimate of the shear modulus, than the model, if the position of the loss peak is shifted by a temperature independent frequency, which in practice could be found from comparing measurements at a single temperature.

TPE

Figure 10.5 and 10.6 show the correspondence between loss peak postions and relaxation shape for TPE shear data, dielectric data and model predictions. The figures reveal that the DiMarzio-Bishop model's prediction regarding TPE are very analogously to the predictions on DC704. The DiMarzio-Bishop model predicts too wide a relaxation peak and gives quite good predictions of the loss peak position.

The main difference is in the temperature dependence of the model predicted loss peak position. The right hand plot in figure 10.5 shows that for TPE there is only a small error on the loss peak position and there is no (or very little) systematics in the temperature dependence of the error. This indicates that the temperature dependence of ε_i has been better extrapolated in the case of TPE than in the case of DC704. This is not surprising because the temperature dependence of ε_i has in all cases been approximated from the temperature dependence of TPE's ε_h values (See section 9.3).

The model predicted TPE relaxation curve can of course be made narrower by choosing a smaller ε_i. We have not depicted such a figure, as we have no known refraction index to give a lower limit on the possible ε_i in the case of TPE. Refraction indexes are not given because TPE is solid at room temperature.

It is possible that the too wide model curves in both the case of TPE and DC704 are partly due to errors in the determination of the shear loss peak, and not to inadequateness of the DiMarzio-Bishop model. If this is the case, then it indicates that we systematically measure too high shear loss peaks. Our analysis of the errors on the shear loss peak, due to erroneous determination of the degree of filling of the shear transducer, and due to the inversion algorithm used when shear data are extracted from the raw capacitance data, signal that such a systematic overestimation is in fact likely.
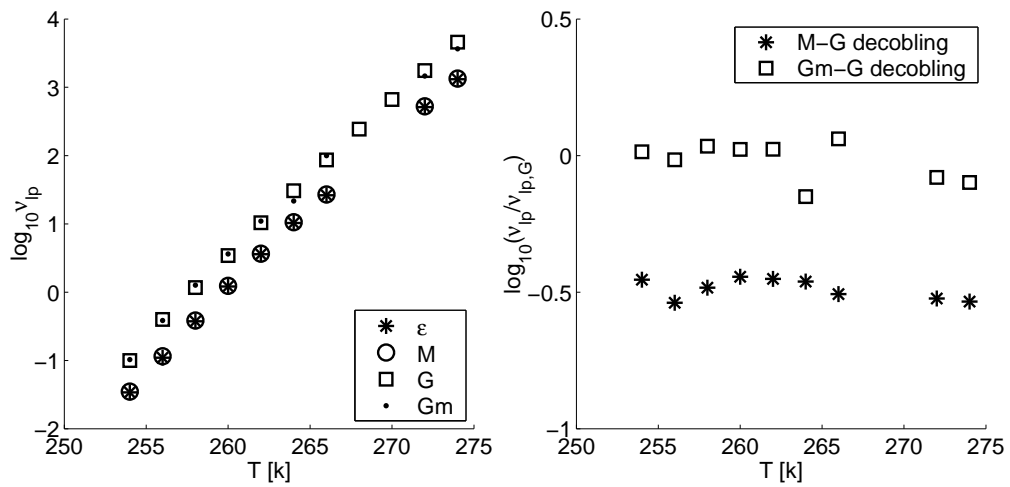
Figure 10.5 TPE. The loss peak position predicted by the DiMarzio-Bishop model, G_m, shear data and pure dielectric data. The model curves are the same as in figure 9.2. This means that ε_i is found from an overall fit at 262.0K and extrapolated to other temperatures. The right figure shows $\log_{10}$ of the decoupling index between the shear modulus, G, and the dielectric modulus, M, and the $\log_{10}$ of the decoupling index between the shear modulus, G, and the shear modulus given by the DiMarzio-Bishop model, G_m. The latter is simply the residual of the shear and model data in the left figure, hence the slope reveals a systematic error in the determination of loss peak as a function of temperature.
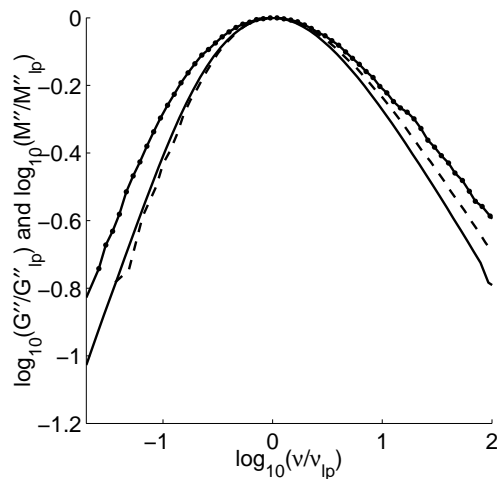

Figure 10.6 TPE. The shape of the relaxation peak predicted by the DiMarzio-Bishop model (solid dotted line), shear data (solid line) and pure dielectric modulus (dashed line) at 256.0K. All curves are scaled by peak position, to allow for a comparison of the shape alone. The model curve is the same as in figure 9.2. This means that ε_i is found from an overall fit at 262.0K and extrapolated to 256.0K.

10.3 Fits of the real part of the shear modulus

The general picture from the analysis in this section is that quantitative agreement between the DiMarzio-Bishop model and the data is quite good though not perfect. If the DiMarzio-Bishop model really holds quantitatively, it should also agree with the real part of the shear modulus. The real part of the predicted modulus is also crucial if the DiMarzio-Bishop model is to bee used for making qualified estimates regarding G_∞ and its temperature dependence. Such estimates could (as described in our motivation) be of great importance in testing the shoving model.

The problem with including the real part of the signal is that the two other parameters play an important part. We have this far paid little attention to a proper determination of K_1 (the parameter which scales the loss peak) and none to K_2, which is a real number added to the signal (see equation 4.7.8). These parameters are both of great importance when the real part of the DiMarzio-Bishop model is studied.
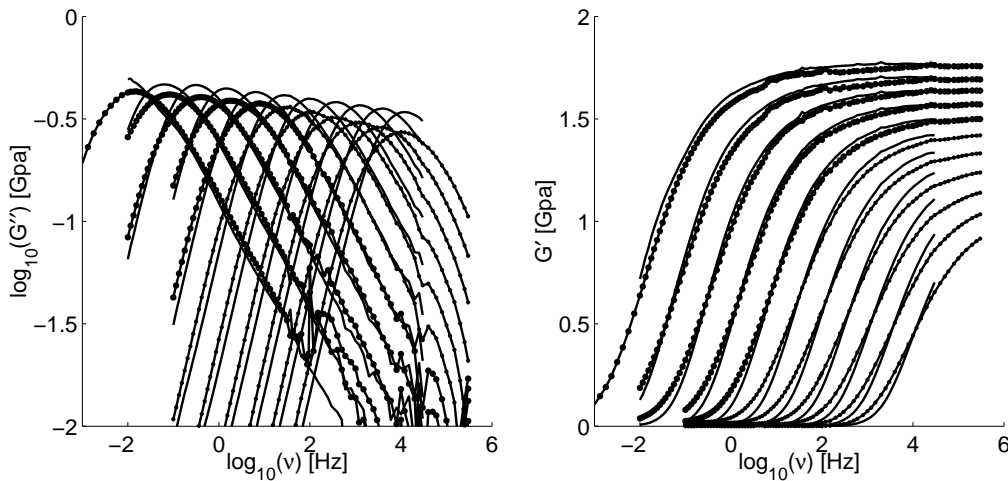

Figure 10.7 DC704. Test of the DiMarzio-Bishop model's ability to fit the real and imaginary part of the spectrum. Shear data (solid line) and shear spectra calculated from the DiMarzio-Bishop model and dielectric data (solid dotted line). The temperatures are $211.4 - 231.6$K in steps of approximately 2 degrees. The high temperature model curves, which are plotted with a thinner line have been determined by extrapolating the parameter temperature dependence found from the low temperature data. See the text for more details.

Figure 10.7 shows DC704 model and shear data with imaginary and real parts. In these calculations the second form of the simple formulation of the model, see equation 4.7.8, is used, that is we use, ε_i, $\varepsilon_e - \varepsilon_i$ and the lumped parameter K_3 as the three parameters. The ε_i values used are those which were determined in section 9.3. ε_e values used are taken directly from dielectric data and K_3 is determined such that the high frequency plateau value of the calculated shear modulus agrees with the shear data. For the temperatures, where we have not been able to make proper determination of high and low frequency limits for shear and dielectric data, a simple linear extrapolations was used to estimate the temperature dependence of ε_e and K_3.

The agreement is reasonable, for the data where we have a good determination of high and low frequency values of shear as well as dielectric data. The loss peak is too wide as always, and this broadening can also be seen in the real part of the model predicted spectra.

The extrapolated model curves are difficult to evaluate as it is impossible to decide if the G_∞ values are in agreement with the real G_∞.

10.4   Summary

The quantitative agreement is reasonable for TPE and DC704, but the model significantly overestimates the width of the relaxation peak.

It would be a great improvement if estimations of the shear modulus could be made directly from the dielectric data. This does not seem as a realistic prospect in our opinion, because it has been necessary to find the K_3 values via G_∞. An alternative route would be to use the microscopic parameter r, if its value was claimed to be known somehow. By isolating the value of r from the K_3 values we have used, we find an r value of approximately 0.7Å which is weakly increasing with increasing temperature ($\approx$ 3% in 10 degrees). We have made similar test on the other liquids, and the finding of an unreasonably small molecular radius is general. This indicates that the stokes friction term used in the DiMarzio-Bishop model need to be modified or reinterpreted, if the model should give even coarse shear data estimates with dielectric data and a molecular radius as starting points. A possibility is to extrapolate the modes parameters from ranges where they are well defined in both shear and dielectric measurement, but the result is no better than an equivalent extrapolation made by using an phenomenological fitting function on the shear data.

To test the shoving model (see section 2.2 and the introduction) the high frequency shear modulus is needed, and it is exactly in the cases where the high frequency behavior is unknown that it is impossible to use the DiMarzio-Bishop model to predict the shear behavior. So the hope of using this approach to get better tests of the shoving model does not seem realistic.

11 Significance of local field

In chapter 9 poor quantitative agreement between the DiMarzio-Bishop model and the data was seen for all the substances which have a larger strength than approximately 10%. The general picture is that the DiMarzio-Bishop model predicts too wide relaxation curves and too high loss peak positions.

In section 4.7 we argued that the choice of local field is of minor importance in the case of liquids with a small strength. Contrary the choice of local field might have greater importance in the case of liquids with a great dielectric strength. It is therefore possible that the poor agreement seen for substances with a great strength is due to the inadequateness of the Maxwell or Lorentz field[1]. We will in this chapter examine how the local field alters the results in practice, in order to test this hypothesis.

PPE is the only of the relevant substances with no visible beta relaxation peak. This makes matters much more simple and we will therefore restrict the detailed analysis to PPE.

11.1 Possible experimental explanations of poor fits

Before looking at the local field we analyze if the deviation could be due to uncertainties or errors in the measurements, but find that this is not the case.

Figure 11.1 illustrates how the model strongly overestimates the width of the relaxation peak, and that the peak shapes disagrees especially at the high frequency end of the spectrum. Likewise, figure 11.2 shows that the model strongly overestimates the position of the loss peak. The analysis in section 10.1 shows us that both these deviations could be a sign of an overestimated ε_i value. Agreement between model and shear data for both shape and loss peak position could in fact be obtained by using an ε_i value which was considerably lower than the smallest physically reasonable value.

A small value could be explained if the capacitor had been poorly filled. This is unlikely because the liquid is quite viscous at room temperature, which made it possible to over-fill the capacitor, and because we have made two different dielectric measurements on PPE which agree perfectly. The deviation of 1 decade in loss peak position and the large deviation in shape is much too dramatic, to be accounted for by the uncertainty on the shear measurements. Unless the error is due to a bad shear experiment. To test this we performed a second measurement which agreed nicely with the first one both in shape, loss peak and absolute values indicating that the shear transducer was properly filled both times. An alternative explanation could be that the n^2 value of the liquid was smaller than the one reported in table 4.1. To test this we made a measurement of the refraction index using a "PZO RL3 refractometer" and found that $n^2 = 2.653$ at $28°C$,

---

[1] In the test of the model, which we presented in chapter 9, there was no distinction between using the Maxwell or the Lorentz field. See section 4.7.
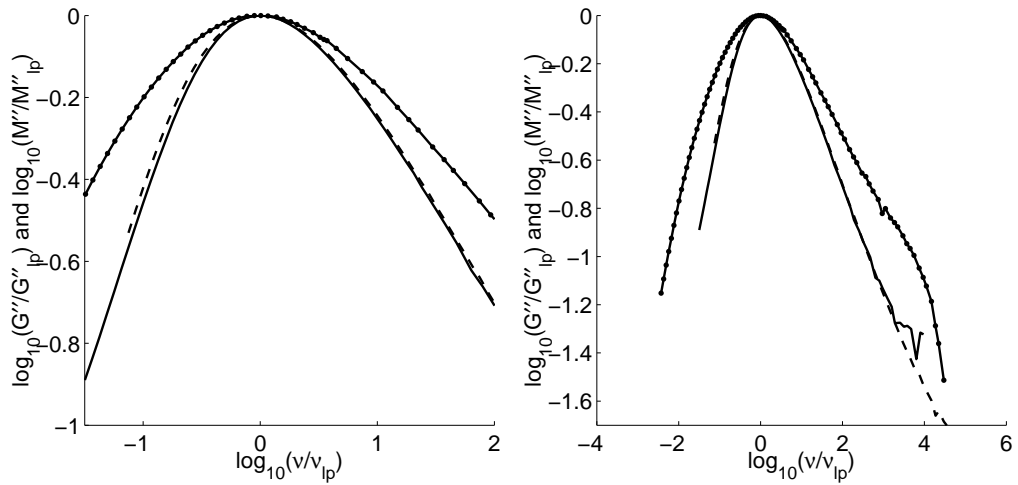
Figure 11.1 PPE. The shape of the relaxation peak found from dielectric data and the DiMarzio-Bishop model (solid dotted line), shear data (solid line), and pure dielectric modulus (dashed line) at 254.0K. All curves are scaled by peak position, to allow for a comparison of the shape alone. The model predicted curve is the same as in figure 9.5. This means that ε_i is set to 2.7 at 256.0K and extrapolated to other temperatures. The two figures show the same curves with different scaling.
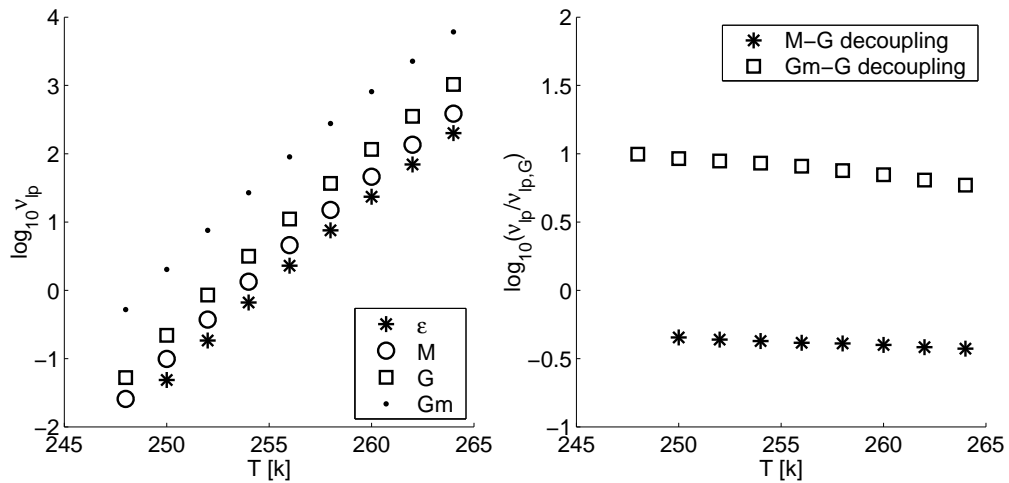

Figure 11.2 PPE. The loss peak position predicted by the DiMarzio-Bishop model, G_m, shear data and pure dielectric data. The model data are the same as in figure 9.5. This means that ε_i is set to 2.7 at 256.0K and extrapolated to other temperatures. The right figure shows $\log_{10}$ of the decoupling index between the shear modulus and the dielectric modulus M, and the $\log_{10}$ of the decoupling index between the shear modulus and the shear modulus given by the model G_m. The latter is simply the residual of the shear and model data in the right figure.

in good agreement with the table value. A final possibility for having a smaller n^2 than the table value could be that the assumption about the temperature independence of α_i is wrong, and it decreases with temperature (this would destroy our argument for the lower limit of ε_i). We performed a measurement of the refraction index at approximately $20°C$ below room temperature and found a significant increase in n as expected from our assumption, but this does of course not guarantee that the temperature dependence is the same at lower temperatures.

We are confident that the poor agreement we have found between the DiMarzio-Bishop model and data is due to a genuine poor agreement and will thus proceed by discussing the possible physical explanations.

11.2   Different local field tested on data

In order to analyze the significance of the local field, and how this depends on the dielectric strength, we have compared the result of the model in the Maxwell (equation 4.7.6), Lorentz (equation 4.4.7), and Fatuzzo-Mason (equation 4.5.3) field formulations for PPE and TPE respectively.

Figure 11.3 shows a comparison of the three versions of the model made on TPE. The same value of ε_i, ε_e and r has been chosen. r has been determined such that the high frequency plateau value agrees in the Maxwell formulation of the DiMarzio-Bishop model. There is no visible difference, as expected for TPE, which has very small ($\approx 2\%$) dielectric strength (see section 4.7).

The same type of comparison is shown for PPE in figure 11.4. It is clearly seen that the results of the three versions of the model differ largely in the predicted absolute value, but the predicted peak shape and loss peak position is hardly affected. A closer inspection shows that the loss peak position differs by as little as 0.003 decade, and the shape of the relaxation curves when scaled to agree in hight are indistinguishable.

The comparison above is analogous to the comparison between the Fatuzzo-Mason and the Lorentz versions of the field, which is presented in Díaz-Calleja et al. [1993]. A different approach is to use the same ε_e and ε_i but let r be a fitting parameter in the three versions of the model. We have presented such a comparison in figure 11.4. r is in all three cases determined such that the high frequency plateau values agree. The Maxwell and the Lorentz fields give *exactly* the same prediction when this approach is used, as it has been accounted for in section 4.7.2. The figure illustrates that the Fatuzzo-Mason curve agree with the two other curves as well[2].

The three versions of the model predict different values of r, but they are all of the same order of magnitude ($1.1\text{Å} - 1.3\text{Å}$) and it is impossible to say if any of these values is more reasonable than the others. (A discussion on how r should or could be interpreted is found in section 12). This shows that if the model is used or tested by a fitting procedure, then there is virtually no difference between the three versions of the model which we have discussed, even for a liquid with a relatively large dielectric strength. This strongly suggests that the poor model predictions we have seen for PPE should not be explained by the chosen local field, because if this was the case, then the three fields used should be expected to give different results, due to their differences. It is of course possible, that all the fields we have used are equally dissatisfactory. We find that

---

[2]A close inspection reveals a difference between the Fatuzzo-Mason curve and the two others, because they are not theoretically the same, whereas the Lorentz and the Maxwell curve are (see section 4.7).

this is most likely the case if no chosen average continuum local field is adequate. If this is the case then it is difficult to make any sense of the DiMarzio-Bishop model itself, as it is derived from an overall continuum and average approach.
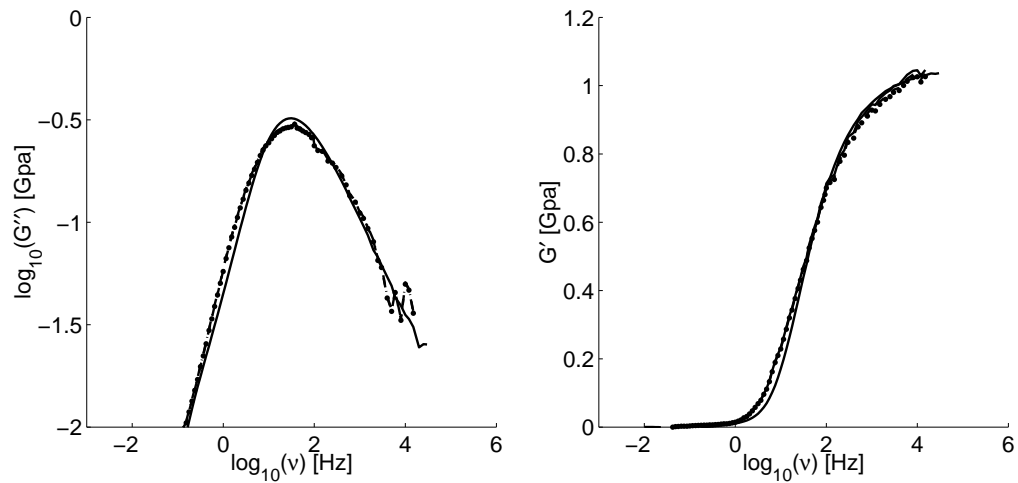

Figure 11.3 Test of the significance of the chosen field on the results of the DiMarzio-Bishop model made on TPE (264K). The shear modulus (solid line), Maxwell version of the model (solid dotted line), Lorentz field formulation (dotted line), and the model with Fatuzzo-Mason field (dashed line). The same values of r, ε_i and ε_e are used in the three versions of the model.

Figure 11.4 Test of the significance of the chosen field on the results of the DiMarzio-Bishop model made on PPE (254K). The shear modulus (solid line), Maxwell version of the model (solid dotted line), Lorentz field formulation (dotted line), and the model with Fatuzzo-Mason field (dashed line). The same values of r, ε_i and ε_e are used in the three versions of the model. r is chosen such that the G_∞ value of the Maxwell formulation of the model agrees with the actual G_∞ of the shear data.
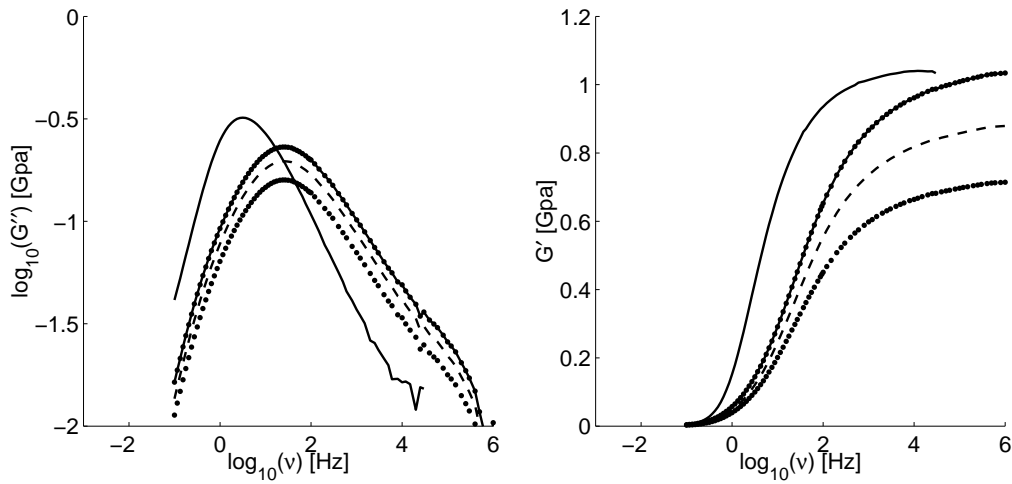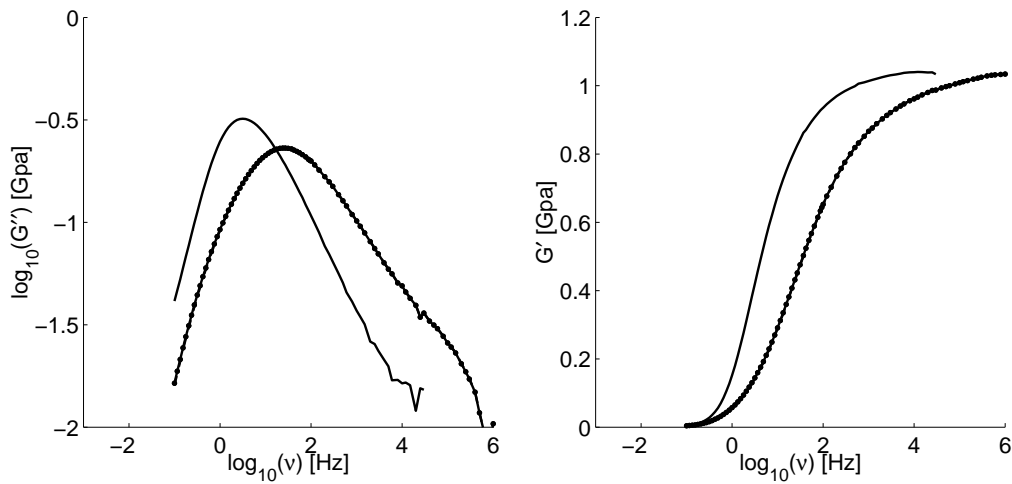

Figure 11.5 Test of the significance of the chosen field on the results of the DiMarzio-Bishop model made on PPE (254K). The shear modulus (solid line), Maxwell version of the model (solid dotted line), Lorentz field formulation (dotted line), and the model with Fatuzzo-Mason field (dashed line). The same values ε_i and ε_e are used in the three versions of the model, r is in each case chosen such that the high frequency value of the calculated shear modulus agrees with the G_∞ of the shear data. The three versions of the model yield almost identical results, therefore, the curves are indistinguishable.

12 Discussion of the DiMarzio-Bishop model

12.1 Status of the model

In physics models serve many different purposes: From simple models, which aim to capture the "underlying physics" and predict only the characteristic features of the phenomena in question, to detailed models, which aim at making accurate quantitative predictions. In theory, the latter is easy to test; either the predictions of the model are true or they are false. In contrast, the first kind of models is much harder to test, since the success criteria is not well defined. It has to be decided firstly, what the characteristic properties of the physical system are, and secondly how to evaluate if the model captures these properties. Furthermore, if the model can be pushed to make quantitative prediction, it equally has to be assessed, how these predictions should be compared to the details of the physical phenomena. Finally it should be established how the model can be falsified!

It could be argued that some of our (and other's) work on the DiMarzio-Bishop model push it far in the quantitative direction compared to what was the original ambition of DiMarzio and Bishop.

In their introduction DiMarzio and Bishop write:

> The venerable Debye theory of the dielectric susceptibility predicts that the Cole-Cole plot is a semicircle. However, for many systems of viscous liquids and glasses (especially polymer systems) the Cole-Cole plot is a flat skewed arc. [Dimarzio & Bishop, 1974]

and later in the introduction, they write the following about their results:

> It is thereby suggested that the skewed-arc behavior is a manifestation of the variation of the viscosity of the medium with frequency. [Dimarzio & Bishop, 1974]

From these quotes and from looking at the model predictions, which they evaluate as "a fair god fit", it is seen that the original success criteria for the DiMarzio-Bishop model, was that it should predict the right type of shape in a Cole-Cole plot. The impression is thus that DiMarzio and Bishop think of the model as a "coarse grained" model, which captures the essence of the underlying physics. The DiMarzio-Bishop model is successful from this original point of view. It does in fact serve as an explanation for the non-Debye dielectric relaxation spectra. (Though it is little surprise that a non-Debye behavior emerges from a model, when a non-Debye shear modulus is used as input.)

This is of course a very modest demand on what phenomenology the DiMarzio-Bishop model should capture. Seen in this light, the qualitative results we find in chapter 8 and 7 are of great importance, as they give new testable predictions.

The DiMarzio-Bishop model gives an explanation of the difference which is always seen between the shear loss peak position and the dielectric loss peak position. A connected result of the DiMarzio-Bishop model, is that the shape of the loss peaks in the two signals should be slightly different. In general this result holds, however, exceptions exist.

The two predictions, mentioned above, are both directly testable, but have different status. The predicted change in peak position is large and thus robust to small deviations due to details that are not incorporated in the model. On the contrary, the predicted difference in shape is small, and it is therefore sensitive to smaller differences between the model and the actual physics involved.

A third, but not directly testable, qualitative prediction is the prediction of an elastic contribution to the high frequency plateau value of the dielectric constant. This prediction would be testable if precise absolute values of the dielectric constant and the refraction index at the relevant temperature were accessible. This is unfortunately not the case since experimental problems interfere with the test. However by recasting the prediction to a question of the temperature dependence of the high frequency plateau value of the dielectric constant, the prediction becomes testable in practice. However, the drawback is that the analysis becomes much more complex and moreover the effect might not be seen in all substances.

With regard to quantitative predictions, the DiMarzio-Bishop model predicts the shape and position of one relaxation process from the other via a few parameters. Needless to say there are different ways to test if this connection holds, and our "on parameter test" is one of them. Albeit the one parameter test places even higher demands on the model, as the physically acceptable values of the parameter are limited.

The final test of the DiMarzio-Bishop model's strength as a quantitative prediction model is our test on the real part of the spectrum. Here the question is whether or not the model can be used to find the high frequency shear modulus.

The general picture from our different tests is that when more demands are added to the DiMarzio-Bishop model it starts to fail. In all cases we see the predicted change in loss peak and in most cases we also see the predicted change in shape of the loss peak, yet the difference in shape are generally small. The elastic contribution to the high frequency plateau value of the dielectric constant is in fact seen for the one substance, where we would expect the temperature dependency of the elastic contribution to dominate the experimental problems. In the test on the entire relaxation spectrum, which involves the exact connection of shape and position, there are several examples where the DiMarzio-Bishop model fails. This shows that the model is inadequate for making reliable quantitative predictions, however, this might also effect how the DiMarzio-Bishop model is perceived as a qualitative good model. One of the issues that will be discussed in the following is the question of why the model gives much better fits for some substances than for others.

12.2   The physical limits on the fitting parameter

The DiMarzio-Bishop model was in section 8.1 rewritten, by using the high frequency limit of the dielectric constant ε_h, and the high frequency limit of the shear modulus G_∞ (see equation 8.1.1):

$$\frac{\varepsilon(\omega) - \varepsilon_i}{\varepsilon_e - \varepsilon_i} = \frac{1}{1 + \frac{1/a-1}{G_\infty} G(\omega)} \quad \text{where} \quad a = \frac{\varepsilon_h - \varepsilon_i}{\varepsilon_e - \varepsilon_i}$$

In the summary of the chapter "One parameter test of the model" (section 9.4) it was discussed that the better fits on liquids with small dielectric strength might be due to a larger freedom in the fitting parameter when expressed in terms of a. In the following we will elaborate on this possibility.

The table below presents an overview of how the value of a controls the shift in loss peak position (the precise values does of course depend on shape of the mechanical signal, but the changes are minor. The shear data used here are the fictive data described in figure 8.1).

$a = \frac{\varepsilon_h - \varepsilon_i}{\varepsilon_e - \varepsilon_i}$	$\log_{10}(\nu_{lp,G}/\nu_{lp,\varepsilon})$
0.05	1.6
0.1	1.3
0.2	1.0
0.4	0.6

ε_h and ε_e are given by data and n^2 is a lower limit on ε_i. Therefore a becomes bounded by 0 and the maximum value $(\varepsilon_h - n^2)/(\varepsilon_e - n^2)$. On a practical level this yields a tighter bound for liquids with large dielectric strength as the value $(\varepsilon_h - n^2)$ is relatively small compared to $(\varepsilon_e - n^2)$.

By looking at figure 8.3 it can be observed that typical shifts in loss peak position are about half a decade (TPG being a extreme with a shift of one decade). This signifies that good fits require that the value of a should be around 0.4. High values like these can be obtained, by using physically reasonable ε_i values, in the case of liquids with small strength, whereas it is impossible for liquids with large dielectric strength.

The described model calculations were performed by calculating the dielectric constant from a shear modulus, but the conclusion regarding the shift in loss peak position will of course also hold when the DiMarzio-Bishop model is tested by the one parameter test. For liquids with large dielectric strength the maximal value of a is small, thus the model predicts a big difference between dielectric and shear mechanical loss peak positions. This might be the reason why the shear peak position is overestimated in these cases while it is well approximated for liquids with small dielectric strength.

The above discussion raises the question of whether the good fits for liquids with small dielectric strength are merely due to the freedom of a, rather than an actual better agreement between model and data. It should, however, be recalled that the DiMarzio-Bishop model makes reasonable fits of both shape and position with the same physically reasonable ε_i (and hereby a) value for the liquids with small dielectric strength. It is therefore very possible that the DiMarzio-Bishop model actually describes the dynamics of liquids with smaller strength better than the dynamics of liquids with larger dielectric strength.

12.3   The significance of the local environment

According to our quantitative tests, the DiMarzio-Bishop model is inadequate for describing the alpha process in the case of large dielectric strength, and moreover the model generally gives a poor description of the beta process. As we have argued that the choice of local field does not explain the poor agreement it indicates that the microscopic model itself, gives a poor description for the beta relaxation and of the relaxation in liquids with large dielectric strength.

It is very likely that the assumption about uncorrelated dipoles is good for liquids in which the dipole is very weak, since other types of intermolecular forces will dominate over dipole-dipole interactions; whereas it is a poor assumption for very dipolar liquids, where the dipole-dipole interactions might introduce local order. The consequence of such a local order in the liquid, is that each molecule "sees" a different environment, and that the properties of this local environment will differ largely from the average behavior of the liquid. This could be an explanation for the poor agreement between the DiMarzio-Bishop model and data on substances with a large dipole.

It is likely that some local order exits even for liquids with small permanent dipoles, and even if this is not the case, the local behavior will still differ from the average behavior of the liquid.

The beta process is believed to be a local process. Such a local process is probably more dependent on the local order of the liquid than the larger structural rearrangements of molecules in the alpha process. This could offer an explanation to why the DiMarzio-Bishop model fails to give a quantitative description of the beta process, while it works better for the alpha process.

It could of course be argued that the shear modulus also depends on the intermolecular forces, but as mentioned in an introductory chapter (section 2.3) it is easy to imagine two different relaxation processes representing the underlying dynamics in two different ways. Hence it is possible that the local structure has a different influence on the shear modulus and the dielectric constant respectively.

12.4   The friction term and the molecular radius

In the test of the DiMarzio-Bishop model, which are presented in the literature, r is normally used as a fitting parameter (see section 4.6).

By relating r to the elastic contribution in terms of $a = (\varepsilon_h - \varepsilon_i)/(\varepsilon_e - \varepsilon_i)$ we can use the physical limits on ε_i to determine limits for reasonable values of r.

Using the Maxwell formulation of the DiMarzio-Bishop model (equation 4.7.5) the following connection is found:

$$a = \frac{1}{1 + \frac{4\pi r^3}{k_B T} G_\infty} \quad \text{giving} \quad r^3 = (1/a - 1)\frac{k_B T}{4\pi G_\infty}. \tag{12.4.1}$$

If the Clausius-Mossotti approximation is used, a $\frac{\varepsilon_i + 2}{\varepsilon_e + 2}$ term enters the equation.

It can be seen that a large elastic contribution (large a) could be due to a small molecular radius or a small G_∞. Equally it is seen that bounds on r can be given from the bounds on ε_i, if ε_h, ε_e and G_∞ are known from the measurements. A lower bound on ε_i, corresponding to an upper bound on a, yields a lower bound on r. An example, using

standard reasonable values of T (200K), and G_∞ (1GPa), is that a bound of $a < 0.05$ corresponds to $r > 1.6\text{Å}$.

The differences we see between the shear and the dielectric loss peak positions correspond to a values ranging from $a = 0.1$ to $a = 0.4$. Using physically reasonable values for T, and G_∞ (the results are rather robust regarding the precise values) it is found that $a = 0.1$ leads to $r \approx 1\text{Å}$ and that $a = 0.4$ leads to $r \approx 0.7\text{Å}$. Reasonable fits made with r as a parameter will therefore give r values of this order of magnitude.

The radii found in the literature based on fits with the DiMarzio-Bishop model, agree reasonably well with the above. However, a molecular radius of approximately 1Å is smaller than physically reasonable for a molecular liquid. Hence, these r values could be seen as an argument against the model, but the DiMarzio-Bishop model can easily be adjusted to avoid this problem.

The actual form of the friction term $\zeta(\omega)$ does not enter in the derivation of the DiMarzio-Bishop model. It is therefor possible to choose this function after the general derivation of the model.

In the derivation of the model it was assumed that the rotational friction is given by a Stokes friction term in the no slip case. A simple modification could be a smaller constant connecting $\zeta(\omega)$ and $\eta(\omega)$. Changing the factor connecting $\zeta(\omega)$ and $\eta(\omega)$ could be interpreted as allowing some degree of slip. Such an approach will not lead to any differences regarding the DiMarzio-Bishop model's ability to describe the data. It merely opens the possibility of using values of r, which are more physically reasonable, without changing the essentials of the model.

The DiMarzio-Bishop model gives a very simple and consistent connection between the shear modulus and the dielectric constant. Hence, the notion of a sphere rotating in the liquid is not fundamental for the DiMarzio-Bishop model. It is the simple coupling between rotation and macroscopic shear behavior which is essential.

The above discussion emphasizes how profitable it is to express the DiMarzio-Bishop model in terms of macroscopic parameters, as the acceptable values of the macroscopic parameters stay unaffected by the physical interpretation of the model.

12.5 The dynamics

One of the overall conclusions on our work is that it is reasonable to use the DiMarzio-Bishop model as a tool for understanding the fundamentals of rotational dynamics. This raises the question of which kind of dynamics the DiMarzio-Bishop model suggests.

The fluctuation dissipation theorem (equation 2.4.3) tells us that the response function in terms of $\chi(t)$ is directly proportional to $\langle (P(t) - P(0))^2 \rangle$. Therefore, the interpretation of the model can be made in terms of the fluctuation in polarization, which is directly related to the mean fluctuation in orientation.

The rotation of the molecules was in the original Debye model described by ordinary (rotational) diffusion. This meant that the squared polarization fluctuation was predicted to be continuous and exponential. In the DiMarzio-Bishop model the dynamics of the equilibrium liquid is somewhat different. At very short times the mean molecule performs an angular jump, which brings it a finite distance away form the starting point, whereas the molecular dynamics becomes dominated by ordinary diffusion at very long

time scales. In the intermediate time ranges the dynamics changes gradually from very fast dynamics to the diffusion regime.

An alternative way of receiving information about the rotational dynamics is NMR experiments. By varying an experimental parameter in the NMR experiments a parametrized correlation function can be obtained, and this yields information about the rotational dynamics (see for example Hinze [1998] and Böhmer et al. [2001]).

The general framework for interpreting results from this kind of NMR experiments is in terms of angular jump models[1]. The main parameters in the jump models are the jump angle distribution and the distribution of waiting times (rotational diffusion is a special case of jump models where the jump angle goes to zero). The data are analyzed by simulating a given jump dynamics and calculating the NMR signal, which would emerge form a sample with this dynamics. A simple distribution consisting of a mixture of small jumps (in the order of $5°$) and large jumps (in the order of $20 - 50°$) is usually sufficient to describe the data[2].

A simple interpretation is proposed in Hinze [1998], where the large jumps are the fundamental reorientation of the molecules and the small jumps are attributed to local reorganization after a large jump has perturbed the local potential. Alternatively the small jumps could initiate the large jumps, however, it is unknown if the first or the second scenario is most correct [Böhmer et al., 2001].

The NMR-based understanding of the rotational dynamics is not necessarily in contradiction with the DiMarzio-Bishop model. The DiMarzio-Bishop model incorporates the jump dynamics via the shear modulus, which in itself is believed to be controlled by jump dynamics.

We have studied the simple NMR-based jump picture by performing a small simulation[3] where $\langle (P(t) - P(0))^2 \rangle$ was calculate for a system with this type of jump dynamics. No abrupt differences between short time and long time behavior could be seen in $\langle (P(t) - P(0))^2 \rangle$, thus no sign of an instantaneous contribution was found. This implies that the elastic contribution that enters in $\langle (P(t) - P(0))^2 \rangle$ according to the DiMarzio-Bishop model cannot be seen in the simple NMR-based jump picture.

12.6 The connection between shear mechanical and dielectric relaxation

A final point to consider, is how the relation between shear and dielectric behavior could be understood, if the DiMarzio-Bishop model really does give an adequate tool for understanding the relation.

We picture this by two different scenarios. The first of these scenarios is tightly connected to the traditional derivation of the model, whereas the latter is more abstract.

The rotation of a molecule in the liquid is inhibited by its interaction with its neighbor molecules via intermolecular forces. This interaction will obviously be determined by

---

[1]The concept of jump dynamics is, as described in the introduction to "glass forming liquids", part of todays paradigm for understanding very viscous liquids.

[2]The ratio between large and small jumps depends much on the substance, it is as an example found in Hinze [1998] that 80% small jumps and 20% large jumps should be used in the case toluene.

[3]The simulation method (a continuous time random walk algorithm) and choice of parameter, are based on Hinze [1998]. The distribution of the size of jumps were: 80% $4°$ jumps and 20% $25°$ jumps. The waiting time distribution was taken to be an exponential distribution. The average was taken over 10^5 trajectories.

the local configuration around the molecule. The assumption of the DiMarzio-Bishop model is that the *averaged* interaction is equivalent to the interaction between a macroscopic entity and the continuum liquid - a continuum liquid which is characterized by the macroscopic shear modulus. The shear modulus is an average property, which is directly related to the microscopic intermolecular forces. Hence, the DiMarzio-Bishop model gives a prescription of how two different macroscopic quantities should be connected.

When, recalling that both shear and dielectric behavior are governed by the liquids fluctuation in the $6N + 1$ dimensional energy landscape, the scene is set for a more abstract interpretation. A movement in the landscape will be reflected some way in the shear stress and some other way in the rotational polarization. The two do not a priori need to be connected. However, if it is assumed that they are in fact connected, then the DiMarzio-Bishop prescribes a simple and consistent connection.

The topology of the energy landscape is determined by the intermolecular forces. Hence, it is the relation between the intermolecular forces, the shear stress, and the polarization which is the key point, in both of the above interpretations. Therefore we think of them as two different ways of picturing what might happen, rather than two competing suggestions.

13 A few other points

The aim of this chapter is to report and discuss our data in relation to some of the fundamental questions of the phenomenology of relaxation in glass forming liquids. These points are not directly linked to the DiMarzio-Bishop model, however they are very central to the research area, and this is why we chose to include them. Needless to say, the comparison of shear and dielectric behavior is in focus in this chapter as it for the rest of our work.

13.1 Time temperature superposition (TTS)

An interesting question is whether or not the shape of the alpha peak is temperature dependent (see section 2.5.2). This question relates closely to the question of the differences between the shape of the dielectric spectrum and the shape of the shear mechanical spectrum, since these differences will be temperature independent if TTS is be obeyed in both relaxations.

TTS plots of both the shear and the dielectric relaxations are shown in figures 13.1 to 13.5. In the plots it is seen that for the alpha substances (TPE, DC704 and PPE) the dielectric constant and the shear modulus show an almost temperature independent shape of the loss peak (see figure 13.1, 13.2 and 13.3). Especially the shear modulus of DC704 and PPE and the dielectric constant of DC704 is seen to fall on master curves.

In the case of substances with a beta peak TTS breaks down. On TPG where the beta peak is much less pronounced than in the case of DHIQ it does, however, look very much as if the alpha peak alone exhibits TTS. The shear alpha peak of both DHIQ and TPG get narrower as the temperature decreases. Equally this means that the alpha peak gets narrower as the beta peak and the alpha peak separate from each other. (see figure 13.5 and 13.4). A close inspection of the dielectric data on DHIQ and TPG reveals a more complicated temperature dependence. At high temperatures, where the alpha peak is at higher frequencies than the beta peak, the alpha peak is rather narrow. As the temperature is decreased the peak gets broader, and the beta peak appears as a shoulder. At even lower temperatures the two peaks separate and the alpha peak becomes narrower again. (see figure 13.6). This suggests that it is the merging with the beta peak which gives the temperature dependence of the alpha peaks width, hence that the alpha peak itself has a temperature independent shape. Unfortunately, we are not able to test if this scenario is also found in the shear mechanical relaxation, because we do not have any substances where the beta peak appears at sufficient low frequencies.
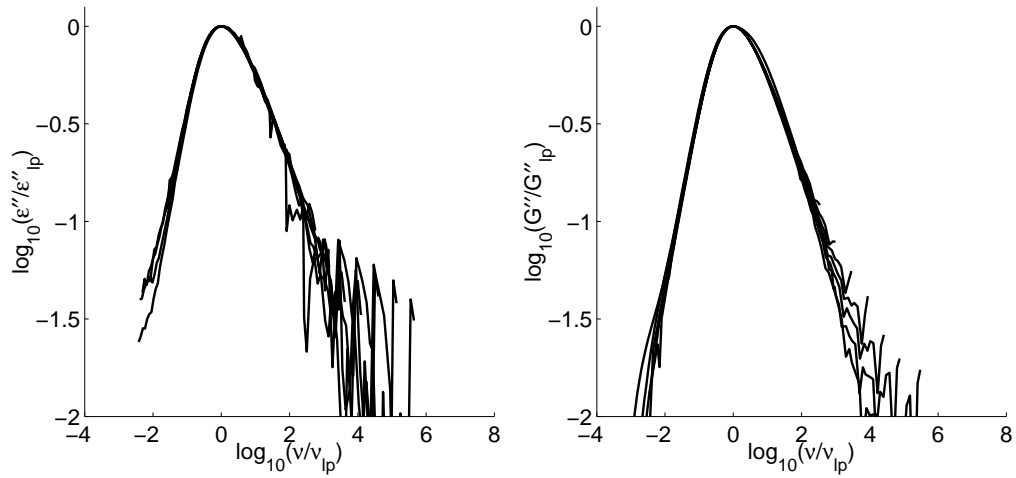
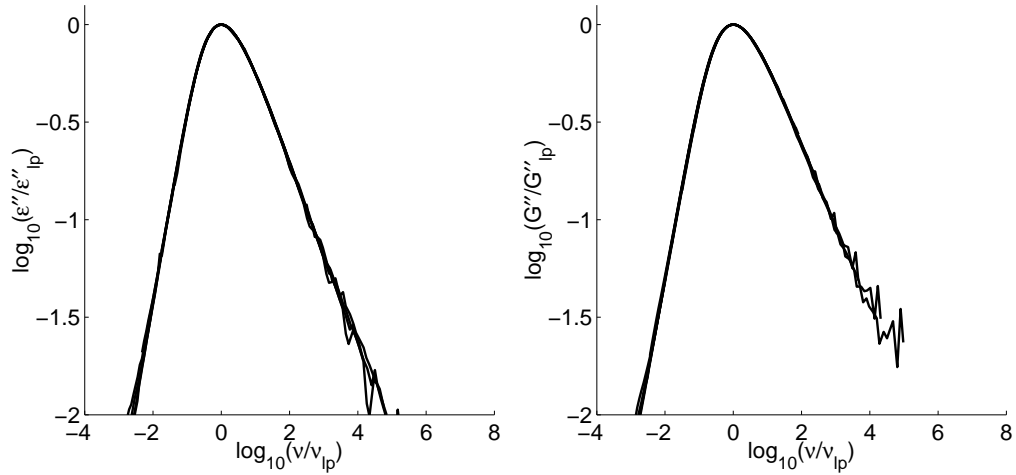**Figure 13.1** TTS plot of TPE data, at 254.0K to 266.0K in steps of 2K.

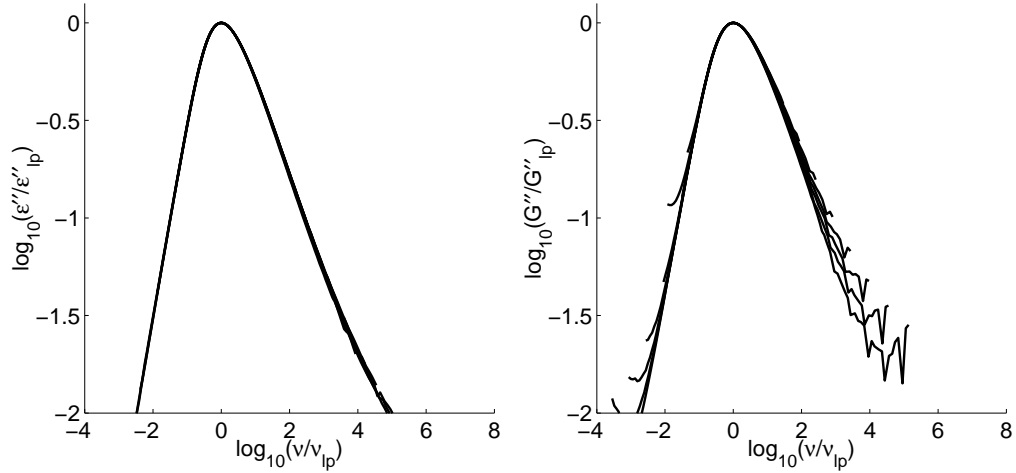**Figure 13.2** TTS plot of DC704 data, at 215.4K to 231.6K in steps of approximately 2K.

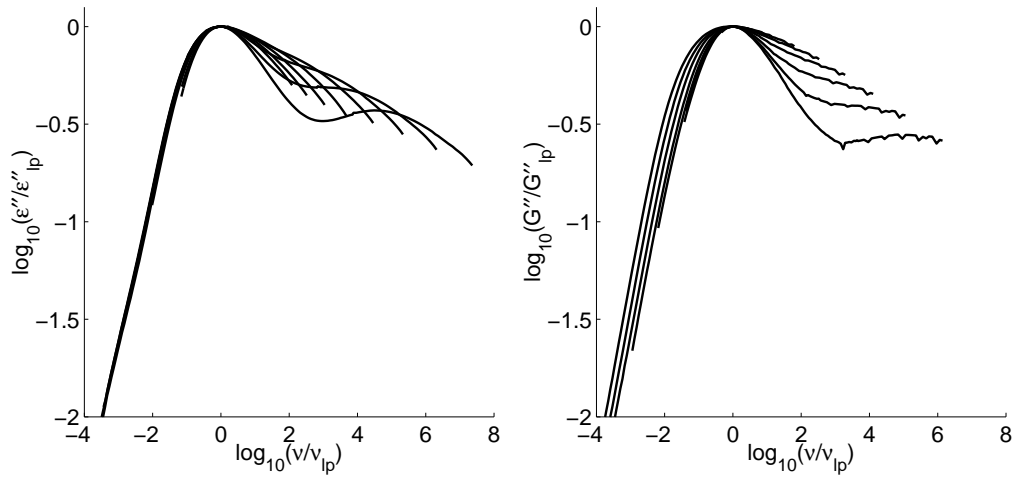**Figure 13.3** TTS plot of PPE data, at 250.0K to 264.0K in steps of 2K.

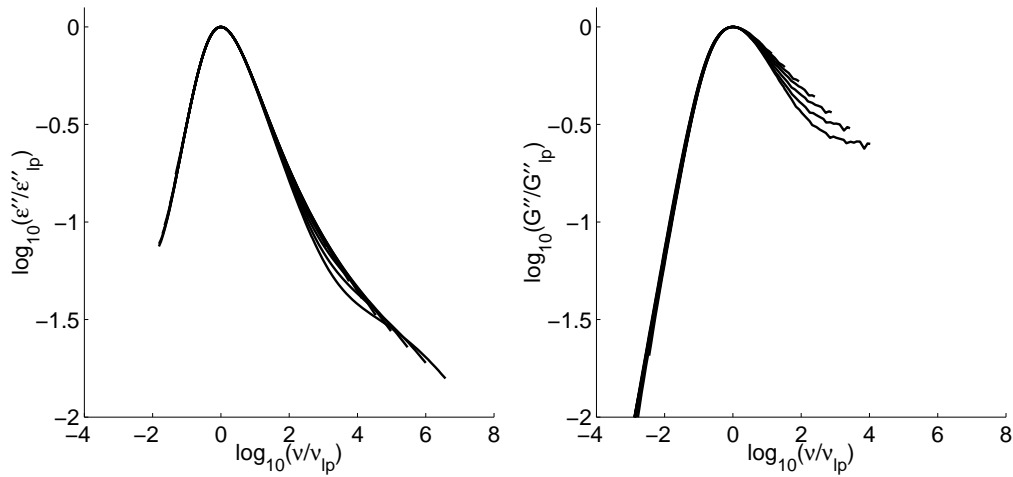**Figure 13.4** TTS plot of DHIQ data, at 180.0K to 190.5K in steps of 1.5K.

Figure 13.5 TTS plot of TPG data, at 196.0K to 212.0K in steps of 2K.
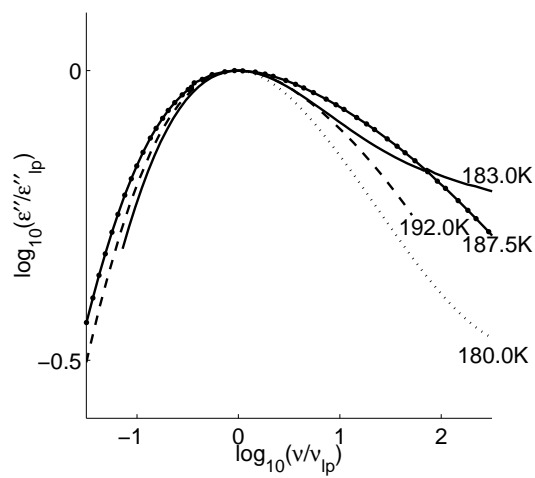

Figure 13.6 TTS plot of DHIQ dielectric data at the temperatures given on the figure. Note the scale on the x-axis, the beta peak is outside this zoom.

13.2 Dielectric modulus versus dielectric constant

When comparing dielectric and shear mechanical data, it is often discussed which dielectric response function should be used. In this section we make a few comments concerning this discussion.

13.2.1 Brief background

The most common ways of presenting the relaxations respectively are via the dielectric susceptibility in terms of ε and the shear modulus G, and these two functions are compared in several cases. An alternative which is sometimes used is a comparison of the dielectric modulus M with G. We are not aware of any model based predictions regarding a direct connection between M and G, but it is a general assertion that moduli ought to be compared to other moduli and susceptibilities to susceptibilities [Angell et al., 2000], [Paluch, 2000].

It is difficult to compare the shear compliance to the dielectric constant because the former diverges as the frequency approaches zero, while the dielectric constant has a finite equilibrium value. Using the retardation part of the compliance (see section 3.1 for a definition) does, however, offer a way around this problem [Schröter & Donth, 2002], [Angell et al., 2000].

13.2.2 Our work in this view

We did find that the dielectric modulus, according to the DiMarzio-Bishop model, should be closer to the shear modulus than the dielectric constant. This could on one hand, be used to support the view that the dielectric modulus should be compared to the shear modulus. On the other hand, we found that the behavior of the relation between the dielectric modulus and the shear modulus was dependent on the dielectric relaxation strength, whereas this was not the case for the dielectric constant, (see section 8.1.1).

In our quantitative analysis we cast the dielectric data into a modulus form, though it was not the pure modulus ($M = 1/\varepsilon$) but a *rotational dielectric modulus* ($1/(\varepsilon - \varepsilon_i)$). However, it is almost trivial that a model that gives the shear *modulus* from the dielectric data should include something *modulus*-like.

The discussion on whether the modulus or the dielectric constant should be used is of limited relevance on a practical level with regard to substances with a little dielectric strength, as the two relaxation peaks have the same shape and position in these cases[1]. An example of this can be seen in the right plot of figure 13.7.

For liquids with great relaxation strength very different curves are seen when going from the susceptibility picture to the modulus, hence the conclusions drawn will certainly depend on which formulation is chosen. The dielectric relaxation spectra of TPG, which has a very large dielectric strength and a beta relaxation, serves an example of

---

[1]The general relation between the two losses is $M''(\omega) = \frac{-\varepsilon''(\omega)}{(\varepsilon'(\omega))^2 + (\varepsilon''(\omega))^2}$. The dielectric constant can be expressed as, $\varepsilon(\omega) = \varepsilon_h + \delta(\omega) + i\varepsilon''(\omega)$, where $\delta(\omega)$ and $\varepsilon''(\omega)$ are small compared to ε_h if the dielectric strength is small. Thus the relation between the losses reduces to the proportionality $M''(\omega) \approx \frac{-\varepsilon''(\omega)}{\varepsilon_h^2}$, for substances with small strenght

pronounces differences between the susceptibility and the modulus curves. The dielectric modulus and the dielectric constant are shown for TPG on the left hand plot of figure 13.7. The peak of the modulus is wider, furthermore it can be seen that the beta relaxation is much more pronounced in the dielectric modulus than in the dielectric constant.
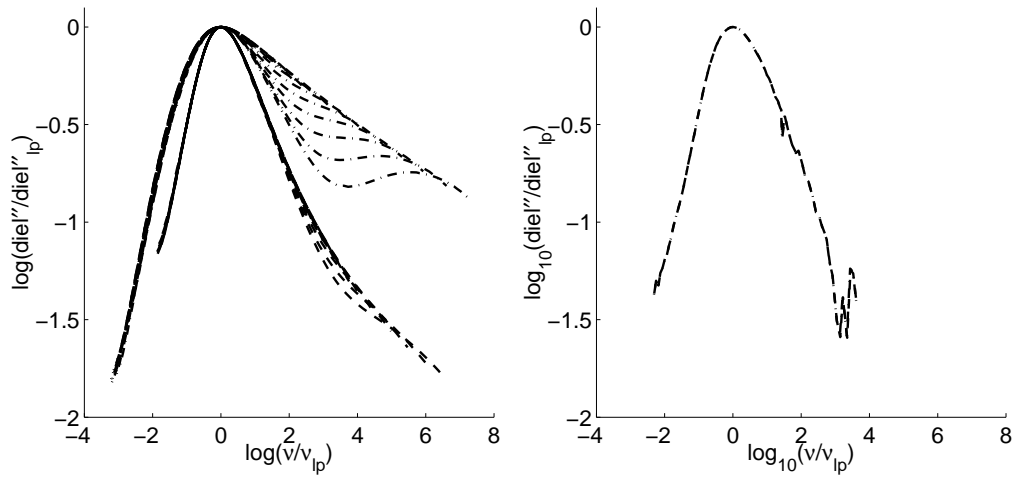

Figure 13.7 Comparison of the shape of the dielectric constant (dashed line) and the dielectric modulus (dash dotted line). The left figure shows TPG at 190K to 224K in steps of two degrees. The right plot shows TPE at 262K, it is almost impossible to distinguish the two curves.

13.3   Fragility

The temperature dependence of the loss peak position, is as we mentioned numerous pages back a thoroughly studied area. In this section we report how the liquids we have studied behave in this respect. The focal point is an evaluation of how the results depend on whether shear or dielectric data are used.

We have found both the Olsen index at T_g and the Angell fragility index (see section 2.2 for definitions). We have found that the uncertainties on determining the indexes is large. Furthermore the result is strongly dependent on what exact procedure is used, and on which precise definitions (eg. of T_g) are used. However, the general order of the liquids on the fragile to strong scale seems to be the same for different methods as long as the same method is used for all liquids. Therefore, we have used the exact same method in determining the indexes for all liquids and for shear and dielectric data alike[2].

The results are shown in table 13.1. We have earlier reported that the shear loss peak position is at a higher frequency than the dielectric loss peak position. The same result is seen here as a lower shear T_g than dielectric T_g. Squalane falls out of this pattern; it is seen in figure 8.3 that the difference between the two loss peaks approaches zero as T_g is approach in the case of squalane, this is consistent with identical T_g.

The general trends regarding fragility is that the liquid appears to be more fragile when studied via the shear relaxation, than when studied by the dielectric relaxation. It is very dependent on substance how pronounced the difference is. The most important conclusion to be drawn from table 13.1 is thus that very exact agreement should not be expected for models that aim to explain the fragility if the model is not related to the characteristic time of a specific relaxation. There is little qualitative difference regarding which liquids are found to be strong or fragile respectively, but it should be kept in mind that all the liquids (except DHIQ) have very similar fragility. It is therefore possible that the picture changes if a greater span of fragilities is included.

The greatest differences seem to be seen for liquids with a beta relaxation. Recalling figure 8.3 we also found that the loss peak positions of the two relaxations show stronger decoupling for the beta liquids. These results might be due to our simple treatment of the data, and might therefore be altered if the alpha loss peak position was found after subtracting the beta relaxation by some appropriate procedure.

---

[2]

- The alpha loss peak positions, is taken to be the point of maximum loss and $\nu_{lp}(T)$ is found by using a fitting routine.

- $\tau(T)$ is defined as $1/\nu_{lp}(T)$.

- The glass temperature is defined as the temperature where $\tau(T_g) = 10^3$s. This leads to a difference in T_g depending on whether shear of dielectric data are used.

- $\tau_0 = 10^{-13}$s is assumed.

- $E(T) = k_B T(\ln \tau(T) - \ln \tau_0)$ is determined.

- The slopes $\gamma(T_g) = - \left. \frac{d \log E(T)}{d \log T} \right|_{T_g}$ and $m = \left. \frac{d \log_{10}(\tau)}{dT_g/T} \right|_{T_g}$ are estimated by using the last measured point and the theoretical point $(T_g/T, \tau) = (1, 10^3 \text{s})$. In this step much care is taken in order to determine T_g correctly such that this estimate of the slope is actually right. The uncertainty of the determination of T_g is the main flaw of this procedure. In the cases where we have a data point close to T_g the uncertainty is much smaller, this is seen because the difference in m as found directly from the definition and found via γ becomes significantly smaller.

Contrary to what we generally see DHIQ comes out more fragile by the dielectric data. DHIQ also deviates from the other liquids by being very fragile and by having an extremely pronounced beta relaxation, and both these features could affect the fragility or the fragility found by the procedure we have used.

	Dielectric			Shear		
	T_g	γ	m	T_g	γ	m
TPE Triphenylethylene	248.7K	3.8	73	247.5K	4.1	78
DC704 Tetramethyltetraphenyl- trisiloxane	210.5K	4.2	83	209K	4.6	83
PPE Polyphenyl Ether	244.7K	4.2	80	243K	4.6	85
Squalane Perhydrosqualene	166.7K	3.2	64	166.7K	4.5	87
Pb20 Polybutadiene	175.7K	4.0	79	175.2K	5.7	105
DHIQ Decahydroisoquinoline	178.7K	9.0	154	178.2K	8.0	143
TPG Tripropylene glycol	189K	3.3	65	187K	4.6	86

Table 13.1 The glass temperature and the fragility (in terms of the Olsen index $\gamma(T_g)$, and the Angell index m.) found from dielectric and shear relaxation respectively. Equation 2.2.5 does not hold exactly due to numerical uncertainties.

14   Conclusion

The DiMarzio-Bishop model which is a generalization of the Debye model has been analyzed and tested.

We have given a macroscopic formulation of the model, which gives a correct treatment of the high frequency behavior of the dielectric relaxation and have thereby avoided earlier simplifying, but unphysical assumptions.

Measurements have been made on seven different liquids and we have in all cases taken both shear mechanical and dielectric relaxation spectra under the same physical conditions. All seven liquids exhibit different phenomenology when categorized by whether a secondary relaxation can be seen and by their dielectric relaxation strength.

The DiMarzio-Bishop model predicts an elastic contribution to the high frequency dielectric constant. We have shown that an increase in the high frequency dielectric constant with increasing temperature has to be due to such an elastic contribution, and we have demonstrated that this behavior can in fact be found in data.

Furthermore we have shown that the model predicts the shear loss peak to be found at higher frequencies than the loss peak of the dielectric constant. This prediction concerns both the primary alpha relaxation and the secondary beta relaxation. The prediction is found to hold in all our data as well as in data, which are reported in the literature.

The model also predicts a shear relaxation that is broader than the dielectric relaxation and that the secondary relaxation is more pronounced in the shear relaxation than in the dielectric relaxation. Our data generally behave in accordance with these predictions. There are, however, exceptions, and the broadening is not as unambiguous as it should be expected from the DiMarzio-Bishop model.

We have formulated the DiMarzio-Bishop model in a version where the loss peak shape and loss peak position of the shear modulus can be found from the dielectric constant by using only one macroscopic parameter, ε_i. By using this formulation, the DiMarzio-Bishop model can give reasonable quantitative fits for liquids with small dielectric strength and no beta relaxation. For liquids with a small strength and a beta relaxation we see reasonable fits around the alpha peak, while the beta peak is overestimated. The model cannot give reasonable fits for liquids with a large dielectric strength, if a physically reasonable value is to be used for the macroscopic parameter, ε_i. The physically determined limit we have on ε_i is relatively stronger when applied to liquids with large strength. It is therefore impossible to know if the strength dependent difference in the quality is the fit is due to different physics or due to this practical difference.

By using different local fields in the DiMarzio-Bishop model, and by specifically studying how the effects of the chosen local field is strength dependent, we have shown that the deviations between data and model are unlikely to be due to the local field approximation.

The quantitative agreement between the DiMarzio-Bishop model and data are all in all moderate to poor. Resultantly, we do not think it is a realistic prospect to predict

shear behavior from dielectric data by using the DiMarzio-Bishop model, nor to understand the details of dielectric relaxation in terms of the DiMarzio-Bishop model. The qualitative predictions of the DiMarzio-Bishop model do, however, capture a lot of the phenomenology. Therefore, we believe that the model serves as a tool for understanding the fundamental physics of dielectric relaxation. This implies that shear relaxation and dielectric relaxation are in fact closely related.

Bibliography

Angell, C. A., Ngai, K. L., McKenna, G. B., McMillan, P. F. & Martin, S. W. [2000]. Relaxation in glassforming liquids and amorphous solids, *J. Appl. Phys.* **88**: 3113.

Bauer, C., Böhmer, R., Moreno-Flores, S., Richert, R., Sillescu, H. & Neher, D. [2000]. Capacitive scanning dilatometry and frequency-dependent thermal expansion of polymer films, *Phys. Rev. E* **61**: 1755.

Bauer, C., Richert, R., Böhmer, R. & Christensen, T. [2000]. Dynamic thermal expansivity near the glass transition, *J. Non-cryst Solids* **262**: 276.

Böhmer, R., Diezemann, G., Hinze, G. & Rössler, E. [2001]. Dynamics of supercooled liquids and glassy solids, *Prog Nucl Mag Res Sp* **39**: 191.

Böttcher, C. J. F. [1973]. *Theory of electric polarization*, Vol. 1, 2 edn, Elsevier Scientific Publishing Company.

Chang, I. & Sillescu, H. [1997]. Heterogeneity at the glass transition: Translational and rotational self-diffusion, *J. Phys. Chem. B* **101**: 8794.

Christensen, T. & Olsen, N. B. [1994]. Comparative measurements of the electrical and shear mechanical response function in some supercooled liquids, *Journal of Non-Chrystaline Solids* **172**: 357.

Christensen, T. & Olsen, N. B. [1995]. A rheometer for the measurement of a high shear modulus covering more than seven decades of frequency below 50 kHz, *Rev. Sci. Instrum* **66**: 5019.

Cole, R. H. [1938]. Dielectric absorbation in polar media and the local field, *J. Chem. Phys.* **6**: 385.

Díaz-Calleja, R., Riande, E. & Román, J. S. [1993]. Interconversion between mechanical and dielectric relaxations for poly(cyclohexyl acrylate), *J. Polym Sci. Pol Phys.* **31**: 711.

Debye, P. [1929]. *Polar Liquids*, The Chemical Catalog Company, Inc.

Deegan, R. D., Leheny, R. L., Menon, N., Nagel, S. R. & Venerus, D. C. [1999]. Dynamic shear modulus of tricresyl phosphate and squalane, *J. Phys. Chem. B* **103**: 4066.

Deegan, R. D. & Nagel, S. R. [1995]. Dielectric susceptibility measurements of the primary and secondary relaxation in polybutadiene, *Phys. Rev. B* **52**: 5653.

Dimarzio, E. A. & Bishop, M. [1974]. Connection between macroscopic electric and mechanical susceptibilities, *J. Chem. Phys.* **60**: 3802.

Doi, M. & Edwards, S. F. [1986]. *The Theory of Polymer Dynamics*, Oxford University Press.

Donth, E., Beiner, M., Reissig, S., Korus, J., Garwe, F., Vieweg, S., Kahle, S., Hempel, E. & Schröter, K. [1996]. Fine structure of the main transition in amorphous polymers: Entanglement spacing and characteristic length of the glass transition. Discussion of examples, *Macromolecules* **29**: 6589.

Dyre, J. C. & Olsen, N. B. [2003]. Landscape equivalent of the shoving model. To appear i Phys. Rev. E, cond-mat/0211042.

Dyre, J. C., Olsen, N. B. & Christensen, T. [1996]. Local elastic expansion model for viscous-flow activation energies of glass-forming molecular liquids, *Phys. Rev. B* **53**: 2171.

Ediger, M. D., Angell, C. A. & Nagel, S. R. [1996]. Supercooled liquids and glasses, *J. Phys. Chem.* **100**: 13200.

Einstein, A. [1905]. Über die von der molekularkinetishen Theorie der Wärme geforderte Bewegung von in ruhenden Flüssigkeiten suspendierten Teilchen, *Annalen der Physik* **17**: 549.

Etienne, S., Elkoun, S., David, L. & Magalas, L. B. [2003]. Mechanical spectroscopy and other relaxation spectroscopies, *Sol St Phen* **89**: 31.

Fatuzzo, E. & Mason, P. [1967]. A calculation of the complex dielectric constant of a polar liquid by the librating molecule method, *Proc. Phys. Soc. Lond.* **90**: 729.

Ferri, D. & Castellani, L. [2001]. Fine structure and thermorheological complexity of the softening dispersion in styrene-based copolymers, *Macromolecules* **34**: 3973.

Ferry, J. D. [1961]. *Viscoelastic properties of polymers*, second edn, John Wiley & Sons, INC.

Gemant, A. [1935]. The conception of a complex viscosity and its application to dielectrics, *Trans. Faraday. Soc.* **31**: 1582.

Goldstein, M. [1969]. Viscous liquids and glass transition - a potential energy barrier picture, *J. Chem. Phys.* **51**: 3728.

Harrison, G. [1976]. *The Dynamic Properties of Supercooled Liquids*, Academic press (INC.) London LTD.

Havriliak, S. [1990]. Equilibrium polarization of polar polymers in a matrix of arbitrary compliance, *Macromolecules* **23**: 2384.

Havriliak, S. & Havriliak, S. J. [1995]. Comparison of dielectris theories that explicitly include viscoelastic parameters, *J. Polym Sci. Pol Phys.* **33**: 2245.

Hinze, G. [1998]. Geometry and time scale of the rotational dynamics in supercooled toluene, *Phys. Rev. E* **57**: 2010.

Johari, G. P. [1973]. Intrinsic mobility of molecular glasses, *J. Chem. Phys.* **58**: 1766.

Johari, G. P. [2002]. Localized molecular motions of beta-relaxation and its energy landscape, *J. Non-cryst Solids* **307**: 317.

Johari, G. P. & Goldstein, M. [1970]. Viscous liquids and glass transition. II. secondary relaxations in glasses of rigid molecules, *J. Chem. Phys.* **53**: 2372.

Jonscher, A. K. [1983]. *Dielectric Relaxation in Solids*, Chelsea Dielectric Press Ltd.

Lautrup, B. [1999]. *Continuum Physics*, draft 6, march 3, 1999 edn. Unpublished, new edition can be acquired from NBI, Copenhagen university.

Lunkenheimer, P. & Loidl, A. [2002]. Dielectric spectroscopy of glass-forming materials: alpha-relaxation and excess wing, *Chem. Phys.* **284**: 205.

Menon, N., Nagel, S. R. & Venerus, D. C. [1994]. Dynamic viscosity of a simple glass-forming liquid, *Phys. Rev. Lett.* **73**(7): 963.

Olsen, N. B. [1998]. Scaling of beta-relaxation in the equilibrium liquid state of sorbitol, *J. Non-cryst Solids* **235**: 399.

Olsen, N. B. [2003]. Personal communication.

Olsen, N. B., Christensen, T. & Dyre, J. C. [2000]. Beta relaxation of nonpolymeric liquids close to the glass transition, *Phys. Rev. E* **62**: 4435.

Olsen, N. B., Christensen, T. & Dyre, J. C. [2001]. Time-temperature superposition in viscous liquids, *Phys. Rev. Lett.* **86**: 1271.

Onsager, L. [1936]. Electric moments of molecules in liquids, *J. Am. Chem. Soc.* **58**: 1486.

Paluch, M. [2000]. Dielectric and mechanical relaxation in epoxy systems with molecules of differing topology, *J. Phys-condens Mat* **12**: 9511.

Rasmussen, T. S. [2003]. Personal communication, Technical staff IMFUFA, RUC.

Ribierre, J. C., Mager, L., Fort, A. & Méry, S. [2003]. Effects of viscoelastic properties on the dielectric and electrooptic responses of low-T_g guest-host polymers, *Macromolecules* **36**: 2516.

Richert, R. [2002]. Heterogeneous dynamics in liquids: fluctuations in space and time, *J. Phys-condens Mat* **14**: R703–R738.

Richert, R. [2003]. Dielectric squalane data. Unpublisehd.

Richert, R. & Angell, C. A. [1998]. Dynamics of glass-forming liquids. V. On the link between molecular dynamics and configurational entropy, *J. Chem. Phys.* **108**: 9016.

Richert, R., Duvvuri, K. & Duong, L. T. [2003]. Dynamics of glass-forming liquids. VII. Dielectric relaxation of supercooled *tris*-naphthylbenzene, squalane, and decahydroisoquinoline, *J. Chem. Phys.* **118**: 1828.

Rössler, E. [1990]. Indications for a change of diffusion mechanism in supercooled liquids, *Phys. Rev. Lett.* **65**(13): 1595.

Schrøder, T. B., Sastry, S., Dyre, J. C. & Glotzer, S. C. [2000]. Crossover to potential energy landscape dominated dynamics in a model glass-forming liquid, *J. Chem. Phys.* **112**: 9834.

Schröter, K. & Donth, E. [2000]. Viscosity and shear response at the dynamic glass transition of glycerol, *J. Chem. Phys.* **113**: 9101.

Schröter, K. & Donth, E. [2002]. Comparison of shear response with other properties at the dynamic glass transition of different glassformers, *J. Non-cryst Solids* **307**: 270.

Scientific Instrument Services, Inc. [n.d.].
URL: *http://www.sisweb.com/*

Sigma-Aldrich [n.d.].
URL: *http://www.sigmaaldrich.com*

Suchanski, W., Jurga, S., Pakula, T., Paluch, M. & Ziolo, J. [2000]. Molecular dynamics in supercooled di-isobutyl phthalate close to the glass transition, *J. Phys-condens Mat* **12**: 9551.

Vogel, M. & Rössler, E. [2001]. Slow beta process in simple organic glass formers studied by one- and two-dimensional ^2H nuclear magnetic resonance. I, *J. Chem. Phys.* **114**: 5802.

Yang, M. & Richert, R. [2002]. Solvation dynamics and probe rotation in glass-forming liquids, *Chem. Phys.* **284**: 103.

Zorn, R., McKenna, G. B., Willner, L. & Richter, D. [1995]. Rheological investigation of polybutadienes having different microstructures over a large temperature-range, *Macromolecules* **28**: 8552.

Zorn, R., Mopsik, F. I., McKenna, G. B., Willner, L. & Richter, D. [1997]. Dynamics of polybutadienes with different microstructures. 2. Dielectric response and comparisons with rheological behavior, *J. Chem. Phys.* **107**: 3645.

A   Reaction field

A dipole in a dielectricum (which in our case is made up of the same type of dipoles) will polarize its surroundings and this polarization of the surroundings will give rise to an electric field at the position of the original dipole. This field is called the reaction field. In the following we outline how the reaction field is found following the presentation in Böttcher [1973].

The first step is to consider the case of a permanent dipole that cannot be further polarized. That is no further polarization is induced when a field acts on the dipole.

The dipole itself is modeled as a spherical vacancy, with radius a, with an ideal dipole in the center. The vacancy is labeled domain 2. The surroundings of vacancy are modeled as a continuum with a dielectric constant ε. The surroundings are labeled area 1.

The potentials in the two domains φ_1 and φ_2 are found by using the standard solution of Laplace's equation in spherical coordinates with the z-axis pointing the same direction as the dipole. This is combined with the boundary conditions, which are standard when solving the equation over an interface between vacuum and a dielectricum

$$\varphi_1\big|_{r=a} = \varphi_2\big|_{r=a}, \quad \varepsilon \frac{\partial \varphi_1}{\partial r}\bigg|_{r=a} = \frac{\partial \varphi_2}{\partial r}\bigg|_{r=a}, \tag{A.1}$$

the condition that the field goes to zero at long distances from the dipole

$$\varphi_1\big|_{r \to \infty} = 0, \tag{A.2}$$

and the condition that the divergence in the center has to correspond to the divergence due to the ideal dipole that is placed there. Accordingly the only diverging term in φ_2 should be

$$\frac{\mu}{r^2} \cos(\theta). \tag{A.3}$$

This procedure yields the following potential within the cavity

$$\varphi_2 = \frac{\mu}{r^2} \cos(\theta) - \frac{2(\varepsilon - 1)}{2\varepsilon + 1} \frac{\mu}{a^3} r \cos(\theta). \tag{A.4}$$

The first term is the potential of the field due to the point dipole itself. The second term is the potential of the reaction field. From this it follows that the reaction field is given by

$$\boldsymbol{R} = \frac{2(\varepsilon - 1)}{2\varepsilon + 1} \frac{\mu}{a^3} \hat{z}, \tag{A.5}$$

which is seen to be proportional to the dipole moment, $\boldsymbol{\mu}$:

$$\boldsymbol{R} = f\boldsymbol{\mu}, \quad f = \frac{2(\varepsilon - 1)}{2\varepsilon + 1} \frac{1}{a^3} \tag{A.6}$$

The next step is to generalize this to the case of a dipole that can be polarized. Such a dipole will be polarized by the reaction field and this additional dipole moment will also contribute to the reaction field. This means

$$
\begin{aligned}
\boldsymbol{R} &= f(\boldsymbol{\mu} + \alpha_i \boldsymbol{R}) \ \Leftrightarrow & \text{(A.7)} \\
\boldsymbol{R} &= \frac{f}{1 - f\alpha_i}\boldsymbol{\mu}, & \text{(A.8)}
\end{aligned}
$$

where α_i is the induced polarization coefficient.

B   Fitting functions

In this appendix we will present the fitting functions and models, which we have used in our analysis. Both shear and dielectric fitting functions have been used to determine high frequency plateau values, and the equilibrium values have also been found in the case of dielectric data. The limiting values found in this manner have been used in 7, 10 and 11. There shear fitting functions have also been used for generating the fictive shear data, which are used in chapter 8 and 10.

Havriliak-Negami function

This phenomenological fitting function is used to describe dielectric data.

$$\varepsilon = \varepsilon_h + \frac{\varepsilon_e - \varepsilon_h}{(1 + (i\omega\tau_D)^a)^b}. \tag{B.1}$$

$0 \leq a \leq 1$ and $0 \leq b \leq 1$.

If $b = 1$ the function reduces to the Cole-Cole function, if $a = 1$ the function reduces to the Cole-Davidson function, and finally if $a = b = 1$ the function reduces to the Debye function.

Extended Maxwell

This is a generalization of the Maxwell model based on the BEL model. The Extended Maxwell model is in this thesis used to describe the alpha relaxation in the shear modulus.

$$G = G_\infty \frac{1}{1 + \frac{1}{i\omega\tau_M} + q\left(\frac{1}{i\omega\tau_M}\right)^a} \tag{B.2}$$
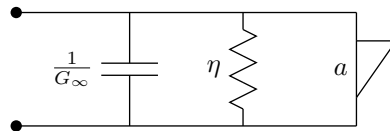

Figure B.1 Electric diagram showing the extended Maxwell model, the outer right element is a generalized diffusion chain.

The mechanical alpha–beta–model

We use this model to describe shear modulus spectra with both an alpha and a beta relaxation.

The mechanical shear response is modeled as a parallel combination of an extended maxwell element and a mechanical Cole-Cole element.
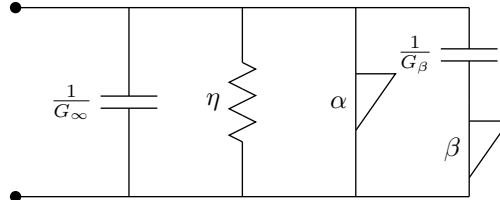

Figure B.2 Electric diagram showing the mechanical α–β–model. The α- and β-elements are generalized diffusion chains.

The shear modulus is given as

$$G(\omega) = \frac{G_\infty}{1 + \frac{1}{i\omega\,\tau_\alpha} + q\left(\frac{1}{i\omega\,\tau_\alpha}\right)^\alpha + \frac{G_f}{(i\omega\,\tau_\beta)^\beta + 1}} \tag{B.3}$$

where $\tau_\alpha = \frac{\eta}{G_\infty}$, $G_f = \frac{G_\infty}{G_\beta}$. The prefactor on the $(i\omega\tau_\beta)^\beta$ term has been set to one, but a different value can be chosen with out loss of generality because τ_β is a free parameter.